CHALMERS

The operating cycle representation of road transport missions

LUIGI ROMANO

Department of Mechanics and Maritime Sciences
CHALMERS UNIVERSITY OF TECHNOLOGY
Göteborg, Sweden 2023

Thesis for the degree of doctor of philosophy
in
Machine and Vehicle Systems

The operating cycle representation of road transport missions

LUIGI ROMANO

Department of Mechanics and Maritime Sciences
CHALMERS UNIVERSITY OF TECHNOLOGY
Göteborg, Sweden 2023

The operating cycle representation of road transport missions

LUIGI ROMANO
ISBN 978-91-7905-888-3

Doctoral thesis at Chalmers University of Technology
Series number: 5354
ISSN 0346-718X

Department of Mechanics and Maritime Sciences
Chalmers University of Technology
SE–412 96 Göteborg
Sweden
Telephone: +46 (0)731431356

Cover: A truck driving in a stochastically generated environment, surrounded by a stream of data.
Generated with DALL · E2 (available from https://openai.com/dall-e-2/).

Chalmers Reproservice
Göteborg, Sweden 2023

To my family: Mom, Dad, Francesco
&
my beloved Yulia.

Men's fortunes are on a wheel, which in its turning suffers not the same man to prosper forever.

–Herodotus

The operating cycle representation of road transport missions
Luigi Romano
Department of Mechanics and Maritime Sciences
Chalmers University of Technology

Abstract

The difficulties that conventionally road vehicles are facing in meeting regulation standards require *ad-hoc* solutions. Moreover, the impellent shift of paradigm towards full electrification and partial automation is posing great challenges to the automotive industry, which has set a zero-emissions target to be reached within a short time horizon. In this context, the energy performance of commercial vehicles may be dramatically improved if the characteristics of the transport application, that is, the intended usage, are known prior to prototype development and design selection. To tailor the vehicle's specifications, however, a representative description of the mission and the surroundings is needed.

Where many conventional approaches fail, the operating cycle format (OC) has revealed great potential in describing road operations in a way that is, to a large extent, independent of both vehicle and driver. More specifically, the framework consists of three levels of representation. The first, called the *bird's-eye view*, serves mainly as a classification tool and makes use of metrics and labels to completely characterise the overall application of a vehicle during its lifetime. The second description, the *stochastic operating cycle* (sOC), condenses the main properties of a road operation using elementary statistics. It is conceived as an intermediate representation with a higher resolution. Finally, the *deterministic operating cycle* (dOC) is the most detailed description of a transport mission and collects deterministic models to be used in simulations. In previous studies, the OC format was demonstrated to work in theory, but some margins for improvement could still be identified. Furthermore, the benefits deriving from the use of the OC were explored only partially.

The first objective of this thesis consists in extending the OC representation to include stochastic models for weather, traffic, and mission properties, which were missing in the original formulation. The new models are built to be parsimonious and to facilitate parametrisation and implementation starting from real data. This enables reproducing and simulating realistic environments where a transport mission may take place, with a substantial gain in accuracy. The second purpose of this work is to showcase how the OC concept can be used in practical applications concerning the design and sale phases. To this end, the relationships existing between the three levels of representation included in the format are formalised mathematically by exploiting the stochastic nature of the sOC, which acts as a bridge between the bird's-eye view and the dOC. It is argued that the three descriptions can work synergically to support manufacturers in their internal processes of classification, optimal development and selection, and virtual testing of energy-efficient vehicles.

Keywords: operating cycle, road mission, transport application, energy estimation,

stochastic processes, probability distributions

Acknowledgments

My PhD journey has finally come to an end and I have accumulated a long list of names that deserve a proper acknowledgement. First, I would like to express my gratitude to my academic supervisors, Professors Bengt Jacobson and Fredrik Bruzelius, and my former industrial supervisor Sixten Berglund. They have believed in me since the very beginning and offered me a position as a PhD student at Chalmers in the first place. Bengt's peculiar way of thinking and framing problems has, in particular, always been an inexhaustible source of inspiration. Concerning both technical and practical issues, I have always valued preciously Bengt's guidance and extreme availability beyond what was required. In Fredrik, my main supervisor, I soon found a friend, also. Fredrik has always tried to spur my inventiveness and excite my curiosity towards my PhD topic and the COVER project. Despite the frustration and the difficulties sometimes encountered in this sense, he has been very successful in his purpose. Besides that, Fredrik has always encouraged me firmly while conducting some other research in parallel, allowing me to broaden my interests with patience and support: I really appreciate that. With Sixten, I have perhaps spent less time than desirable; nonetheless, his company has been extremely precious, especially at the very beginning of my PhD. Our running sessions in the Lundby area were a good incentive for some physical activity after a rather stagnant period of motionless life.

At RISE, my first co-supervisor Pär Johannesson owns the great merit of introducing me to the fascinating world of statistics and deserves a big thanks for that. Also at RISE, I am indebted to Michele Godio for his enthusiastic and irreplaceable contribution to the COVER project. With my second co-supervisor and friend Toheed Ghandriz, I have shared a considerable amount of time as a PhD student, other than a common interest in sci-fi movies. I will always enjoy a good chat about work and science fiction over a cold beer. At Volvo Trucks, I want to thank the amazing people that have assisted me in carrying out my research, especially Rickard Andersson, Anders Eriksson, and my former students Erik Nordström and Carl Emvin. Carl has now started his own PhD journey, and I am sure he will be a great candidate for continuing the work initiated with COVER.

The beginning of my PhD studies coincides with that of a life-lasting friendship with Milo Viviani, whose apartment I also inherited as the last member of a long tradition of Italian mathematicians (and mathematicians to be). The succession ends here, but I am proud of having been part of the exclusive club of Barytongatan 8. Milo has been one of my best

friends in Gothenburg and first indicated a more rigorous, methodic approach to the problems I was investigating. In the past years, he has been a tireless revealer of many thrilling secrets about the mysteries of pure and applied mathematics, finally persuading me to pursue a Master's degree at the University of Gothenburg. In fact, at the Department of Mathematics, I would like to thank Simone Calogero and Axel Målqvist for the stimulating discussions that we had about PDEs, FEMs and semigroup theory. To Axel, my Master's thesis advisor, I am particularly grateful for his enthusiasm in supervising me without even knowing whether I would be admitted to the program or not.

Apart from exposing me to advanced mathematical topics, Milo also introduced me to my extended family in Gothenburg: the Kantarellers. Among them, I have made friends for life, especially Giovanni, Antonio, and Matteo. Giovanni, in particular, has been to me a mentor-father-like figure during the past years. He fed me with amazing food, unorthodox ideas, and uncountable linguistic acnedotes. The honorary member Matteo Tamini has also been a fun and sometimes crazy companion of adventures.

At VEAS, I want to express my gratitude to all my colleagues and friends, especially those that have accompanied me through this journey from the beginning till the very end: Anandh, Sachin, Juliette, Johannes, Arun, Adam, Alexey, Björnborg, and Krister. Dragan, with his calm wisdom and his spirituality, has also been a close friend to me in the past years; I hope to meet him again in future. With Marco Virgolin, I made a particularly strong bond, and our friendship has continued even outside Chalmers: we meet regularly in Amsterdam for a delicious Neapolitan pizza when I am there visiting my girlfriend. I also want to thank Simone and Sonja for all the hard administrative work, for the attention dedicated to making the environment welcoming and pleasant for everyone, and for their great coffee. Sonja, with her luminous smile, really incarnates the true spirit of VEAS. At Chalmers, I have also made many good friends outside VEAS. In Michele Maglio, I have found a generous and sincere friend. I enjoyed very much talking about cinema, art, and literature during our relaxed lunches and coffees. At E2, I had the pleasure of attending the control courses with some talented PhD students, particularly Carl-Johan Heiker and Sondre Wiersdalen: it was a great experience to meet and study with them both. Finally, with my first and greatest friends at Chalmers, Alireza Marzbanrad and Afshin Houshang, I share priceless and joyful memories that will never fade.

Concerning my stay in Trondheim, I am particularly grateful to Professor Ole Morten Aamo for hosting me at NTNU and providing kind and very insightful feedback on my work for the entire duration of the visit. I also met new friends there, whom I hope to see again in future. At my home university in Naples, I will always be in debt to Professor Francesco Timpone for introducing me to the discipline of vehicle dynamics. On the same subject, I had extremely interesting discussions with Professor Massimo Guiggiani, who has always been a source of inspiration to me and a role model to tend to. I hope to meet him in person soon. At CNR Istituto Motori, special thanks go to Professor Pietro Capaldi for giving me the opportunity of approaching the modelling of driving cycles already in 2016. Now that I look in retrospect, it really seems that the research conducted during my PhD studies is a

natural continuation of what I did in Naples some years ago. I like to glimpse some sort of romantic fatalism in this somewhat circular epilogue.

Finally, with all the love and tenderness of my heart, I would like to thank my family – Mom, Dad, and my brother Francesco –, and my beloved *piccerella* Yulia, for always being there for me. You are the brightest light of my life.

Luigi Romano
Göteborg, September 2023

PS: I hope I did not forget anyone, but if so, please do not take offence: if you are reading this thesis, you have probably contributed a little bit to it.

Thesis

This thesis comprises an extended summary and is based on the following appended papers:

A **L. Romano**, P. Johannesson, F. Bruzelius, and B. Jacobson, "An enhanced stochastic operating cycle description including weather and traffic models", *Transportation research part D: transport and environment*, vol. 97, 2021.

B **L. Romano**, P. Johannesson, E. Nordström, et al., "A classification method of road transport missions and applications using the operating cycle format", *IEEE Access*, vol. 10, pp. 73087-73121, 2022.

C **L. Romano**, M. Godio, P. Johannesson, et al., "Development of the Västra Götaland operating cycle for long-haul heavy-duty vehicles", *IEEE Access*, vol. 11, pp. 73268-73302, 2023.

D **L. Romano**, M. Raathimiddi, F. Bruzelius, et al., "A method to build energy-metric-optimal (EMO) classification systems for road transport missions", to be presented at *2023 IEEE Vehicle Power and Propulsion Conference*, Milan, Italy, 2023.

E **L. Romano**, C. Emvin, F. Bruzelius, et al., "Stochastic modeling of mission stops and variable cargo weight for heavy-duty trucks", to be presented at *2023 IEEE Vehicle Power and Propulsion Conference*, Milan, Italy, 2023.

Concerning the first four appended papers, the doctoral candidate Luigi Romano established the theory and was responsible for the conceptualisation, methodology, model and software development, validation, formal analysis, investigation, data curation, writing, review, editing, and visualisation phases. The coauthors contributed with experimental data acquisition, review, editing, and supervision. Concerning Paper E, the doctoral candidate was mainly responsible for the supervision, conceptualisation, formal analysis, and writing phases, with the second author conducting most of the simulations and a large part of the data analysis.

Some other publications by the author, not included in the thesis, are reported below.

1. **L. Romano**, F. Bruzelius, and B. Jacobson, "Transient tyre models with a flexible carcass", to appear on *Vehicle System Dynamics*, 2023.

2. **L. Romano**, M. Maglio, and S. Bruni, "Transient wheel-rail rolling contact theories", *Tribology International*, vol. 186, 2023.

3. **L. Romano**, "Advanced Brush Tyre Modelling", 1st ed. Springer, Cham, 2022.

4. M. Ciavarella, **L. Romano**, and J. R. Barber, "Rolling of a cylinder with slip-dependent friction: the Carter solution revisited", *Theoretical and Applied Fracture Mechanics*, vol. 121, 2022.

5. **L. Romano**, F. Timpone, F. Bruzelius, and B. Jacobson, "Transient Tire Slip Losses Using the Brush Theory", *Tire Science and Technology*, 2022.

6. **L. Romano**, F. Timpone, F. Bruzelius, and B. Jacobson, "Rolling, tilting and spinning spherical wheels: Analytical results using the brush theory", *Mechanism and Machine Theory*, vol. 173, 2022.

7. **L. Romano**, F. Bruzelius, and B. Jacobson, "An extended LuGre-brush tyre model for large camber angles and turning speeds", *Vehicle System Dynamics*, vol. 61, no. 6, pp. 1674-1706, 2022.

8. **L. Romano**, F. Bruzelius, M. Hjort, and B. Jacobson, "Development and analysis of the two-regime transient tyre model for combined slip", *Vehicle System Dynamics*, pp. 1-35, 2022.

9. **L. Romano**, F. Timpone, F. Bruzelius, and B. Jacobson B, "Analytical results in transient brush tyre models: theory for large camber angles and classic solutions with limited friction", *Meccanica*, vol. 57, no. 1, pp. 165-191, 2022.

10. **L. Romano**, F. Bruzelius, and B. Jacobson B, "Brush tyre models for large camber angles and steering speeds", *Vehicle System Dynamics*, vol. 60, no. 4, pp. 1341-1392, 2022.

11. **L. Romano**, S. Strano, and M. Terzo, "Synthesis and comparative analysis of three model-based observers for normal load and friction estimation in intelligent tyre concepts", *Proceedings of the Institution of Mechanical Engineers, Part D: Journal of Automobile Engineering*, vol. 235, no. 6, pp. 1629-1642, 2021.

12. **L. Romano**, F. Bruzelius, and B. Jacobson, "Unsteady-state brush theory", *Vehicle System Dynamics*, vol. 59, no. 11, pp. 1643-1671, 2021.

13. **L. Romano**, S. Strano, and M. Terzo, "A model-based observer for intelligent tire concepts", *2019 IEEE 5th International forum on Research and Technology for Society and Industry (RTSI)*, 2019.

14. G. Breglio, A. Irace, V. R. Marrazzo, et al., "Feel-tire unina: development and modeling of a sensing system for intelligent tires", *2019 IEEE 5th International forum on Research and Technology for Society and Industry (RTSI)*, 2019.

15. D. Garcia-Pozuelo, O. A. Olatunbosun, **L. Romano**, et al., "Development and experimental validation of a real-time analytical model for different intelligent tyre concepts", *Vehicle System Dynamics*, vol. 57, no. 12, pp. 1970-1988, 2019.

16. **L. Romano**, A. Sakhnevych, S. Strano, and F. Timpone, "A novel brush-model with flexible carcass for transient interactions", *Meccanica*, vol. 54, no. 10, pp. 1663-1679, 2019.

17. **L. Romano**, A. Sakhnevych, S. Strano, and F. Timpone, "A hybrid tyre model for in-plane dynamics", *Vehicle System Dynamics*, vol. 58, no. 7, pp. 1123-1145, 2019.

Acronyms and notation

Acronyms and notation are as follows.

Acronyms

OC	Operating cycle
dOC	Deterministic operating cycle
sOC	Stochastic operating cycle
GTA	Global Transport Application
UFD	User-Factor Description
EMO	Energy-metric-optimal
PDF	Probability density function
PMF	Probability mass function
CDF	Cumulative distribution function

Notation

In this thesis, the notation is generally as follows: for a generic random variable $A : \Omega_A \mapsto \mathcal{S}_A$, its realisations are denoted by the corresponding small letter a, unless specified otherwise. The probability and expectation operators are denoted as $\mathbb{P}(\cdot)$ and $\mathbb{E}(\cdot)$, respectively. The set of real numbers is denoted by $\mathbb{R}$; the sets of positive and negative real numbers are denoted by $\mathbb{R}_{\geq 0}$, $\mathbb{R}_{\leq 0}$ when including the zero and by $\mathbb{R}_{>0}$, $\mathbb{R}_{<0}$ when excluding it. The set of positive integer numbers is denoted by $\mathbb{N}$, whereas $\mathbb{N}_0$ denotes the extended set of positive integers including zero, i.e., $\mathbb{N}_0 = \mathbb{N} \cup \{0\}$. Sequences of random variables are denoted by $\{A_k\}$ (the subscript k is often dropped when the clarity allows). Finally, indicator functions are denoted by $\mathbb{1}_{a \in \mathcal{A}}$ and assume a value of one if $a \in \mathcal{A}$ and zero otherwise.

Table of Contents

Chapter 1

Introduction

The present chapter is dedicated to a general outline of the thesis. After discussing in detail the motivations behind the work in Sect. 1.1, the main research questions are formulated in Sect. 1.2. The theoretical background and limitations are presented in Sect. 1.3. Finally, the main contributions are summarised in Sect. 1.4.

1.1 Motivation and background

An appealing way to frame this thesis is to invoke some recently published data that denounce the entity of the anthropogenic factor contributing to the global warming phenomenon (to cite a few documents, one may look at the technical reports authored by individual researchers [1–4], or drafted by governmental agencies [5–10]). A conspicuous contribution to the production of pollutants comes from the release of equivalent CO_2 emissions from human activity, particularly relating to the road transport of people and goods (Fig. 1.1). This incentivised the European Commission to adopt several strict measures which aim at contrasting the increasing temperature and pollution trend and target directly the transportation sector [11–14]. More specifically, emission thresholds have been set for heavy-duty and passenger vehicles. Preliminary tests have been designed with the very purpose of ensuring compliance with such limits and may be carried out physically or by using simulation tools. At the same time, the accelerated shift of paradigm towards full electrification and partly automated driving is also posing enormous challenges to the automotive sector, with vehicle manufacturers announcing the ambitious target of zero emissions to be reached within a relatively short time horizon. Compared to their conventionally fuelled counterpart, electric vehicles are however heavier and sadly associated with the well-known phenomenon of range anxiety, which in turn implies the need for a more energy-efficient design [15–17].

In this context, the energy performance of road vehicles may be dramatically improved if the operating conditions are known prior to prototype development and design selection. These include mission characteristics, driver's behaviour, and external settings like topographical, wind and traffic conditions. All these factors correlate with both the usage itself and the

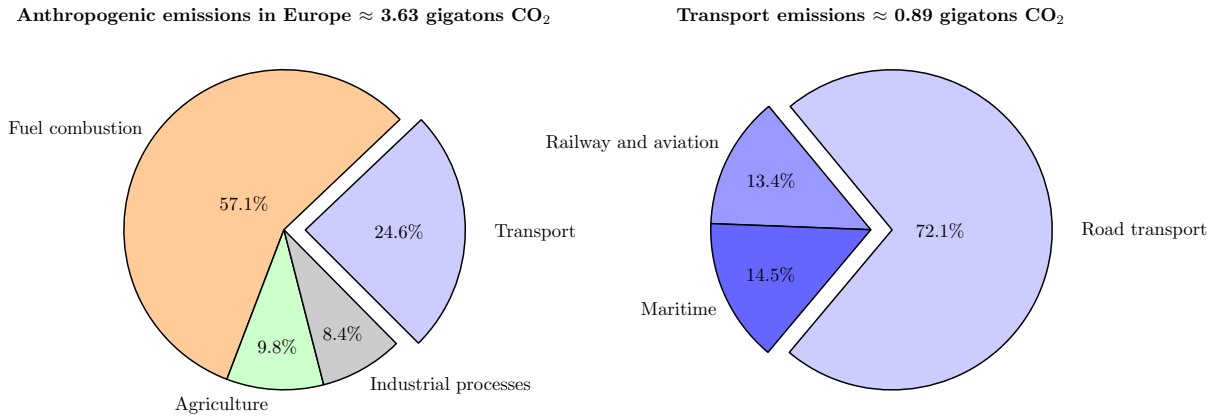

Figure 1.1: Distribution of the CO_2 emissions in Europe for the year 2017 relating to the total human activity and transportation sector. Europe alone contributes with about 10% to the global CO_2 release.

surroundings where the transport operation takes place. Since major variation may occur depending on the location and the time (due to, e.g., the effect exerted by seasonal and diurnal trends), the vehicle's specifications should be tailored to meet the transport application and the relative boundary conditions.

To investigate how these influence the vehicle's response, however, it is necessary to formulate mathematical models. These should of course be realistic, and ideally sufficiently simple to allow a fundamental understanding of the physical problem. On the one hand, limiting the attention to the vehicle and driver as separate entities, several models have been developed over the years with different goals in mind. On the other hand, a synthetic but complete description of a transport operation has been rarely attempted in literature. One obvious difficulty encountered when defining a transport operation relates to the notion *per se*, which might appear to be rather obscure and vague. Provided that this first obstacle can be overcome, another question to address is how to identify all the relevant features and then represent them in a useful manner, in a way that is independent of the vehicle itself. This is sometimes referred to as the *representation problem* [18].

Accurate modelling of transport operations may also serve different purposes than those outlined so far. For heavy-duty vehicles, an important aspect to consider is that virtual testing is often required before a physical prototype can be built. One reason for that relates to the immense degree of diversification that may be achieved in the actual configuration. Indeed, whilst only a few predetermined alternatives are available for passenger cars, the panorama of different combinations is virtually infinite for trucks. Considering the combinatorial nature of the problem, it becomes soon obvious that physical testing is prohibitive in terms of both costs and times, and other options should be preferred. Tailoring the vehicle for the right mission – or spectra of missions – is an extremely delicate process. Besides, if all the relevant factors are not accounted for properly, a solution derived analytically, or even numerically,

may easily result in a suboptimal configuration in practice.

1.1.1 The driving cycle representation

The aspects outlined so far are themselves sufficient to legitimate the enormous research effort lavished on addressing the representation problem. One well-established approach consists in describing a transport mission using a driving cycle. Intuitively, a driving cycle is a mapping[1] from the time or vehicle's position along its trajectory to a speed profile, which should capture the salient features of the operation. Speed profiles may be synthesised by using different types of information, and several approaches have been proposed in the literature. In particular, there exist two main variants of a driving cycle: modal and transient. The former type is usually employed for standard tests regulated by legislation, since it allows for straightforward comparison. Examples of modal driving cycles include the WLTC shown in Fig. 1.2 and those used in VECTO [20]. However, such driving cycles are not very realistic and are currently considered obsolete. More specifically, a major shortcoming of using them resides in the fact that performance is inherently built into the model, and there is no clear separation between the vehicle and the driving cycle itself.

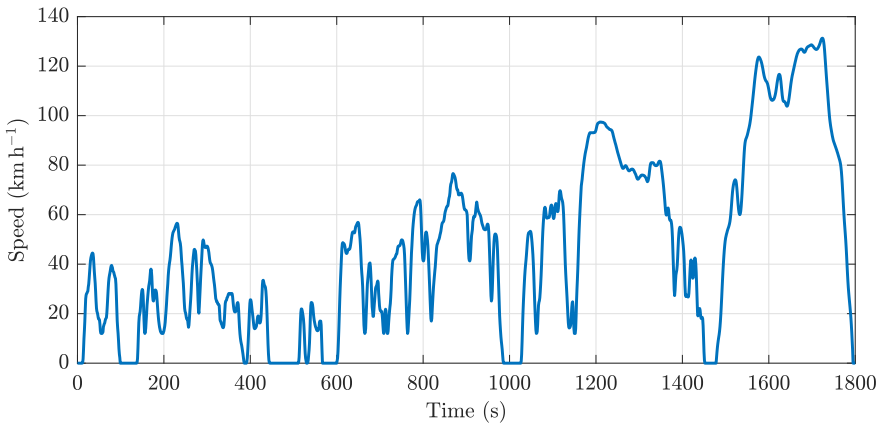

Figure 1.2: The WLTC class 3 driving cycle.

Transient cycles are often preferred for powertrain optimisation and design purposes, which require accurate feasibility studies, as those performed in [21–31]. In this context, a crucial aspect of the efficient design is the accurate description of a transport operation, with exhaustive information about the surroundings. Indeed, to correctly replicate the real-world performance, it is necessary to take into account all the external factors and stimuli which may affect the vehicle's behaviour. These include road and mission properties, but also weather and traffic conditions [32–35].

[1] For an interested reader, a more formal definition in mathematical terms may be found in [19].

How to synthesise representative transient cycles is an interesting and open question, and different approaches have been explored over the years [36–49]. In particular, it is possible to distinguish between rule-based methods and statistical ones. Rule-based methods are very sensitive to experts' opinions and aim to replicate a limited number of characteristics from the measured driving cycles [50, 51]. Such a criterion may be represented by the percentages of city, suburb, and highway speeds. By contrast, the advantage of resorting to statistical techniques resides in the fact that generated synthetic speed profiles correlate with certain operating conditions of the vehicle, e.g., cruising, idling, acceleration or braking events. This enhanced approach makes use of Markov chains or machine learning techniques, and combines different information (mostly inferred by speed and acceleration signals) to reflect the characteristics of real-driving scenarios. Improved algorithms also account for external sources of excitation (for example road grade) which are anticipated to have a major influence on a vehicle's overall performance [19, 52–63]. Traffic conditions are also modelled empirically, often based also on the characteristics of a certain road type [35].

The above mentioned approaches are all aimed at addressing the representation problem by synthesising a unique representative transient cycle starting from a large amount of data. In fact, a single driving cycle is often sufficient when it comes to apply conventional algorithms and routines for the purposes of vehicle design optimisation and selection. On the other hand, reproducing variation in transport operations may lead to a more accurate prediction of the energy performance of road vehicles. Ideally, departing from a single representation of the usage, driving cycles may be constructed to be statistically equivalent, so as to produce a meaningful spread in performance. This line of research was pioneered in [64, 65], where a procedure was proposed that allows for the synthesis of multiple driving cycles, departing from a single trip. More specifically, it was shown in [64, 65] that the energy performance of electric city buses is highly sensitive to fluctuations in both the number of stops and passenger load. Indeed, by treating both quantities as random variables, the authors deduced that the energy consumption follows approximately a normal distribution. The variability connected to the randomness of the external surroundings, concerning for example temperature and rolling resistance, was also investigated in [66], where the inherent uncertainty was modelled by adding a noise term to the assumed nominal value for the quantities in interest. These fundamental contributions essentially explored the *variation problem*, which was defined by Pettersson [18] and is concerned with similarities and differences between road missions and within transport applications (Fig. 1.3). Limitedly to the driving cycle description, the notion of equivalence has been defined according to different sets of measures, for example considering the effect that a certain speed profile may have on the vehicle's performance [54].

Along with the representation and variation problems, however, Pettersson [18] also defines the so-called *classification problem*, in conjunction with the need to properly qualify a road mission (or an entire transport application) using a simplified set of metrics and labels. This is mainly motivated by the fact that, rather than referring to a certain speed profile, vehicle manufacturers and operators usually describe the usage concerning the characteristics of the environment, which are easier to interpret. In this context, whilst the conventional

Figure 1.3: An example of different road transport missions.

description in terms of a driving cycle has been successful in addressing the first two problems indicated by Pettersson [18], the latter still deserves particular attention. In fact, a major limitation connected with the driving cycle representation is that the information about the operating environment – including parameters that may dramatically impact energy consumption [32–35, 67–73] – is often lost or accounted for only implicitly during the synthesis of a representative speed profile.

1.1.2 The operating cycle representation

Expanding on the discussion initiated above, there are two main arguments which may be raised against these conventional descriptions in terms of a driving cycle. The first is that their pathological nature makes them inadequate to compare different vehicles. With "pathological", it is here intended that there exists an implicit correlation between the reference vehicle and the speed profile. This intrinsic contamination may jeopardise the general validity of the resulting speed profile. Another demerit point is that, when a driving cycle is recorded, all the external effects (due to, e.g., traffic or wind conditions) are automatically incorporated. This is done implicitly, meaning that their influence cannot be understood or examined. Intuitively, it might be argued that a general, reliable representation of a transport mission should be independent of both the vehicle and the driver.

The *operating cycle* (OC) format introduced by Pettersson certainly fulfils these requirements [18, 74, 75]. In fact, this type of representation is not based on the concept of a driving cycle, and therefore no speed profile needs to be postulated as an input to the longitudinal vehicle model. On the contrary, the properties of both the mission and the external surround-

ings are modelled separately, and then a driver model is used to translate dynamically the external stimuli into the desired speed. This allows for circumventing the need to incorporate the information coming from the surroundings into the speed profile.

The OC consists of three main levels of representation, each of them designed for a specific role. Before commenting on their relative functions, the notions of *transport application*, *transport operation* and *transport mission* according to [18] should be clarified. In particular, Pettersson defines the transport application as the overall purpose of a vehicle during its lifetime [18]. This is something antecedent to the vehicle itself, and towards which the specifications should be tailored. The difference between transport operation and mission is less formal: the former consists of a countable number of tasks along a given route, whereas the latter integrates the operation with details from the surroundings[2]. Both the operation and the mission presume the existence of a vehicle to make sense, i.e., are defined *a posteriori*.

Given the definitions above, the intuition suggests that having a realistic description of a transport mission is not sufficient to characterise the application. There are two additional requirements that should be imposed, which again connect to the variation and classification problems introduced above. Specifically, the classification problem concerns the existence of different sorts of relationships between individual representations [18]. In nature, things may be grouped and labelled into different categories depending on certain common properties. Identifying differences and similarities between transport missions is crucial when it comes to defining the overall application. If transport missions can be classified based on some well-defined metrics, then the complexity of the problem decreases significantly. Provided that suitable metrics can be identified, even missions which belong to the same transport application cannot be expected to be identical when interpreted as individual realisations. Ideally, one would like to quantify the variation inside each category in a simple way. This implies, however, the need for an intermediate description, which should be ideally built around this principle and make use of elementary statistical tools. This is again the variation problem indicated by Pettersson [18].

The three levels of representation comprised in the OC format, namely the *bird's-eye view*, the *stochastic operating cycle* (sOC), and the *deterministic operating cycle* (dOC), respond exactly to these needs. In this very context, it is important to mention that the enormous potential of the OC format was illustrated through several examples in previous works [18, 74, 75]. However, the version delivered by Pettersson left still space for an ample margin of improvement. In particular, concerning the representation problem, models for weather, traffic and mission parameters had not been included. Moreover, the synergies between the three levels of representation were explored only partially, with the consequence that the applicability of the OC framework to the optimal vehicle design and selection processes could not be demonstrated in practice. Such deficiencies mainly motivate the present thesis.

[2]In the following chapters, it will be shown that such a definition is still ambiguous from the modelling perspective. However, subordinate to some specific stochastic models, the notions of road transport operations and mission, respectively, might be rendered equivalent concerning any sequence of tasks.

1.2 Research questions

The three problems identified in the preceding discussion, namely the representation, variation, and classification problems, may be more formally stated as research questions. A fourth question may also be formulated that connects to the notion of usefulness, and is called in this thesis the *application problem*[3].

I. **Representation problem:** How can a road transport mission be described mathematically to enable a realistic representation of the usage in a way that is independent of both the vehicle and driver?

   This research question intimately connects to the need of building a comprehensive mathematical description of the operating environment, including all the relevant factors that may have an impact on energy performance. In conducting such an operation, there are many aspects that need to be carefully pondered. For example, the main parameters to consider, the level of detail required to balance accuracy and simplicity, and the fundamental principles to follow. The scope is instead limited to individual transport missions.

II. **Variation problem:** How can variation between road operations be measured and reproduced mathematically?

   The first part of this research question concerns the need for measuring the variation between individual road missions and entire applications, using simple yet rigorous statistical tools. The second aspect relates instead to the possibility of reproducing such a variation through mathematical modelling. In doing so, the ambition is to bridge together a more accurate description of the usage and a higher-level representation, idoneous for classification purposes.

III. **Classification problem:** How can transport applications be classified concerning geographical and operational features, in a way that is independent of both the vehicle and driver?

   This question formalises the need for classifying the usage of road vehicles by resorting to scalar metrics and labels, capable of condensing the relevant information about differences and similarities between entire applications. The chosen indicators should target directly the characteristics of the environment, allowing for an intuitive interpretation of the usage based on measurable physical quantities, for example concerning geographical or operational features. A natural subquestion that arises in this context is how to specify these metrics in a meaningful way, and how to prescribe limits and thresholds to optimise diversification between different classes and groups of missions.

[3]The term *application* is preferred here to *usefulness* or *applicability* because the OC machinery should be explicilty applicable to the analysis and optimisation of transport applications.

IV. **Application problem:** How can the representation, variation, and classification problems be addressed in order to support and facilitate the optimal vehicle development and selection processes?

The models and methods delivered whilst answering the first three questions should be successfully employed to assist vehicle manufacturers in designing more energy-efficient vehicles, based on the characteristics of the intended application, and on the user's needs. That is, they should be useful in practice.

1.3 Theory, methods, and limitations

The present Section provides an overview of the theory and methods presented in this thesis, along with possible limitations.

1.3.1 Theory and methods

Albeit eventually touching upon more classical topics like simulations and dynamical systems, the present is not a conventional thesis in vehicle dynamics. Quite the opposite, the focus is more on what surrounds the vehicle, including road properties, weather, and traffic conditions. More specifically, in the sOC description, the modelling of the operational environment is mainly based on a collection of stochastic processes. These, together with other elementary tools borrowed from the disciplines of probability and statistics, constitute the true core of the present research. Markovian and autoregressive processes, in particular, play both a pivotal role in the development of some of the stochastic models introduced in Papers A, B and E. However, to the extent that is necessary to appreciate the results advocated in this thesis, the reader is only required to have a minimal understanding of probability laws and random variables. Indeed, a rather friendly approach to these subjects is consistently preferred, with emphasis on the physical aspects that motivate the inclusion of certain quantities and models. Excellent and, in fact, more mathematically rigorous introductions to the Markovian and autoregressive processes used in the building of the sOC format may be found, for example, in [76, 77].

The methodology presented in Paper D presumes some knowledge about multi-objective optimisation, including the notions of Pareto-optimality and efficiency [78]. However, the results of Paper D are only briefly mentioned in this thesis, and thus an introductory discussion on the above-mentioned topics is omitted for the sake of both conciseness and consistency.

Concerning more directly the simulation aspect, conventional models for (longitudinal) vehicle dynamics are mainly based on systems of *differential-algebraic equations* (DAE). In fact, even the dynamics of mechanical components described by *partial differential equations* (PDEs) may be fairly approximated using simplified ODE-based representations. Examples of such subsystems may include, for instance, tyres, combustion engines, and batteries, for which even the quasi-static approach is frequently adopted [79–82]. The reader is presumed

to be familiar with these topics, which are not covered explicitly in the thesis. In this context, Appendix A provides a sufficient introduction to VehProp, which constitutes the principal simulation tool used in the investigations conducted in the appended papers.

1.3.2 Limitations

The scope of the present research being extremely broad, some assumptions have been introduced to simplify the analysis. This has inevitably led to some limitations.

In particular, from a pure vehicle modelling perspective, the analysis has been confined to longitudinal dynamics. This implies that the effects from, e.g., suspension compliance and roll dynamics have been neglected systematically. The influence from tyre slip losses has been investigated both theoretically and numerically in other publications [83, 84], but disregarded in simulation. In [84], it was also shown that considering the transient behaviour of the tyre during acceleration and deceleration phases may lead to different results than those advocated in other studies, but, to the best of the author's knowledge, a proper ODE-based model to account for the non-steady state slip losses has not been developed yet. The research has also been conducted from a single-vehicle perspective, meaning that complex dynamics arising from vehicle or fleet interaction have not been considered.

Some limitations are strictly connected to the stochastic models introduced in the operating cycle description. In particular, the physical quantities labelled in the road and weather categories have been assumed to only depend either on space or time, respectively. Furthermore, the proposed traffic model is based on the assumption of stationary flow and homogeneous road conditions, as discussed more extensively in Sect. 2.2.3 and in Paper A. Weather and traffic models have been built in isolation and parametrised using real data available from external databases. For both, the fitting procedures have been chosen such as to minimise the error between the model prediction and measurements. Finally, concerning the actual mission properties, the development and validation of stochastic models were restricted to a specific vehicle topology in Paper E.

The examples adduced throughout the thesis mainly deal with heavy-duty trucks equipped with diesel engines. Concerning again heavy vehicles, an illustrative example connected with the more recent shift of paradigm towards electrification is presented in Paper C. However, the OC format has been conceived to be generally applicable to any (road) vehicle category, provided that a suitable model is available. Lastly, the driver model employed in this thesis is based on a simple PID controller and tries to replicate a human driver. Simulation results seem to suggest a realistic behaviour, but no experimental validation has been conducted.

Finally, an exhaustive discussion about the applicability of the OC machinery to the processes of vehicle design optimisation, selection, and testing is presented in Chap. 4. In this context, it should be mentioned that optimisation problems cover a domain which is immensely vast *per se* and are not dealt with explicitly in the thesis, nor were they in the appended papers. Instead, a summary of interesting methods and results has been presented recently by Ghandriz [25, 85–87], who followed a similar approach to that outlined in Chap.

4. Some of these findings are also reported in Paper C.

1.4 Thesis outline and contribution

The remainder of this thesis is organised as follows. Chapter 2 is devoted to the description of the OC format and discusses all three levels of representation. The core of the chapter focuses on the sOC, which may be thought of as a bridge between the bird's-eye view and dOC models. The relationships existing between the three representations are also analysed in detail, and their mutual interactions and synergies are revealed. Building upon the results presented in Papers B, C and E, Chap. 3 introduces the notions of *operating classes* and *composite variables*, whose definition is propaedeutic to address the classification problem within the theoretical framework established by the OC format. The chapter concludes with a brief discussion on how to optimally design a classification system for road transport missions. In Chap. 4, the practical usage of the OC format is exemplified starting from the investigations conducted in Papers B and C. More specifically, the conceptual example adduced in Chap. 4 covers the optimal design, selection and virtual testing phases. The discussion is integrated with additional comments on some technical aspects which concern the parametrisation and the implementation of the stochastic models presented in the thesis. Chapter 5 concludes the thesis by summarising what done and opening possible perspectives for future studies. Finally, an introduction to the simulation tools used to in this thesis is given in Appendix A, whereas Appendix B provides additional details about two classification systems adopted by vehicle manufacturers for their internal processes: the *Global Transport Application* (GTA) and the *User-Factor Description* (UFD).

1.4.1 Scientific contributions

Recalling previous works on the OC description, the representation and variation problems were addressed to a certain extent in [74, 75], where deterministic and stochastic road models were introduced. However, the versions of the dOC and sOC delivered by Pettersson were deficient in weather and traffic models. Concerning a possible solution to the classification problem, only a tentative proposal was made in [18], which was also limited to a single stochastic model for the road topography. Finally, given the still partially unstructured nature of the format, its applicability to product development and selection was not investigated in earlier studies.

In this context, the main scientific contributions of this thesis are as follows.

- Concerning the representation and variation problems, an enriched version of the sOC that includes new stochastic models for the weather and traffic categories has been developed in Paper A. It must be remarked that the stochastic models for weather and traffic do not constitute a novelty when considered in isolation, since a great deal of research has been already lavished on dedicated studies. Instead, the main contribution

of Paper A should be sought in that it makes this collection of stochastic models useful for studies in vehicle dynamics. Similarly, a stochastic model capturing variations in cargo weight has been introduced in Paper E and validated using real-world data logged from a single truck.

- Taking inspiration from two existing descriptions adopted by vehicle manufacturers, a methodology to classify road transport missions using stochastic models and statistical indicators has been presented in Paper B. The proposed approach exploits the intrinsic relationship existing between the bird's-eye view and sOC descriptions, thus also enabling to accurately quantify similarities and differences between individual operations, as well as entire applications, based on physical quantities that are easy to interpret. This contribution relates to the variation and classification problems.

- An operating cycle for long-haul heavy-duty vehicles, complete with the majority of the road models presented in this thesis, has been parametrised in Paper C using log-data collected from real-world missions. In the same paper, a technique to build a single representative sOC for an entire application, starting from a multitude of dOCs and sOCs, has also been discussed. The potential of the resulting description has been elucidated by considering two examples dealing with the development of an electrified fleet tailored to the characteristics of the transport application, and with emissions certification, respectively. Paper C is mainly concerned with the variation, classification, and application problems.

- A methodology to specify limits and thresholds to optimally design a classification system has been presented in Paper D. Starting with the theoretical results advocated in Paper B, the proposed approach relies on the definition of some vehicle-independent metrics that may be used to characterise the usage from the perspective of energy efficiency and builds upon some well-established concepts from multi-objective optimisation. Paper D focuses almost exclusively on the classification problem.

The connections between the appended papers are illustrated in Fig. 1.4. More explicitly, in Paper A, some of the stochastic models analysed in Paper B are presented. The research directions explored in Papers C and D are not directly related, but the corresponding findings build upon the results advocated in Paper B. Finally, Paper E continues mainly in the same direction as Paper A, by introducing a stochastic model to describe payload variations. A formal statistical analysis is also conducted in the same spirit of Paper B.

Before moving to the technical chapters, it is worth clarifying that this thesis should be intended as a collection of concepts, theories, and methods established with the intent of addressing the problems identified in Sect. 1.2, and specifically with the aim of assisting manufacturers in the development of more energy-efficient vehicles. Whilst the perspective may undoubtedly be seductive, the monumental futility of constructing an all-embracing theory of the operating cycle representation is, however, not undertaken here: the models presented

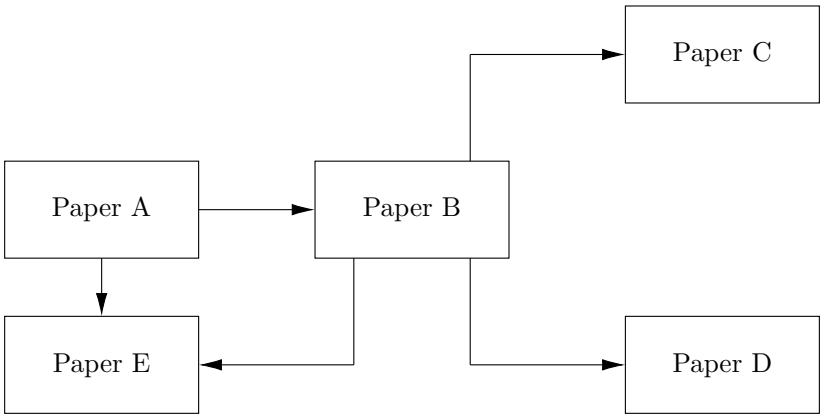

Figure 1.4: Connections between the appended papers. Paper A focuses on the representation and variation problems. Some of the models developed in Paper A are analysed in Paper B, where a theoretical framework to address the variation and classification problems is established. The results from Paper B are utilised independently in Papers C and D, which are concerned with the application and classification problems, respectively. Paper E partially addresses the representation and variation problems, concerning specifically the mission modelling.

in the following should be regarded as mostly indicative, and everything but definitive. Refinements and generalisations are of course always possible and certainly encouraged. Besides, modularity and simplicity constitute the very inspiring principles of the operating cycle.

Chapter 2

The operating cycle description

The present chapter is dedicated to the mathematical description of road transport missions and applications in terms of an operating cycle (OC). The aim of the operating cycle is fourfold and satisfies the needs for representation, variation, classification, and application, as already mentioned in the introduction. From the modelling perspective, the first three ambitions of the OC format naturally result in a composite representation that is built upon three different levels: the *bird's-eye view*, the *stochastic operating cycle* (sOC) and the *deterministic operating cycle* (dOC). These three descriptions complement each other and attempt to address the classification, variation and representation problems, respectively. The practical applicability of the OC to the optimal design and selection processes of road vehicles is instead revealed by the synergies existing between its three levels of representation. As shown in Fig. 2.1, these are arranged in a pyramidal structure, which reflects their hierarchical order and their resolution. A common feature shared amongst all three levels of description is that they discriminate between four different categories to model a transport operation: road, weather, traffic, and mission. The first three categories relate to the description of the operating environment, whereas the last one concerns the modalities by which a vehicle is operated. For each of the above-mentioned categories, the necessary models to be included may be preliminarily deduced starting from a simple set of equations for longitudinal dynamics, like those reported in Appendix A, Paper A, or in most of the textbooks dedicated to the description of energy efficiency and consumption of road vehicles [82, 88].

In what follows, the three building levels of the OC format will be reviewed in order, with particular emphasis on the sOC, which constitutes the very core of the framework. All the models presented in this chapter may be found in similar form in [18, 74] and in Papers A and E.

2.1 The bird's-eye view

Descending the hierarchical order between the descriptions, the bird's-eye view collocates on the top of the pyramid. It is specifically conceived to address the classification problem, and

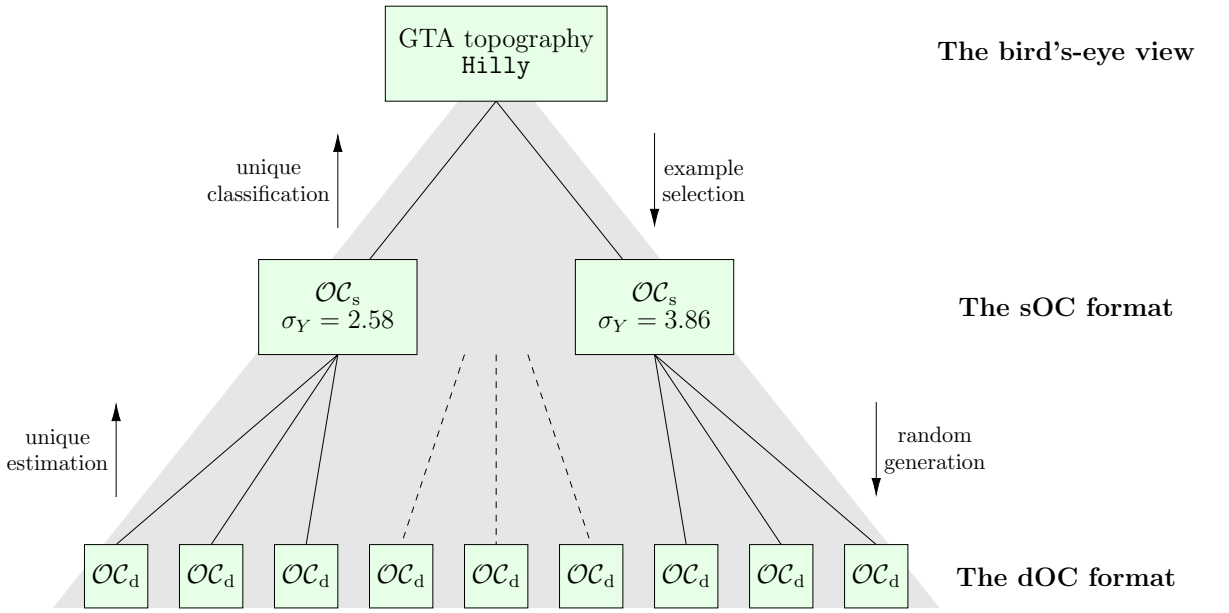

Figure 2.1: Schematic representation of the pyramidal structure of an OC, using the topography parameter as an example. All the missions being equivalent in the sense of a GTA class belong to the same transport application (the bird's-eye view). The individual statistical properties may however differ within the transport application (sOC). Finally, transport missions can be statistically equivalent but significantly different in practice. This is captured by the dOC representation.

targets individual road missions, as well as entire transport applications. The bird's-eye view representation makes use of simplified metrics and labels, which may easily be translated into statistical indicators [74, 75, 89, 90]. These should be ideally chosen to be representative of some variation in usage, performance, or properties. The metrics and labels for the bird's-eye view may be defined from scratch or borrowed from existing classification systems, as exemplified briefly for the topography parameter in the following. In particular, the GTA system introduced by Volvo specifies four different levels [91]:

I. `FLAT` if slopes with a grade of less than 3% occur during more than 98% of the driving distance.

II. `P-FLAT` if slopes with a grade of less than 6% occur during more than 98% of the driving distance.

III. `HILLY` if slopes with a grade of less than 9% occur during more than 98% of the driving distance.

IV. `V-HILLY` if the other criteria are not fulfilled.

In the above example, the bird's-eye view labels clearly correspond to the operating classes `FLAT`, `P-FLAT` (predominantly flat), `HILLY` and `V-HILLY` (very hilly), whilst the metrics are the values imposed on the road grade (3%, 6% and 9%, respectively) and the probability of occurrence, always set to 0.98. On the other hand, the UFD adopted by Scania[1] proposes only three classes:

I. `FLAT` if max 20% of the road section inclines more than 2%.

II. `HILLY` if between 20-40% of the road section inclines more than 2%.

III. `V-HILLY` if more than 40% of the road section inclines more than 2%.

In both cases, the given thresholds are ambiguous, and there is no guarantee that they can reflect any significant variation in usage or performance. Furthermore, it is worth observing that the UFD targets single road sections, whilst the GTA specifies the different classes based on the vehicle usage, and therefore mixes the characteristics of the environment with those of the transport operation. One main advantage of such a vague description resides in its colloquial tone. In fact, the bird's-eye view is the most appropriate representation when a vehicle manufacturer is interfacing with a customer, who cannot be expected to have a deep understanding of stochastic models and parameters. Similar to the topography parameter, a system of classes is specified by the GTA and UFD descriptions for most of the stochastic road models presented in this thesis, and for some of the weather models. An exhaustive list may be found in Paper B, and in reduced form also in Paper C, along with their mathematical formalisations in terms of probabilities and expectations.

Formally, the complete set of bird's-eye view metrics may be defined mathematically as

$$\mathcal{OC}_{\mathrm{b}} = \{\mathcal{R}_{\mathrm{b}}, \mathcal{W}_{\mathrm{b}}, \mathcal{T}_{\mathrm{b}}, \mathcal{M}_{\mathrm{b}}\}, \tag{2.1}$$

in which $\mathcal{R}_{\mathrm{b}}$, $\mathcal{W}_{\mathrm{b}}$, $\mathcal{T}_{\mathrm{b}}$ and $\mathcal{W}_{\mathrm{b}}$ are the sets containing all the respective bird's-eye view metrics in the road, weather, traffic, and mission categories. The subscript $(\cdot)_{\mathrm{b}}$ in (2.1) stands for *bird's-eye view*.

2.2 The stochastic operating cycle

The stochastic operating cycle (sOC) may be considered a mid-level description of a transport mission, and addresses the variation problem. In its general formulation, it consist of a complete set of stochastic models grouped into four different categories: road, weather, traffic and mission.

Each sOC model is provided with its own set of stochastic parameters, which are chosen to condense the relevant statistical properties (mean, variance, etc.) of the corresponding quantity. These may also be related to physical entities, but the interpretation is often less

[1]The information on the UFD has kindly been supplied by Scania through personal communication.

straightforward. The structure of the sOC is conceived to be as simple as possible, and the models are thought to be independent of each other. In a more formal way, the complete set of sOC parameters may be defined mathematically as

$$\mathcal{OC}_{\mathrm{s}} = \{\mathcal{R}_{\mathrm{s}}, \mathcal{W}_{\mathrm{s}}, \mathcal{T}_{\mathrm{s}}, \mathcal{M}_{\mathrm{s}}\}, \tag{2.2}$$

where $\mathcal{R}_{\mathrm{s}}$, $\mathcal{W}_{\mathrm{s}}$, $\mathcal{T}_{\mathrm{s}}$ and $\mathcal{W}_{\mathrm{s}}$ are the sets containing all the sOC parameters marked as road, weather, traffic and mission, respectively. The subscript $(\cdot)_{\mathrm{s}}$ in Eq. (2.2) stands for *stochastic*. Models and parameters for the road category have been introduced by Pettersson [74], whilst the traffic and weather categories have been more recently developed by the author of this thesis in Paper A. Finally, a first step towards the stochastic modelling of mission properties has been attempted in Paper E, concerning specifically variations in cargo weight.

It is essential to remark that the overall framework is built with the philosophy of being as simple as possible. This means that complicated multivariate distributions are avoided, thus requiring each individual model to be treated as a separate entity. Disregarding such mutual interaction guarantees modularity and allows for ease of implementation. At the same time, to balance complexity and realism, a certain level of interaction between each model is preserved by arranging the sOC itself in a hierarchical fashion. Concerning the road, weather, and traffic categories, parsimony is thus achieved by defining two separate sets of models: primary and secondary ones (subordinate). In this way, it becomes possible to achieve a modular structure equipped with a high level of diversification. The (main) obvious disadvantage is that the number of effective values needed for each stochastic parameter also increases.

Primary models are introduced to simplify the mathematical description of the format. At present, they include stochastic models for *road type* and *seasonality* falling within the road and weather categories, respectively. Once a mathematical formulation for both primary models has been established, the secondary ones inherit their sets of sOC parameters accordingly. In particular, the sOC parameters for the secondary models in the road and weather categories are supposed to only depend on the corresponding primary counterpart. On the contrary, the stochastic parameters for the secondary traffic model are determined by the specific combination of road type and season. On the other hand, the mission category does not discriminate between primary and secondary models in its current implementation (although such distinction could be made based on different operating conditions of the vehicle, or eventually topologies).

An illustration of the resulting composite edifice is shown in Fig. 2.2, where the hierarchical structure comprising primary and secondary models is shown. For what follows, it is worth clarifying that the stochastic models introduced in Sects. 2.2.1, 2.2.2, 2.2.3, and 2.2.4 may be used to model individual road missions. The extension to entire transport applications may be addressed as explained in Sect. 2.2.5, and later on also in Chap. 3.

In the following, the secondary models for the road, weather, traffic, as well as those for the mission category, will be discussed in detail. The presentation follows those of Papers A, B and E, altough with some simplifications.

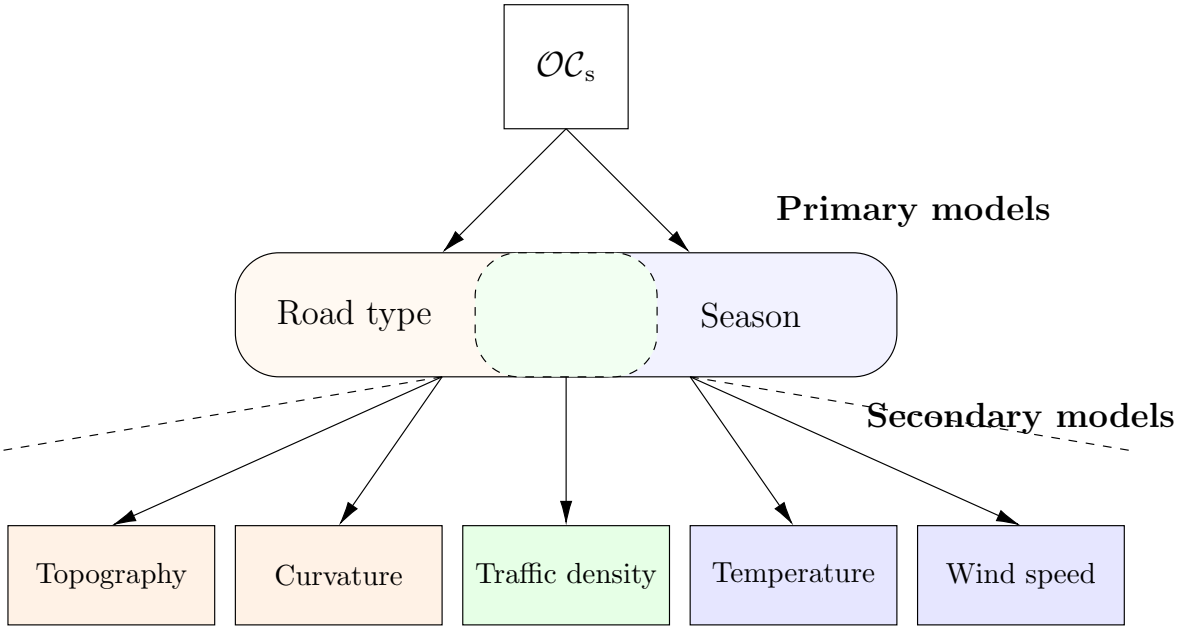

Figure 2.2: Hierarchical structure of an sOC. Road type and season are both primary models and influence the value of the statistical parameters for the secondary models. Whilst the (secondary) road and weather parameters depend only on the respective primary model, the traffic ones are determined by the road type and season simultaneously. Figure adapted from Paper A.

2.2.1 Road models

The road models were originally developed by Pettersson [18], and are adapted from previous formulations. The primary model for the road category concerns the road type, whereas the secondary models presented in this thesis include those for topography, curviness, stop signs and speed bumps, road roughness, speed signs, and ground types.

The road type *per se* is an abstract notion, which cannot be measured nor classified directly. The solution envisioned by Pettersson [74] consists hence in connecting this concept to something which may be more easily understood and quantified: the speed limit [92]. A stochastic model is then constructed by first postulating the existence of n_r different road types. This is done by considering a sequence $\{r_1, \ldots, r_{n_r}\}$, based on $n_r - 1$ characteristic speed signs, ordered in ascending magnitude. These mark the transition from one road type to the next, implying that each speed sign belongs uniquely to a given road type. According to this approach, the road type may be treated as a random variable R_t, assuming values $r_\mathrm{t} \in \mathcal{S}_{R_\mathrm{t}} = \{r_1, \ldots, r_{n_r}\}$ as a function of the speed signs along the route. In particular, a specific number $n_{v|r_i}$ of speed signs is associated to each road type. Moreover, it is assumed that the Markov property holds [76], i.e.,

$$\mathbb{P}\big(R_{\mathrm{t},k+1} = r_{i,k+1} \big| R_{\mathrm{t},1} = r_{i,1}, R_{\mathrm{t},2} = r_{i,2}, \ldots, R_{\mathrm{t},k} = r_{i,k}\big) = \mathbb{P}\big(R_{\mathrm{t},k+1} = r_{i,k+1} \big| R_{\mathrm{t},k} = r_{i,k}\big). \tag{2.3}$$

By modelling the locations X_k for the road types as a Poisson process, that is,

$$X_{k+1} - X_k \sim \mathcal{E}(\lambda_{Ri}), \tag{2.4}$$

the complete model is then described by a continuous-time Markov chain, and parametrised by the entries p_{Rij} of the single-step transition matrix $\mathbf{P}_R \in \mathbb{R}_{\geq 0}^{n_r \times n_r}$ and the n_r intensities λ_{Ri}, reading

$$\lambda_{Ri} = \frac{1}{L_{Ri}}, \tag{2.5}$$

being L_{Ri} the mean length of the road type r_i, collected in a vector $\boldsymbol{L}_R = [L_{R1} \ \ldots \ L_{Rn_r}]^\mathrm{T}$. It should be noticed that, in the construction above, no self-transitions are allowed, i.e., $p_{Rii} = 0$, $i = 1, \ldots, n_r$, which automatically implies $\sum_{j \neq 1} p_{Rij} = 1$, $i = 1, \ldots, n_r$.

Starting from the stochastic model for road types detailed above, the stationary distribution[2] $\boldsymbol{\pi}_R$ of the overall process may be derived as the solution of the system [76, 93, 94]

$$\boldsymbol{\pi}_R \mathbf{G}_R = \mathbf{0}, \tag{2.6a}$$

$$\sum_{i=1}^{n_r} \pi_{Ri} = 1, \tag{2.6b}$$

[2]It is supposed that there exists a unique stationary distribution.

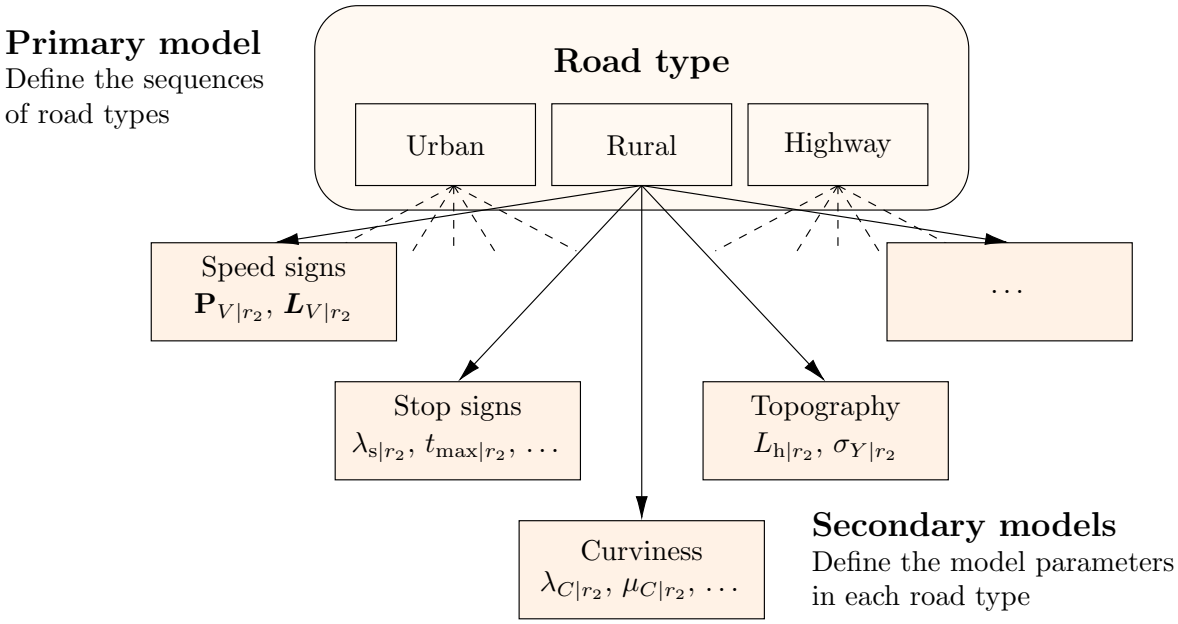

Figure 2.3: The road type is the primary road model. The other parameters are treated as ancillary and inherit their values depending on the road type. Figure adapted from Paper A.

where the entries $g_{Rij} = g_{Rij}(p_{Rij}, L_{Ri})$ of the generator matrix $\mathbf{G}_R$ may be calculated as

$$g_{Rij}\big(p_{Rij}, L_{Ri}\big) = \begin{cases} \lambda_{Ri} p_{Rij} = \dfrac{p_{Rij}}{L_{Ri}}, & i \neq j, \\ -\lambda_{Ri} = -\dfrac{1}{L_{Ri}}, & i = j. \end{cases} \tag{2.7}$$

Equations (2.6) and (2.7) describe the stationary distribution of the road types along a road transport mission, as a function of the observed number of transitions between road types and their mean lengths. An analytical expression for the stationary vector $\boldsymbol{\pi}_R = \boldsymbol{\pi}_R(\mathbf{P}_R, \boldsymbol{L}_R)$ is reported in Paper C concerning the case $n_r = 3$.

As mentioned above, the secondary road models inherit their parameters from the specific road type on which they are defined. In this context, Fig. 2.3 elucidates the hierarchical ordering of the road models for $n_r = 3$ (urban, rural and highway).

Starting with Eqs. (2.6) and (2.7), it should be observed that, for an individual transport mission, the total probability and expectation of a random variable that depends on the road type may be calculated by weighted summation over the different road types, respectively, using the total laws for probability and expectation[3]. Indeed, in the sOC representation,

[3]With the same rationale, the variance of a process defined over different road types may also be calculated using the corresponding formula for the total variance. However, such a formula is not explicitly used in this thesis, nor in the appended papers.

road segments belonging to the same road type are described using the same values for the sOC parameters of the secondary models. Denoting with A a generic random variable, the formulae are hence given as follows:

$$\mathbb{P}(A) = \sum_{i=1}^{n_r} \mathbb{P}(A \mid R_\mathrm{t} = r_i)\, \mathbb{P}(R_\mathrm{t} = r_i) = \sum_{i=1}^{n_r} \mathbb{P}(A \mid R_\mathrm{t} = r_i) \pi_{Ri}(\mathbf{P}_R, \boldsymbol{L}_R), \tag{2.8a}$$

$$\mathbb{E}(A) = \sum_{i=1}^{n_r} \mathbb{E}(A \mid R_\mathrm{t} = r_i)\, \mathbb{P}(R_\mathrm{t} = r_i) = \sum_{i=1}^{n_r} \mathbb{E}(A \mid R_\mathrm{t} = r_i) \pi_{Ri}(\mathbf{P}_R, \boldsymbol{L}_R), \tag{2.8b}$$

where the analytical expressions for the probabilities $\mathbb{P}(A \mid R_\mathrm{t} = r_i)$ and expectations $\mathbb{E}(A \mid R_\mathrm{t} = r_i)$ may be derived starting from the secondary models illustrated in the following, as explained in detail in Paper B.

Road topography

Topography plays a major role in determining the overall energy performance of road vehicles. Indeed, positive road grades are responsible for resistive forces that oppose longitudinal motion, resulting in increased energy consumption [82]. Negative road grades, in contrast, produce forces that accelerate the vehicle downhill, and may considerably impact the life and performance of the mechanical components of the braking system. Negative slopes are also exploited by battery electric vehicles (BEVs) for regenerative braking [25].

In the sOC description, the road topography Y_k is assumed to behave as a stationary, first-order autoregressive AR(1) model [67, 68]. The sequence $\{Y_k\}_{k\in\mathbb{N}}$ along the road is thus given by

$$Y_k = \phi_{Y|r_i} Y_{k-1} + e_{Y,k}, \qquad e_{Y,k} \mid R_\mathrm{t} = r_i \sim \mathcal{N}\Big(0, \sigma^2_{e_{Y|r_i}}\Big), \tag{2.9}$$

where $\phi_{Y|r_i} \in (-1, 1)$ and $\sigma_{e_{Y|r_i}} \in (0, \infty)$ are the two characteristic parameters that depend upon the given road type. In particular, departing from Eq. (2.9), the conditional variance of the process may be deduced as

$$\sigma^2_{Y|r_i} = \frac{\sigma^2_{e_{Y|r_i}}}{1 - \phi^2_{Y|r_i}}, \tag{2.10}$$

where the autoregressive coefficient $\phi_{Y|r_i}$ may be also reinterpreted as a function of the mean hill length $L_{\mathrm{h}|r_i}$ for the road type r_i:

$$\phi_{Y|r_i} = \sin\left(\frac{\pi}{2} - 2\frac{L_\mathrm{s}}{L_{\mathrm{h}|r_i}}\right), \tag{2.11}$$

being L_s the sampling length. Owing to these assumptions, the conditional standard deviation $\sigma_{Y|r_i}$ and the mean hill length $L_{\mathrm{h}|r_i}$ condense all the information about the road topography.

Road curviness

Lateral acceleration due to curves along the road typically induces the driver to decelerate, resulting in increased energy consumption. In this context, two main contributing phenomena may be identified: the reduced efficiency of the prime mover and the losses due to pure or combined slip conditions that take place inside the tire contact patches [95–97]. Moreover, lateral load due to road curvature has a substantial impact on the fatigue of the mechanical components of a vehicle, reducing their useful life [98–100].

The sOC representation treats the curves along the road as isolated events, modelled using a sequence of locations, curvatures, and lengths $\{X_k, C_k, L_k\}_{k\in\mathbb{N}}$. The resulting model – referred to as the *curviness* of the road – was introduced by Petterson [74] based on the description proposed by Karlsson [98]. In particular, for each road type, the locations are assumed to follow a Poisson distribution, i.e.,

$$X_{k+1} - X_k \mid R_\mathrm{t} = r_i \sim \mathcal{E}\Big(\lambda_{C|r_i}\Big), \tag{2.12}$$

where the intensity $\lambda_{C|r_i} \in (0, \infty)$ should be interpreted as the mean number of curves per unit of distance along a certain road type. The curvatures C_k is modelled as a modified lognormal distribution as follows:

$$\frac{1}{C_k} = R'_k + r_\mathrm{turn}, \qquad \ln R'_k \mid R_\mathrm{t} = r_i \sim \mathcal{N}\Big(\mu_{C|r_i}, \sigma^2_{C|r_i}\Big), \tag{2.13}$$

where the parameter $r_\mathrm{turn} \in (0, \infty)$ appears because roads are constructed with a lower bounded radius. In theory, r_turn is not a statistical measure, but rather an inherent property of the road type. In this thesis, and also in the appended papers, the same value of r_turn is used for all the road types. Finally, the curve length L_k is modelled using a lognormal distribution, that is,

$$\ln L_k \mid R_\mathrm{t} = r_i \sim \mathcal{N}\Big(\mu_{L|r_i}, \sigma^2_{L|r_i}\Big). \tag{2.14}$$

Stop signs, give way signs, traffic lights and speed bumps

Speed bumps along the vehicle's trajectory force the driver to reduce their cruising speed, often resulting in increased energy consumption. A similar effect is produced by the stop signs, which clearly impose a driving speed of zero. Speed bumps and stop signs are modelled similarly in the sOC representation. More specificaly, they are treated as independent events and described by the sequences $\{X_k, T_{\mathrm{s},k}\}_{k\in\mathbb{N}}$ and $\{X_k, V_{\mathrm{b},k}\}_{k\in\mathbb{N}}$, respectively, where X_k is again the location, $T_{\mathrm{s},k}$ is interpreted as a recommended time, and $V_{\mathrm{b},k}$ as a recommended speed. A Poisson process similar to that in Eq. (2.12), but with intensities $\lambda_{\mathrm{s}|r_i}$ and $\lambda_{\mathrm{b}|r_i}$, may be used to model the distance between two consecutive stops or speed bumps.

The standstill time is then allowed to range uniformly between a minimum t_min and maximum t_max:

$$T_{\mathrm{s},k} \mid R_\mathrm{t} = r_i \sim \mathcal{U}\big(t_{\mathrm{min}|r_i}, t_{\mathrm{max}|r_i}\big). \tag{2.15}$$

Similarly, the recommended speed may be assumed to be uniformly-distributed between a minimum $v_{\min}$ and maximum $v_{\max}$:

$$V_{\mathrm{b},k} \mid R_{\mathrm{t}} = r_i \sim \mathcal{U}\big(v_{\min|r_i}, v_{\max|r_i}\big). \tag{2.16}$$

For a given road type r_i, each model is fully described by three parameters. Additional quantities, such as give way signs and traffic lights, may be modelled following a similar rationale.

Road roughness

Road roughness plays an important role when it comes to durability and fatigue of mechanical components, but has a minor impact on energy efficiency [101]. Nonetheless, it is often included in bird's-eye view descriptions in use by vehicle manufacturers, like the GTA and UFD classification systems developed by Volvo and Scania, respectively.

In this thesis, the model for road roughness is only discussed briefly, whilst a more exhaustive treatment may be found in [67, 68, 102–105]. In this context, road profiles are traditionally modelled using Gaussian processes [106]. This choice works satisfactorily for small sections of roads, whereas variability between sections may be better explained using generalised Laplace models. These may be interpreted as Gaussian processes with randomly varying variance. In the sOC representation, on each road type $i = 1, \dots, n_r$, the model for the road profile $Z(x)$ is based on the definition given by the ISO standard 8608 [107], which uses a two-parameter spectrum:

$$S_Z(\Omega) = C_{\mathrm{r}|r_i} \left(\frac{\Omega}{\Omega_0} \right)^{-w}, \qquad \Omega_1 \leq \Omega \leq \Omega_2, \tag{2.17}$$

and zero otherwise. In (2.17), Ω is the spatial angular frequency, $\Omega_0 = 1$, $\Omega_1 = 2\pi \cdot 0.011$, $\Omega_2 = 2\pi \cdot 2.83$ are two cut frequencies expressed in radians per metre, and $C_{\mathrm{r}|r_i}$, $i = 1, \dots, n_r$, is the conditional degree of unevenness, also called the roughness coefficient [107]. Finally, the waviness parameter w is assumed to be constant and set to $w = 2$. The sOC description employs a Laplace ISO model [67, 68, 102–104], parametrised on each road type by its conditional mean roughness $C_{\mathrm{r}|r_i}$ and the conditional Laplace shape parameter $\nu_{\mathrm{r}|r_i}$ (or, equivalently, its conditional variance and kurtosis).

Speed signs and ground type

The legal speed dramatically impacts the energy performance of road vehicles. In fact, whilst constant cruising speeds may be observed to be apparently optimal from an energy efficiency perspective, frequent variations in driving speed result in increased consumption [25].

On the other hand, the ground type and the asphalt properties play an important role in determining the maximum traction forces that the tyres can generate, and have also a substantial effect on rolling resistance [79–81, 108, 109]. These two aspects are particularly

significant for electric vehicles, in conjunction with both the higher instantaneous torques that the wheels may experience and the well-known phenomenon of range anxiety.

In what follows, only the model for road types is discussed, since the sequence of ground types along the vehicle's route may be modelled using exactly the same rationale. In particular, for a given road type[4] r_k, the speed signs are regarded as piecewise constant, right-side continuous functions of the position [74]. Specifically, the speed signs are modelled as a random process $V = V(x)$ along with the position on the road. Accordingly, the variable $V(x)$ assumes discrete values in the state space $\mathcal{S}_{V|r_k} = \{v_{1|r_k}, \dots, v_{n_{v|r_k}|r_k}\}$, where $n_{v|r_k}$ denotes the finite number of possible speed limits for the road type r_k. Also in this case, the complete model collects a sequence of positions, marked with the corresponding values for the legal speed, i.e., $\{X_k, V_k\}_{k\in\mathbb{N}}$. Similarly as for the road types, the sequence of speed limits is approximated by using a Markov chain [76, 110], and assumes discrete values $v_{i|r_k}$ organised into the speed vector $\boldsymbol{v}_{|r_k} = [v_{1|r_k} \ \dots \ v_{n_{v|r_k}|r_k}]^{\mathrm{T}}$.

Consequently, the entries of the conditional Markov probability matrix $\mathbf{P}_{V|r_k} \in \mathbb{R}_{\geq 0}^{n_{v|r_k} \times n_{v|r_k}}$ fully characterise the discrete chain, with $p_{Vij|r_k}$ modelling the conditional probability of transitioning from state i to state j. Since no self-transition are allowed, as usual, they satisfy $\sum_{j\neq i}^{n_{v|r_k}} p_{Vij|r_k} = 1$, $i = 1, \dots, n_{v|r_k}$. The speed sign locations are again modelled as in Eq. (2.12). For each road type, the $n_{v|r_k}$ intensities $\lambda_{V1|r_k}, ..., \lambda_{Vn_{v|r_k}|r_k}$ may be deduced from the corresponding mean lengths $L_{Vi|r_k}$:

$$\lambda_{Vi|r_k} = \frac{1}{L_{Vi|r_k}}, \tag{2.18}$$

collected into a vector $\boldsymbol{L}_{V|r_k} = [L_{V1|r_k} \ \dots \ L_{Vn_{v|r_k}|r_k}]^{\mathrm{T}}$. The resulting model is completely parametrised by the conditional probabilities $p_{Vij|r_k}$ and the $n_{v|r_k}$ mean lengths $L_{Vi|r_k}$ (or, alternatively, the intensities $\lambda_{Vi|r_k}$). Additionally, it should be observed that the speed $V(x)$ itself behaves as continuous-time Markov chain [76], since the distance between consecutive transitions is modelled using a Poisson process. In particular, the stationary distribution $\boldsymbol{\pi}_{V|r_k}$ of the overall process may be derived departing from its generator matrix $\mathbf{G}_{V|r_k}$, and satisfies the usual set of equations

$$\boldsymbol{\pi}_{V|r_k}\mathbf{G}_{V|r_k} = \mathbf{0}, \tag{2.19a}$$

$$\sum_{i=1}^{n_{v|r_k}} \pi_{Vi|r_k} = 1, \tag{2.19b}$$

where the entries $g_{Vij|r_k} = g_{Vij|r_k}(p_{Vij|r_k}, L_{Vi|r_k})$ of $\mathbf{G}_{V|r_k}$ are given by

$$g_{Vij|r_k}\big(p_{Vij|r_k}, L_{Vi|r_k}\big) = \begin{cases} \lambda_{Vi|r_k} p_{Vij|r_k} = \dfrac{p_{Vij|r_k}}{L_{Vi|r_k}}, & i \neq j, \\ -\lambda_{Vi|r_k} = -\dfrac{1}{L_{Vi|r_k}}, & i = j. \end{cases} \tag{2.20}$$

[4]Here the index k is used for the road type to avoid confusion with the indexing of the model parameters for the speed signs.

Closed-form expressions for $\boldsymbol{\pi}_{V|r_k} = \boldsymbol{\pi}_{V|r_k}(\mathbf{P}_{V|r_k}, \boldsymbol{L}_{V|r_k})$ are again reported in Paper C for the cases $n_{v|r_k} = 2$ and 3, respectively.

2.2.2 Weather models

The stochastic models for the weather category discussed in this paper are based on the formulations presented in Paper A, and were validated using data collected from the Swedish Meteorological and Hydrological Institute (SMHI)[5]. In particular, the primary model for the weather category consists of the season [111]. This is regarded as a random variable S, whose possible realisations are $s \in \mathcal{S}_S = \{s_1, s_2, s_3, s_4\}$ with probabilities p_{s_i}, $i = 1, 2, 3, 4$, respectively[6]. It is worth emphasising that the seasons considered in the sOC representation are the meteorological ones, as opposed to the astronomical. In this context, even though the probabilities p_{s_i} should be calculated differently depending on the location of the road segment (boreal or austral hemisphere), they may fairly be approximated as $p_{s_i} \approx 1/4$, $i = 1, 2, 3, 4$.

On the other hand, the secondary weather models include ambient temperature, atmospheric pressure, precipitation, wind velocity and relative humidity. The major assumption is that the weather properties remain approximately constant in space. Therefore, only the explicit dependence upon time is modelled. As for the stochastic models in the road category, the secondary models inherit their parameters from the season, as illustrated schematically in Fig. 2.4.

Owing to the above premises, using A to denote a generic random variable (either continuous or discrete) for a weather model, the total probability $\mathbb{P}(A)$ and expectation $\mathbb{E}(A)$ may be computed starting from the conditional probabilities $\mathbb{P}(A \mid S = s_i)$ and expectations $\mathbb{E}(A \mid S = s_i)$ as

$$\mathbb{P}(A) = \sum_{i=1}^{4} \mathbb{P}\big(A \;\big|\; S = s_i\big)\, \mathbb{P}\big(S = s_i\big) = \sum_{i=1}^{4} \mathbb{P}\big(A \;\big|\; S = s_i\big) p_{s_i}, \tag{2.21a}$$

$$\mathbb{E}(A) = \sum_{i=1}^{4} \mathbb{E}(A \;\big|\; S = s_i)\, \mathbb{P}\big(S = s_i\big) = \sum_{i=1}^{4} \mathbb{E}\big(A \;\big|\; S = s_i\big) p_{s_i}. \tag{2.21b}$$

Ambient temperature and relative humidity

Ambient (or air) temperature and humidity have a profound impact on the performance of the engine and on the batteries of BEVs [69]. Thermal management strategies also need to be adapted based on the combined effect of both quantities, especially for vehicles operating in cold climates [112, 113]. In addition, the air temperature has a secondary effect on air drag.

[5] Available from: https://www.smhi.se/en/weather/sweden-weather/observations#ws=wpt-a,proxy=wpt-a,tab=vader,param=t.

[6] In the sOC description, the realisations s_i, $i = 1, 2, 3, 4$ correspond to winter, spring, summer and autumn, in that order.

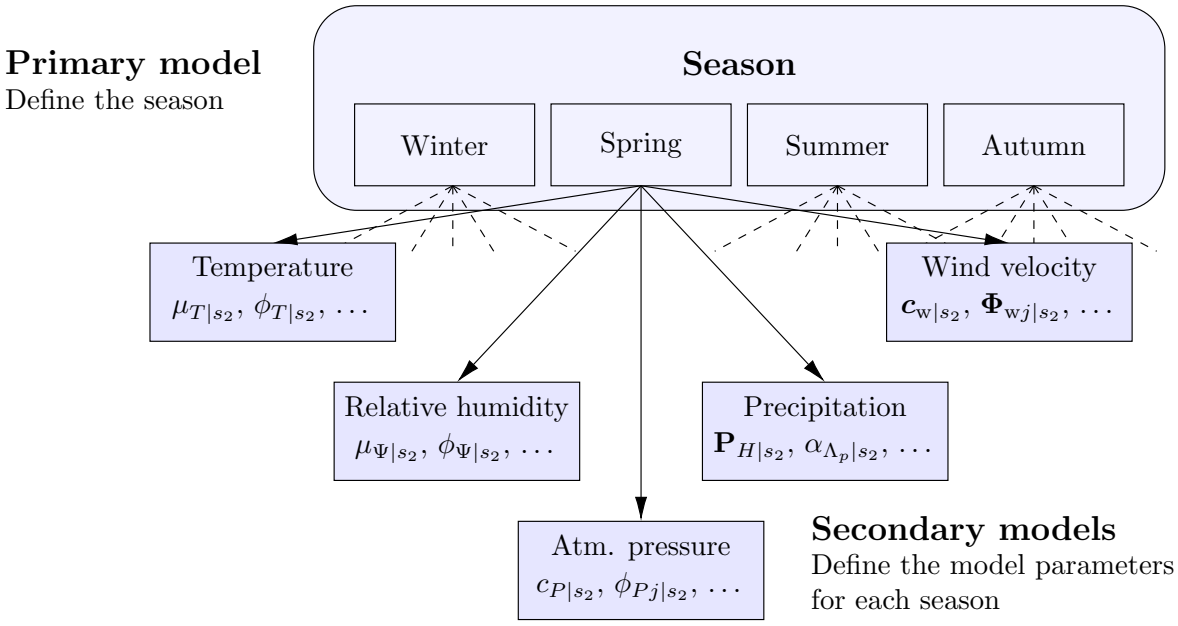

Figure 2.4: The season is the primary weather model. The other parameters are treated as ancillary and inherit their values depending on the season.

From a pure modelling perspective, both ambient temperature and relative humidity exhibit seasonal trends which are deterministic in nature [114, 115]. Therefore, for both physical quantities, a distinction is made between a deterministic component (which tries to capture the diurnal and seasonal trends) and a stochastic one (which replicates the random variations occurring during the day). More specifically, they are described by two sequences $\{T_{\mathrm{air},k}\}_{k\in\mathbb{N}}$, $\{\Psi_{\mathrm{RH},k}\}_{k\in\mathbb{N}}$ assuming values $T^*_{\mathrm{air},k}$ and $\Psi^*_{\mathrm{RH},k}$ in their respective spaces $\mathcal{S}_{T_{\mathrm{air}}}$ and $\mathcal{S}_{\Psi_{\mathrm{RH}}}$. In both cases, the time resolution may be expressed as a fraction of hour $1/K$, with $K \in \mathbb{N}$. Accordingly, the value $k = 1$ refers to the first fraction of the first hour of a first year assumed as a reference. The models are then postulated in the form:

$$T_{\mathrm{air},k} = \bar{T}_k + \tilde{T}_k, \tag{2.22a}$$

$$\Psi_{\mathrm{RH},k} = \bar{\Psi}_k + \tilde{\Psi}_k, \tag{2.22b}$$

in which $\bar{T}$, $\bar{\Psi}$ denote the deterministic trends, and $\tilde{T}$, $\tilde{\Psi}$ capture the residuals [77]. In particular, the deterministic components are modelled as

$$\bar{T}_k = \mu_T + T_{\mathrm{d}} \sin\big(\bar{\omega}_{\mathrm{d}} k + \varphi_{T_{\mathrm{d}}}\big) + T_{\mathrm{y}} \sin\big(\bar{\omega}_{\mathrm{y}} k + \varphi_{T_{\mathrm{y}}}\big), \tag{2.23a}$$

$$\bar{\Psi}_k = \mu_\Psi + \Psi_{\mathrm{d}} \sin\big(\bar{\omega}_{\mathrm{d}} k + \varphi_{\Psi_{\mathrm{d}}}\big) + \Psi_{\mathrm{y}} \sin\big(\bar{\omega}_{\mathrm{y}} k + \varphi_{\Psi_{\mathrm{y}}}\big), \tag{2.23b}$$

where $\bar{\omega}_{\mathrm{d}} = 2\pi/(24 \cdot K)$ and $\omega_{\mathrm{y}} = 2\pi/(24 \cdot 365 \cdot K)$ are the daily and annual frequencies of the periodic signal; the quantities μ_T and μ_Ψ represent the average temperature and humidity

over the year, and the amplitudes T_d, T_y and Ψ_d, Ψ_y model the daily and annual deterministic trends.

On the other hand, a conditional AR(1) process is used to model the stochastic components, i.e.,

$$\tilde{T}_k = \phi_{T|s_i}\tilde{T}_{k-1} + e_{T,k}, \qquad e_{T,k} \mid S = s_i \sim \mathcal{N}\left(0, \sigma^2_{e_T|s_i}\right), \tag{2.24a}$$

$$\tilde{\Psi}_k = \phi_{\Psi|s_i}\tilde{\Psi}_{k-1} + e_{\Psi,k}, \qquad e_{\Psi,k} \mid S = s_i \sim \mathcal{N}\left(0, \sigma^2_{e_\Psi|s_i}\right), \tag{2.24b}$$

where the characteristic parameters are $\phi_{T|s_i}$, $\sigma_{e_T|s_i}$ and $\phi_{\Psi|s_i}$, $\sigma_{e_\Psi|s_i}$ depend explicitly upon the season s_i, $i = 1, 2, 3, 4$, and the process variances may be more conveniently expressed as

$$\sigma^2_{\tilde{T}|s_i} = \frac{\sigma^2_{e_T|s_i}}{1 - \phi^2_{T|s_i}}, \tag{2.25a}$$

$$\sigma^2_{\tilde{\Psi}|s_i} = \frac{\sigma^2_{e_\Psi|s_i}}{1 - \phi^2_{\Psi|s_i}}. \tag{2.25b}$$

Atmospheric pressure

The atmospheric pressure enters directly the definition of the air drag, which opposes the vehicle's longitudinal motion, and also influences the efficiency of the combustion process.

In the sOC, the model for atmospheric pressure is based on that by La Rocca et al. [116] and consists of an ARIMA(p, d, q) process:

$$\phi_{P|s_i}(L)(1 - L)^d P_{\mathrm{air},k} = c_{P|s_i} + \theta_{P|s_i}(L)e_{P,k}, \qquad e_{P,k} \mid S = s_i \sim \mathcal{N}\left(0, \sigma^2_{e_P|s_i}\right), \tag{2.26}$$

where $\phi_{P|s_i}(L)$ is a stable degree p AR lag operator polynomial and $\theta_{P|s_i}(L)$ is an invertible degree q MA operator polynomial. Concerning each season in isolation, the model for atmospheric pressure is fully parametrised by the constant term $c_{P|s_i}$, the autoregressive coefficients $\phi_{Pj|s_i}$, $j = 1, \ldots, p$, the moving average coefficients $\theta_{Pj|s_i}$, $j = 1, \ldots, q$ and the conditional standard deviation $\sigma_{e_P|s_i}$.

Precipitation occurrence and intensity

The intensity of the atmospheric precipitation highly conditions the driver's choice of speed [117, 118], which is clearly reflected in the prime mover operating conditions and, ultimately, in its energy efficiency. Moreover, precipitation accumulated on the ground is responsible for variations in the friction coefficient [119] (usually decreased by the presence of thin layers of water or ice) and rolling resistance, impacting the tyre performance and their ability to produce tractive and braking forces, and exciting the well-known phenomenon of hydroplaning.

According to the sOC representation, the sequence for atmospheric precipitation is modelled in a two-step process [89, 111]. In the first step, the occurrence of the event $\{H_{\mathrm{p},k}\}_{k\in\mathbb{N}}$ is

simulated, and then a suitable probability distribution is used to fit the intensity $\{\Lambda_{\mathrm{p},k}\}_{k\in\mathbb{N}}$, which corresponds to the precipitation amount expressed in millimeters per hour (it assumes value $\lambda_{\mathrm{p},k} \in \mathcal{S}_{\Lambda_\mathrm{p}} \subseteq \mathbb{R}_{>0}$). In particular, the occurrence is modelled by using a Markov chain of fixed interval, similar to what was done in [120, 121]. The stochastic variable $H_{\mathrm{p},k}$ is allowed to take states from the finite space $\mathcal{S}_{H_\mathrm{p}} = \{1, 2\}$, where 1 and 2 correspond to the *dry* and *wet* events. The Markov process for the precipitation is fully characterised by a transition matrix $\mathbf{P}_{H|s_i} \in \mathbb{R}^{2\times 2}_{\geq 0}$. The model for precipitation has only two states, and hence the two following conditions also hold:

$$p_{H12|s_i} = 1 - p_{H11|s_i}, \tag{2.27a}$$
$$p_{H21|s_i} = 1 - p_{H22|s_i}. \tag{2.27b}$$

The transition probabilities $p_{H11|s_i}$ and $p_{H22|s_i}$ may be estimated by counting the number of transitions for the dry and wet events.

For the wet event, the intensity (that is the amount of precipitation per hour) is finally modelled using a Gamma distribution [122, 123]:

$$\Lambda_{\mathrm{p},k|s_i} \sim \mathrm{Ga}\Big(\alpha_{\Lambda_\mathrm{p}|s_i}, \beta_{\Lambda_\mathrm{p}|s_i}\Big). \tag{2.28}$$

Hence, for each season, the precipitation model is fully described by the coefficients $p_{Hij|s_i}$ of the matrix $\mathbf{P}_{H|s_i}$ and the shape and rate parameters $\alpha_{\Lambda_\mathrm{p}|s_i} \in (0, \infty)$ and $\beta_{\Lambda_\mathrm{p}|s_i} \in (0, \infty)$.

Wind speed and direction

Wind speed and direction also enter the definition of the air drag and may favour or oppose the vehicle's motion depending on their relative velocity.

For wind modelling, different approaches have been proposed in the literature, including hybrid and complex multivariate formulations [124, 125]. The main complication when dealing with this parameter is that wind speed and direction often exhibit a strong correlation. Hence, the two signals need to be modelled properly by taking into account their mutual interaction. A natural (and simple) possibility is to resort to a VAR model, which extends the standard notion of an autoregressive series by coupling different random processes. It may be written

$$\mathbf{\Phi}_{\mathrm{w}|s_i}(L)\boldsymbol{Y}_{\mathrm{w},k} = \boldsymbol{c}_{\mathrm{w}|s_i} + \boldsymbol{e}_{\mathrm{w},k}, \tag{2.29}$$

where the vector $\boldsymbol{Y}_{\mathrm{w},k} = [V_{\mathrm{w},k}\ \Theta_{\mathrm{w},k}]^\mathrm{T}$ collects the wind speed $V_{\mathrm{w},k}$ and direction $\Theta_{\mathrm{w},k}$ at each discrete time step k, the parameter $\boldsymbol{c}_{\mathrm{w}|s_i} \in \mathbb{R}^2$ represents a constant offset and $\boldsymbol{e}_{\mathrm{w},k} \in \mathbb{R}^2$ is the vector of normally distributed innovations with covariance matrix given by $\mathbf{\Sigma}_{\boldsymbol{e}_\mathrm{w}|s_i} \in \mathbb{R}^{2\times 2}$. Finally, the matrix operator $\mathbf{\Phi}_{\mathrm{w}|s_i}(L)$ reads

$$\mathbf{\Phi}_{\mathrm{w}|s_i}(L) = \mathbf{I} - \sum_{j=1}^{p} \mathbf{\Phi}_{\mathrm{w}j|s_i} L^j, \tag{2.30}$$

in which every $\mathbf{\Phi}_{\mathrm{w}j|s_i} \in \mathbb{R}^{2\times 2}$ is a matrix of AR coefficients that depend upon the specific season s_i, $i = 1, 2, 3, 4$. An intermediate step is needed for the wind direction, which is a circular variable. This requires the knowledge of the mean wind direction $\mu_{\Theta_{\mathrm{w}}|s_i}$. Further details are given in [126, 127]. To summarise, the wind model is fully described by the average direction $\mu_{\Theta_{\mathrm{w}}|s_i}$, the constant term $\boldsymbol{c}_{\mathrm{w}|s_i}$, the error covariance matrix $\mathbf{\Sigma}_{\boldsymbol{e}_{\mathrm{w}}|s_i}$ and the autoregressive matrices $\mathbf{\Phi}_{\mathrm{w}j|s_i}$, $j = 1, \ldots, p$.

2.2.3 Traffic model

In the sOC representation, the traffic flow is assumed to be stationary on the road section, and thus the unique variable to be considered becomes the density, denoted by ρ_{t}, and expressed as a number of vehicles per unit of distance. Moreover, the parameters for the traffic model are supposed to depend upon both the road type (via the stochastic model for speed signs) and the season. In this context, since the primary models for road type and season are uncorrelated, and each speed sign is associated uniquely to a road type, the total probability for the traffic density model may be calculated considering the conditional probabilities:

$$\begin{aligned}\mathbb{P}(\rho_{\mathrm{t}} \leq \rho^*) = &\sum_{i=1}^{n_r}\sum_{j=1}^{n_{v|r_i}}\sum_{k=1}^{4}\mathbb{P}\big(\rho_{\mathrm{t}} \leq \rho^* \;\big|\; S = s_k \cap R_{\mathrm{t}} = r_i \cap V = v_{j|r_i}\big)\\ &\times \mathbb{P}\big(V = v_{j|r_i} \;\big|\; S = s_k \cap V = v_{j|r_i}\big)\,\mathbb{P}\big(R_{\mathrm{t}} = r_i \mid S = s_k\big)\,\mathbb{P}(S = s_k)\\ = &\sum_{i=1}^{n_r}\sum_{j=1}^{n_{v|r_i}}\sum_{k=1}^{4}\mathbb{P}\big(\rho_{\mathrm{t}} \leq \rho^* \;\big|\; S = s_k \cap V = v_{j|r_i}\big)\pi_{Vj|r_i}\Big(\mathbf{P}_{V|r_i}, \boldsymbol{L}_{V|r_i}\Big)\pi_{Ri}(\mathbf{P}_R, \boldsymbol{L}_R)p_{s_k},\end{aligned} \tag{2.31}$$

where an analytical expression for $\mathbb{P}(\rho_{\mathrm{t}} \leq \rho^* \mid S = s_k \cap V = v_{j|r_i})$ may be deduced starting from the stochastic model described below. A similar formula to that in Eq. (2.31) holds concerning the total expectation. It is worth mentioning that Eq. (2.31) was first derived in Paper B, altough with a different convention for the notation.

Traffic density

Especially in highly-congested scenarios, road traffic excites frequent fluctuations in the driver's choice of speed. As a consequence, the prime mover becomes subjected to transient dynamics and operates in suboptimal conditions. From the perspective of energy efficiency, detailed modelling of the interaction between individual vehicles is not usually required, whereas a macroscopic approach is sufficient [35].

In this context, the stocastic model for traffic density discussed in this thesis is based on that presented in Paper A, and was validated using data collected from the Trafikverket[7].

[7] Available from: https://vtf.trafikverket.se/SeTrafikinformation.

For each road segment, the traffic density is specifically modelled as a sequence $\{\rho_{\mathrm{t},k}\}_{k\in\mathbb{N}}$ assuming values $\rho^*_{\mathrm{t},k} \in \mathcal{S}_{\rho_\mathrm{t}}$, and is expressed as the sum of a deterministic and stochastic component as follows:

$$\rho_{\mathrm{t},k} = \bar{\rho}_k + \tilde{\rho}_k, \tag{2.32}$$

with

$$\bar{\rho}_k = \mu_{\rho|v_{j|r_l}\cap s_i} + \rho_{\mathrm{d}|v_{j|r_l}\cap s_i} \sin\Big(\bar{\omega}_\mathrm{d} k + \varphi_{\rho_\mathrm{d}|v_{j|r_l}\cap s_i}\Big), \tag{2.33a}$$

$$\tilde{\rho}_k = \phi_{\rho|v_{j|r_l}\cap s_i}\tilde{\rho}_{k-1} + e_{\rho,k}, \quad e_{\rho,k} \mid V = v_{j|r_l} \cap S = s_i \sim \mathcal{N}\Big(0, \sigma^2_{e_\rho|v_{j|r_l}\cap s_i}\Big). \tag{2.33b}$$

In (2.33), $\mu_{\rho|v_{j|r_l}\cap s_i}$ is the average density on a specific road segment during the season, $\rho_{\mathrm{d}|v_{j|r_l}\cap s_i}$ is the amplitude of the daily variation, $\bar{\omega}_\mathrm{d}$ is again the the daily frequency, $\varphi_{\rho_\mathrm{d}|v_{j|r_l}\cap s_i}$ the initial phase. It should be noted that, as opposed to the models for the air temperature and humidity, the deterministic parameters in this case depend explicitly upon the combination speed signs/seasonal setting. Thus, in the sOC description, the traffic density is parametrised by the deterministic quantities $\mu_{\rho|v_{j|r_l}\cap s_i}$, $\rho_{\mathrm{d}|v_{j|r_l}\cap s_i}$, $\varphi_{\rho_\mathrm{d}|v_{j|r_l}\cap s_i}$ and the conditional stochastic coefficients $\phi_{\rho|v_{j|r_l}\cap s_i}$, $\sigma_{e_\rho|v_{j|r_l}\cap s_i}$. As usual, the conditional error variance $\sigma^2_{e_\rho|v_{j|r_l}\cap s_i}$ may be rewritten in terms of the process variance as

$$\sigma^2_{\tilde{\rho}|v_{j|r_l}\cap s_i} = \frac{\sigma^2_{e_\rho|v_{j|r_l}\cap s_i}}{1-\phi^2_{\rho|v_{j|r_l}\cap s_i}}, \tag{2.34}$$

which, for a given combination speed sign/season, actually represents the variance of the stochastic component of the traffic density, i.e., $\tilde{\rho} \mid V = v_{j|r_l} \cap S = s_i \sim \mathcal{N}(0, \sigma^2_{\tilde{\rho}|v_{j|r_l}\cap s_i})$.

2.2.4 Mission model

The mission category does not distinguish between primary and secondary models. Moreover, only a stochastic formulation to capture variations in cargo weight is currently implemented in the format.

Cargo weight and standstill time

The cargo weight is regarded as piecewise constant, right-side continuous functions of the position. Specifically, it is treated as a random process $W = W(x)$ along with the position on the road. The entire process is then split into four parts and modelled as a sequence of positions where the payload changes value, stop (or standstill) times, operating states, and cargo weights $\{X_k, T_k, \Xi_k, W_k\}_{k\in\mathbb{N}}$.

In paricular, the sequence of operating states is supposed to behave as a Markov chain, and hence is completely characterised by the Markov probability matrix $\mathbf{P}_\Xi \in \mathbb{R}^{n_\xi\times n_\xi}_{\geq 0}$. Again, an entry $p_{\Xi ij}$ encodes the conditional probability of transitioning from state i to state j and satisfies $\sum_{j=1}^{n_\xi} p_{\Xi ij} = 1$, $p_{\Xi ii} = 0$, $i = 1, \ldots, n_\xi$.

The locations where the vehicle changes its operating state, and accordingly also the transported cargo weight, are then modelled using a Poisson process. Each state ξ_i, $i = 1, \dots, n_\xi$, has therefore its own intensity $\lambda_{\Xi 1}$, which may be deduced directly from the mean distance $L_{\xi i}$ over which the vehicle operates in state ξ_i:

$$\lambda_{\Xi i} = \frac{1}{L_{\Xi i}}. \tag{2.35}$$

The n_ξ mean distances $L_{\Xi i}$ may be organised into a vector $\boldsymbol{L}_\Xi = [L_{\Xi 1} \ \dots \ L_{\Xi n_\xi}]^{\mathrm{T}}$. As usual, the stationary distribution $\boldsymbol{\pi}_\Xi$ of the overall process may be derived starting from the knowledge of the generator matrix $\mathbf{G}_\Xi$, and satisfies the equation

$$\boldsymbol{\pi}_\Xi \mathbf{G}_\Xi = \mathbf{0}, \tag{2.36}$$

where the entries $g_{\Xi ij} = g_{\Xi ij}(p_{\Xi ij}, L_\Xi)$ of $\mathbf{G}_\Xi$ are given by

$$g_{\Xi ij}\big(p_{\Xi ij}, L_{\Xi i}\big) = \begin{cases} \lambda_{\Xi i} p_{\Xi ij} = \dfrac{p_{\Xi ij}}{L_{\Xi i}}, & i \neq j, \\ -\lambda_{\Xi i} = -\dfrac{1}{L_{\Xi i}}, & i = j. \end{cases} \tag{2.37}$$

Combined together, Eqs. (2.36) and (2.37) allow estimating the average normalised distance covered by the vehicle in each operating state.

For the sake of conveniency, the stop time T_k is instead modelled using a Gamma distribution, i.e., $T_k \sim \mathrm{Ga}(\alpha_T, \beta_T)$. It is worth observing that, according to the proposed formulation, the stop time does not depend explicitly upon the specific operating state.

The cargo weight, conditioned to each operating state, is finally modelled using a normal distribution, restricted between zero and a maximum value $w_{\max|\xi_i}$. The limits $w_{\max|\xi_i}$ are prescribed in order to ensure compliance with legislation, and may depend specifically upon the state (for example, the allowed maximum payload may be higher when the trailer is connected). The equations are specifically as follows:

$$W_k = \min\Big(\max\big(0, W'_k \mid \Xi_k = \xi_i\big), w_{\max|\xi_i}\Big), \tag{2.38}$$

and

$$W'_k \mid \Xi_k = \xi_i \sim \mathcal{N}\Big(\mu_{W|\xi_i}, \sigma^2_{W|\xi_i}\Big). \tag{2.39}$$

To summarise, the complete description consists of the transition probabilities $p_{\Xi ij}$, the mean lengths $L_{\Xi i}$ (or, alternatively, the intensities $\lambda_{\Xi i}$), the conditional means $\mu_{W|\xi_i}$, variances $\sigma_{w|\xi_i}$, and maximum values $w_{\max|\xi_i}$, $i, j = 1, \dots, n_\xi$.

It is worth pointing out that, if all the operating states are characterised by the same intensity $\lambda_\Xi \equiv \lambda_{\xi i} = 1/L_{\Xi i} \equiv 1/L_\Xi$, the the distance covered between two generic mission stops follows the same exponential distribution $\mathcal{E}(\lambda_\Xi)$. This introduces some freedom in the mathematical definition of the notion of a road transport mission. Indeed, if the distance

travelled during every operation of pick-up/delivery is exponentially distributed with the same parameter, the length duration of any sequence of n pick-ups/deliveries becomes a Gamma random variable of the type $\mathrm{Ga}(n, \lambda_{\Xi})$. This means that, if the same intensity parameter λ_{Ξ} is used for each state ξ_i, $i = 1, \ldots, \xi_i$, a road transport mission may be defined as a generic sequence of pick-up/delivery tasks to be executed along the road.

The stochastic models for road, weather, traffic and mission are finally summarised in Table 2.1.

2.2.5 Addressing the variation over transport applications

Before concluding the presentation of the stochastic models, it is worth remarking that those falling in the road and mission categories may be (and usually are) parametrised concerning individual operations. As an example, considering the standard deviation $\sigma_{Y|r_i}$, $i = 1, \ldots, n_r$, of the topography model, a single transport mission may be statistically represented using a number of different values corresponding to that of the road types. However, these values may in turn vary over the population of missions that describe an entire transport application. As a result, the standard deviations $\sigma_{Y|r_i}$, $i = 1, \ldots, n_r$, may be regarded as stochastic variables. In Fig. 2.5, the lognormal distributions fitted in Paper C for the conditional standard deviations of the topography model are shown, assuming three different road types (urban, rural, highway). Similar distributions may be generated for all the road parameters described in the preceding sections, as discussed more exhaustively in Paper C, as well as for those falling in the mission category[8].

On the other hand, since the weather and traffic models are usually parametrised by clustering and averaging data collected for a certain geographical region, a single set of values for the sOC parameters may be generally sufficient to characterise a transport application. Alternatively, if the individual missions span multiple areas, then the corresponding application may be characterised by considering the proportions in which the vehicle is operated in each locality[9].

Finally, it should also be observed that, if the sOC parameters are treated as stochastic variables considering a population of road operations, the probabilities and expectations calculated using Eqs. (2.8) and (2.31) become generally functions of stochastic variables, and hence stochastic variables themselves. This aspect plays a crucial role in addressing the classification problem when it comes to entire transport applications, as better explained in the subsequent Sect. 2.4.1 and also in Chap. 3.

[8] In this context, it should be however mentioned that, in Paper E, the stochastic model for cargo weight was parametrised concerning the whole transport application.

[9] In the same context, it should be observed that the different treatment reserved to the road models from the one hand, and to the weather and traffic models on the other one is legitimated by the modalities with which the models themselves are parametrised. This aspect will be clarified later on in Chap. 4.

Table 2.1: Summary of sOC models.

Model	Category	Model type	Number of states	Number of conditional parameters
Road type	Road	Markov process	n_r	n_r^2
Stop signs	Road	Marked Poisson	Continuous	3
Give way signs	Road	Marked Poisson	Continuous	5
Traffic lights	Road	Marked Poisson	Continuous	5
Speed bumps	Road	Marked Poisson	Continuous	3
Speed signs	Road	Markov process	n_v	$n_{v\|r_k}^2$
Topography	Road	Gaussian AR(1)	Continuous	2
Curviness	Road	Marked Poisson	Continuous	6
Road roughness	Road	Laplace AR(1)	Continuous	2
Temperature	Weather	Deterministic Gaussian AR(1)	Continuous Continuous	5 2
Relative humidity	Weather	Deterministic Gaussian AR(1)	Continuous Continuous	5 2
Atmospheric pressure	Weather	Gaussian ARIMA(p, d, q)	Continuous	$2 + p + q$
Precipitation	Weather	Markov process Gamma distributed	2 –	4 2
Wind speed and direction	Weather	Gaussain VAR(p)	Continuous	$6 + 4p$
Traffic density	Traffic	Deterministic Gaussian AR(1)	Continuous Continuous	5 2
Cargo weight	Mission	Markov process	n_ξ	$n_\xi(n_\xi + 3) + 2$

2.3 The deterministic operating cycle

Compared to the first two types of representation already discussed, the deterministic operating cycle (dOC) describes the mission and the external environment with higher accuracy. The dOC is the most adequate way of modelling an operating cycle when it comes to simulation,

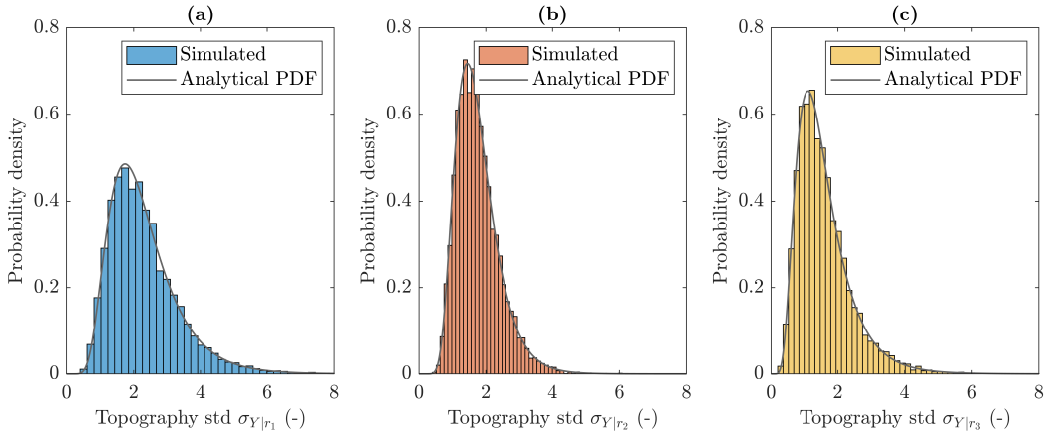

Figure 2.5: Comparison between the measured and fitted lognormal distribution for the conditional standard deviations ($n_r = 3$) of the topography model, concerning the Västra Götaland operating cycle: **(a)** urban; **(b)** rural; **(c)** highway.

and tries to address the representation problem. The central idea is that it may serve as a virtual environment for realistic prediction of the performance of road vehicles, virtual testing and design of control algorithms and development of *ad-hoc* functions.

In the dOC, the same four different categories defined for the bird's-eye view and sOC, namely the road, traffic, weather and mission, are kept. For each of them, a different set of parameters is used. These correspond to the physical quantities which were regarded as *models* in the sOC representation[10], and are defined as discrete functions of time and position. Some parameters are only made dependent on either the position or the time, some others, like the ones marked in the traffic category, depend on both. Additionally, each parameter may be represented by a scalar or a vector-valued signal (see dimensionality in Table 2.2). Any value in between two different discrete times (or positions) may be computed by interpolation using the corresponding model in Table 2.2. For the motivation behind the choice of the specific interpolation strategy for each individual parameter, the reader is referred to [75]. To formalise the dOC format mathematically, the four categories (see Table 2.2) may be defined as the sets containing the parameter sequences: $\mathcal{R}_\mathrm{d}$ is the set containing all sequences labelled as road, $\mathcal{W}_\mathrm{d}$ for weather, $\mathcal{T}_\mathrm{d}$ for traffic, and $\mathcal{M}_\mathrm{d}$ for mission. Then, the dOC format may be defined mathematically as the collection of sets:

$$\mathcal{OC}_\mathrm{d} = \{\mathcal{R}_\mathrm{d}, \mathcal{W}_\mathrm{d}, \mathcal{T}_\mathrm{d}, \mathcal{M}_\mathrm{d}\}, \tag{2.40}$$

where the subscript $(\cdot)_\mathrm{d}$ stands this time for *deterministic*. Interpolation may be then defined as an operator I_dyn acting on the elements in the sets (see Appendix A). However, Eq. (2.40) is only an elegant formalism: it describes the dOC as an algebraic structure, but does not

[10]The relationship between the role of a physical quantity in the sOC and dOC representations is perhaps better understood from Table 2.2, where each entity is labelled under *model* for the sOC and *parameter* for the dOC.

Table 2.2: Stochastic (secondary) models (sOC) and deterministic parameters (dOC parameters) for the sOC and dOC representations. *Linear* and *constant* refer to linear and right-side continuous piecewise constant interpolation models, respectively. The mathematical model of *Dirac delta* occurs when the parameter is regarded as an isolated *event*.

sOC model or dOC parameter	**Category**	**Type**	**Interpolation model**	**Dim**	**Quantity**
Speed signs	Road	Function	Constant	1	Speed limit
Altitude	Road	Function	Linear	1	Vertical coordinate
Curvature	Road	Function	Linear	1	Curvature
Ground type	Road	Function	Constant	2	Surface type, cone index
Roughness	Road	Function	Constant	2	Waviness, roughness coeff.
Stop signs	Road	Event	Dirac delta	1	Standstill time
Traffic lights	Road	Event	Dirac delta	1	Standstill time
Give way signs	Road	Event	Dirac delta	1	Standstill time
Speed bumps	Road	Event	Dirac delta	3	Length, height angle of approach
Longitude	Road	Function	Linear	1	WGS84 longitude
Latitude	Road	Function	Linear	1	WGS84 latitude
Ambient temperature	Weather	Function	Linear	1	Temperature
Atmospheric pressure	Weather	Function	Linear	1	Pressure
Precipitation	Weather	Function	Constant	1	Precipitation amount
Wind velocity	Weather	Function	Constant	2	Velocity vector
Relative humidity	Weather	Function	Linear	1	Humidity
Traffic density	Traffic	Function	Constant	1	Density
Mission stops	Mission	Event	Dirac delta	1	Standstill time
Cargo weight	Mission	Function, event	Linear, constant	1	Payload
Power take-off	Mission	Function	Linear	1	Output power
Charging power	Mission	Function	Constant	1	Input power
Travel direction	Mission	Function	Constant	1	Driving direction

bring much more information about it. The deterministic parameters are simply defined on different spaces, where the relative interpolation operators are allowed to act.

The dOC format provides a detailed view on individual transport operations without making any assumptions about the driver or the vehicle. Furthermore, it is built in a modular way such that parameters may be easily modified, added or removed. To be useful in simulation, the dOC format must be integrated with suitable dynamic models for the vehicle and driver. In the context of this thesis work, and also concerning the attached papers, this has been done by resorting to the VehProp environment, which is an open platform. A detailed description of VehProp is beyond the scope of the present chapter, and is reported in Appendix A. Here, it might be beneficial to briefly comment on how the dOC parameters may be used in practice to reflect variation in usage. A straightforward way to consider the

influence of the different physical entities listed in Table 2.2 is to use an interpretative driver model, which reacts to the external stimuli and sets its reference speed accordingly. For example, the driver may choose to decelerate just before negotiating a curve, based on some comfort threshold on the lateral acceleration (for instance, using a similar relationship to that in Eq. (A.2)); similarly, the cruising speed may be adjusted depending on the traffic density (via, e.g., Eq. (A.4)). This idea, borrowed from [128, 129], has been refined once again by Pettersson [18]. In this context, the complete set of functions currently used to feed the driver model is listed, e.g., in [18] and Paper A, and not reported here for brevity.

2.4 Relationships between the representations

The three levels of representation discussed so far are intrinsically related, and ordered in a pyramidal structure, as shown graphically in Fig. 2.1.

2.4.1 Relationship between the bird's-eye view and the sOC

The first connection which should be explored is that between the bird's-eye view and sOC descriptions. These are both statistical in nature, but with considerably different resolutions. Indeed, whilst the bird's-eye view generally encompasses an entire transport application (but might also be used to classify single operations and even road sections), the sOC mainly targets individual missions. Furthermore, given an sOC, the corresponding bird's-eye view classes may always be deduced uniquely. The inverse operation is not possible since, for a predetermined bird's-eye view class, infinitely many sOCs may exist. This non-bijective nature of the relationship between the sOC and bird's-eye view description is rather typical of the OC format, and persists also at the lower level, in the connection between the sOC and the dOC.

To elucidate the natural relationship between the bird's-eye view and sOC representations, an illustrative example may be adduced concerning the stochastic model for road topography introduced in Sect. 2.2.1, in conjunction with the corresponding bird's-eye view classes prescribed according to the GTA and UFD descriptions. In this context, it is interesting to observe that the criteria specified by both the GTA and UFD systems in Sect. 2.1 may be reformulated in terms of a probability, that is mathematically as $p_{y,\min} < \mathbb{P}(|Y| \leq y) \leq p_{y,\max}$, where y is a limit on the road grade and $p_{y,\min}$ and $p_{y,\max}$ a minimum and maximum threshold targeting the driving distance, expressed as a percentage of the total. In particular, the GTA description sets $y = 3, 6, 9$ and imposes constant limits $p_{y,\min} = 0.98$, $p_{y,\max} = 1$ on the distance, whereas the UFD representation prescribes identically $y = 2$ and considers two different values for $p_{y,\min} = 0.8, 0.6$, respectively, whilst keeping a constant $p_{y,\max} = 1$. Starting with the model presented in Sect. 2.2.1, it may be first noticed that Eq. (2.9) and (2.10) imply that, for a given road mission and on each road type, the road grade itself is

normally distributed, i.e.,

$$Y \mid R_{\mathrm{t}} = r_i \sim \mathcal{N}\Big(0, \sigma^2_{Y|r_i}\Big). \tag{2.41}$$

Since

$$\mathbb{P}\big(|Y| \leq y \;\big|\; R_{\mathrm{t}} = r_i\big) = 2\Phi\left(\frac{y}{\sigma_{Y|r_i}}\right) - 1, \tag{2.42}$$

being $\Phi(\cdot)$ the CDF of the normal distribution, with the aid of Eq. (2.8a), the total probability $p_y(y, \boldsymbol{\sigma}_Y, \mathbf{P}_R, \boldsymbol{L}_R) \triangleq \mathbb{P}\big(|Y| \leq y\big)$ may be calculated as follows:

$$\begin{aligned} p_y(y, \boldsymbol{\sigma}_Y, \mathbf{P}_R, \boldsymbol{L}_R) = \mathbb{P}\big(|Y| \leq y\big) &= \sum_{i=1}^{n_r} \mathbb{P}\big(|Y| \leq y \;\big|\; R_{\mathrm{t}} = r_i\big)\, \mathbb{P}(R_{\mathrm{t}} = r_i) \\ &= \sum_{i=1}^{n_r} \left[2\Phi\left(\frac{y}{\sigma_{Y|r_i}}\right) - 1\right] \pi_{Ri}(\mathbf{P}_R, \boldsymbol{L}_R), \end{aligned} \tag{2.43}$$

where the vector $\boldsymbol{\sigma}_Y$ has been defined collecting the conditional standard deviations for each road type, i.e., $\boldsymbol{\sigma}_Y \triangleq [\sigma_{Y|r_1} \;\; \dots \;\; \sigma_{Y|r_{n_r}}]^{\mathrm{T}}$. Hence, a class for the topography may be specified by considering the inequality

$$p_{y,\min} < p_y(y, \boldsymbol{\sigma}_Y, \mathbf{P}_R, \boldsymbol{L}_R) \leq p_{y,\max}, \tag{2.44}$$

for appropriate values of y and $p_{y,\min}$, and $p_{y,\max}$. The expression in Eq. (2.44) relates the set of sOC parameters for topography and road types to the bird's-eye view thresholds y and $p_{y,\min}$. Such a relationship describes an *operating class*, that is, a mathematical formalism that allows to classify an individual transport mission concerning a certain physical quantity. More generally, the notion of an operating class has been coined in Paper B, where expressions similar to that in Eq. (2.44) have been derived for the vast majority of the models discussed in Sect. 2.1. In the present thesis, a comprehensive theory for the operating classes is better established in Chap. 3.

Moreover, if a single road type is considered, and hence $\sigma_{Y|r_1} \equiv \sigma_Y$, the variance is sufficient to completely characterise an operating class according to the topography parameter. The ranges for σ_Y corresponding to the different topography classes are listed in Table 2.3 for both the GTA and UFD classification systems.

By exploiting the natural connection existing between the bird's-eye view and sOC representations, the non-trivial operation of classifying a road transport mission may be carried out directly in terms of sOC parameters. The obvious advantage is that they are easily quantifyiable and interpretable compared to the vague measures specified by already-existing descriptions like the GTA and UFD. However, relationships similar to that in Eq. (2.44) may only be used to categorise an individual road operation. In fact, when considering an entire transport application, the sOC parameters may be generally allowed to vary over the population of missions, and should thus be regarded as random variables. Expanding upon

Class	GTA system	UFD system
FLAT	$\sigma_Y < 1.29$	$\sigma_Y < 1.56$
P-FLAT	$1.29 \leq \sigma_Y < 2.58$	-
HILLY	$2.58 \leq \sigma_Y < 3.87$	$1.56 \leq \sigma_Y \leq 2.38$
V-HILLY	$3.87 \leq \sigma_Y$	$2.38 < \sigma_Y$

Table 2.3: Topography classes according to the GTA and UFD classification systems with the corresponding intervals for the standard deviation σ_Y.

the discussion initiated in Sect. (2.2.5), the probabilities calculated according to Eqs. (2.42) and (2.43) also become (composite) random variables, and hence the inequality in Eq. (2.44) cannot be employed directly to characterise the usage from a bird's-eye view perspective. In this case, a reasonable choice would be to compute the expectation of Eq. (2.43) (or considering any other representative functional) over the population of missions encompassing the application. When interpreted as a random variable, the probability appearing in Eq. (2.43) is sometimes referred to as *road grade length ratio* (Paper C). The discussion above is propaedeutic to the additional results reported in the subsequent Chap. 3, which summarises some of the findings of Papers B and C.

2.4.2 Relationship between the sOC and the dOC

The level of formality required to illustrate the connection between the sOC and the dOC is much lower compared to the previous case. Generally speaking, starting from a dOC, it is possible to estimate the corresponding stochastic parameters and hence obtain an equivalent description in terms of an sOC. This is usually done by resorting to elementary statistical methods and assuming plausible probability distributions and stochastic models, similar to those already detailed in Sect. 2.2. On the other hand, given a set of stochastic parameters, a dOC may be interpreted as a single realisation of an sOC. Indeed, by simulating its stochastic models, a fully parametrised sOC may be used to synthesise multiple dOCs. Figure 2.6 is a schematic illustration of the typical workflow needed to synthesise a reference dOC, starting from an equivalent sOC. First, the primary models are generated over a specific mission distance, which may either be prescribed or simulated using an opportune distribution (see, e.g., Paper C). For each season, the starting time (day and hour) may also be generated randomly or specified by the user. Another input to the process is the number of days. This then simulates the weather and traffic time series over a finite horizon. The time resolution for this operation is the same as the one used to parametrise each sOC model. The primary models are also simulated simultaneously, since they do not interact explicitly. It is worth mentioning that, whilst the overall road consists of a sequence of road types, the season may be fairly assumed to be constant over the mission. Both models are simulated depending on their stationary distribution, which is trivial for the weather category. The secondary sOC

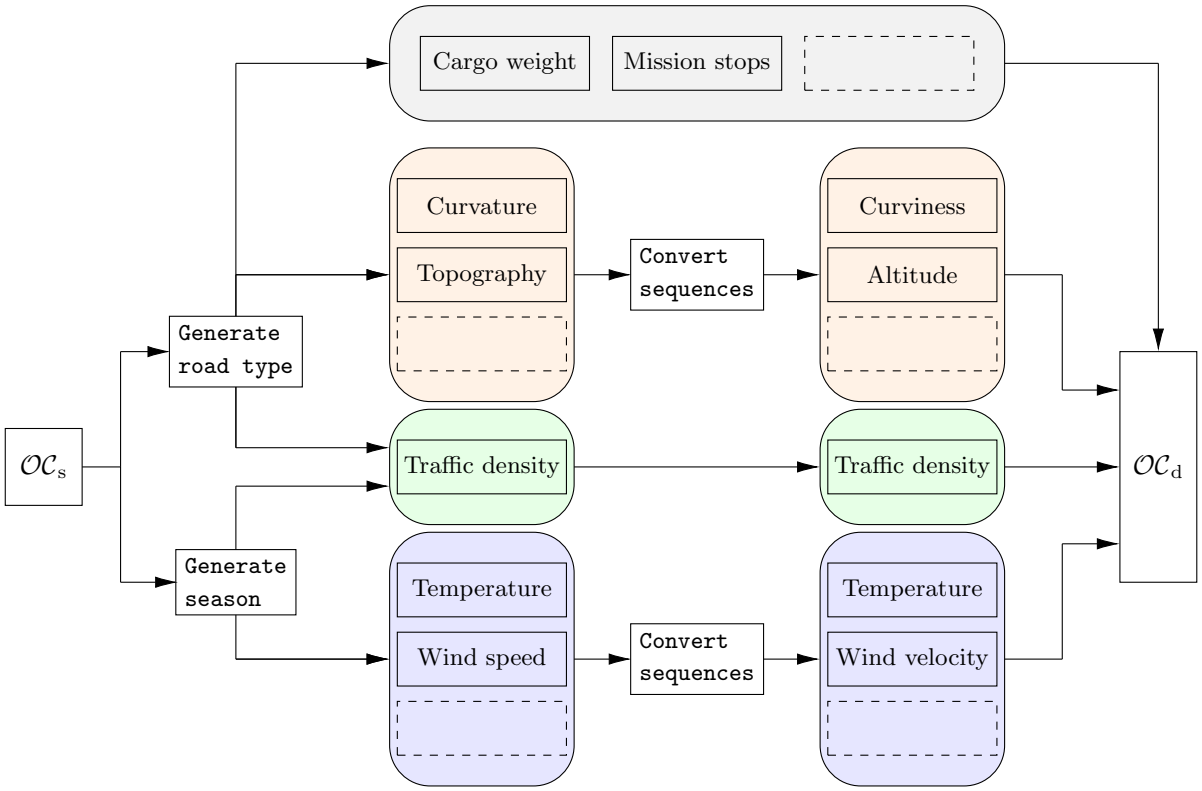

Figure 2.6: Generation process of a deterministic operating cycle (dOC) from a stochastic one (sOC). Whilst the mission category may be assigned *a priori*, all the other models should be generated stochastically. A conversion is needed between the sOC and dOC formalisms. Figure adapted from Papers A and C.

models are then derived from the primary ones. Quantities such as topography and curvature depend only on the road type. On the other hand, weather parameters like temperature, wind speed and direction are only affected by the season in the sOC description. The traffic time series may be only produced when the road has been completely modelled and the season determined. For the secondary models, the simulation of road properties may be carried out using the *ad-hoc* WAFO package implemented in MATLAB® [130, 131], whilst the weather models using a standard Toolbox. The sequences obtained using this procedure need to be converted into the dOC formalism. For example, curvature and topography are translated into curviness and altitude[11]; similarly, wind speed (in magnitude) and direction are instead reformulated in terms of a velocity vector, where the components are specified. Furthermore, wind speed is usually measured at weather stations at approximately 10 m

[11]The sequence $\{z_k\}_{k\in\mathbb{N}}$ is constructed according to $z_{k+1} = z_k + \frac{y_k}{100} L_\mathrm{s} = \sum_{i=0}^{k} y_i + z_0$, being $\{y_k\}_{k\in\mathbb{N}}$ the sequence of realisations for the variable Y_k describing the road grade.

above the ground. Therefore, the value must be converted to ground level[12]. From the signed curvature, the actual road profile and the tangent vector to the trajectory are also deduced numerically using Fresnel integrals. This step is crucial since it allows computation of the relative direction between the vehicle and wind velocity vector. The dOC parameters, plus their location in either space or time (or both for the traffic density), are finally encoded in the dOC description and tabulated.

Concerning the stochastic models for weather and traffic detailed in Sects. 2.2.2 and 2.2.3, an example of generated timeseries (before conversion to the dOC formalisms) is illustrated in Fig. 2.7, considering a time horizon of ten days. The values for the sOC parameters used to generate the plots in Fig. 2.7 coincide with those listed in Paper A. Some realisations for the road models are instead given in [18] for different combinations of sOC parameters, and are not reported here for brevity.

To conclude, it should be emphasised that dOCs originating from the same sOC would eventually be equivalent in a statistical sense but might differ significantly in practice. As for the relationship between the bird's-eye view and the sOC representations, this also implies that the mapping between an sOC and a dOC is not necessarily bijective; quite the opposite. In this context, it should be also mentioned that there is no guarantee that an individual dOC will be realistic. Since the secondary stochastic models are simulated simultaneously, and no explicit interaction is taken into account, it may happen, for instance, that a sharp curve is generated in close proximity to a speed sign marking the transition to a higher speed limit. However, it may be reasonably conjectured that the effect of these unlikely combinations on the vehicle's performance would be eventually filtered out by simulating a large number of dOCs synthesised from the same set of sOC parameters.

[12]For example, using the logarithmic speed profile ([132]).

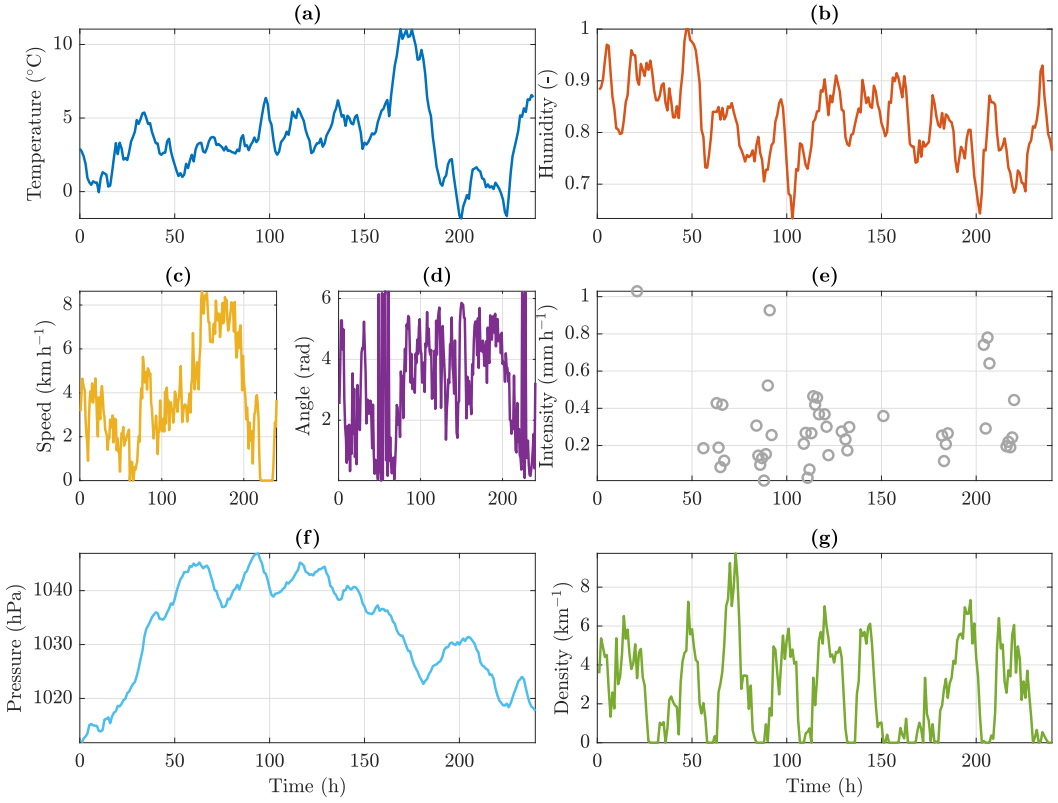

Figure 2.7: Stochastically generated timeseries for the weather and traffic models presented in Sects. 2.2.2 and 2.2.3, over a time horizon of ten days: **(a)** ambient temperature; **(b)** relative humidity; **(c)** and **(d)** wind speed and direction; **(e)** precipitation intensity; **(f)** atmospheric pressure; **(g)** traffic density. Figure adapted from Paper A.

Chapter 3

Operating classes and composite variables

The natural relationship existing between the bird's-eye view and sOC representations may be formulated mathematically by introducing the notion of an operating class, as already anticipated in Sect. 2.4.1. In turn, this formalism offers an indispensable opportunity to address the classification problem indicated by Pettersson [18]. Building upon the findings of Papers B and C, the aim of this chapter is therefore to explore in greater detail the connection between the two above-mentioned levels of representation, and, in doing so, derive the mathematical relationships for the other operating classes presented in the GTA and UFD codifications. This operation may be conducted systematically considering either individual road missions or entire applications. In the latter case, it is necessary to resort to a similar approach to that discussed in Sect. 2.2.5. The analysis proposed in the present chapter is finally concluded by suggesting a possible strategy to optimally specify the thresholds and limits of the bird's-eye view description, following the approach proposed in Paper D.

3.1 Operating classes

The definition of the bird's-eye view metrics and sOC parameters according to Eqs. (2.1) and (2.2), respectively, is not merely a sterile formalism. Indeed, mutual relationships between the elements in the sets $\mathcal{OC}_\mathrm{b}$ and $\mathcal{OC}_\mathrm{s}$ may be deduced by combining an opportunely defined system of classes (for example, according to the GTA and UFD descriptions) with the stochastic models presented in Chap. 2.

More precisely, it has been shown in Paper B that, for a generic model ξ in the road,

weather, and traffic categories, a relationship exists in the form[1]

$$\boldsymbol{a}_{\xi}(\boldsymbol{\eta}_{\mathrm{b},\xi}) < \boldsymbol{\Upsilon}_{\xi}(\boldsymbol{\eta}_{\mathrm{s}}, \boldsymbol{\eta}_{\mathrm{b}}) \leq \boldsymbol{b}_{\xi}(\boldsymbol{\eta}_{\mathrm{b},\xi}), \tag{3.1}$$

where $\xi \in \mathcal{X}_{\mathcal{R}}$, $\mathcal{X}_{\mathcal{W}}$ or $\mathcal{X}_{\mathcal{T}}$ is a generic sOC model, $\mathcal{X}_{\mathcal{R}}$, $\mathcal{X}_{\mathcal{W}}$, and $\mathcal{X}_{\mathcal{T}}$ denote the sets of sOC models for the road, weather, and traffic categories, respectively, $\boldsymbol{\eta}_{\mathrm{s},\xi} \in \mathcal{R}_{\mathrm{s},\xi}$, $\mathcal{W}_{\mathrm{s},\xi}$, $\mathcal{T}_{\mathrm{s},\xi}$ and $\boldsymbol{\eta}_{\mathrm{b},\xi} \in \mathcal{R}_{\mathrm{b},\xi}$, $\mathcal{W}_{\mathrm{b},\xi}$, $\mathcal{T}_{\mathrm{b},\xi}$ are vectors of sOC parameters and bird's-eye-view metrics for the model ξ, $\boldsymbol{\eta}_{\mathrm{s}} \in \mathcal{OC}_{\mathrm{s}}$, $\boldsymbol{\eta}_{\mathrm{b}} \in \mathcal{OC}_{\mathrm{b}}$ are generic vectors of sOC parameters and bird's-eye view metrics, $\mathcal{R}_{\mathrm{s},\xi} \subset \mathcal{R}_{\mathrm{s}}$, $\mathcal{W}_{\mathrm{s},\xi} \subset \mathcal{W}_{\mathrm{s}}$, $\mathcal{T}_{\mathrm{s},\xi} \subset \mathcal{T}_{\mathrm{s}}$ are subsets of sOC parameters for the model ξ, and $\mathcal{R}_{\mathrm{b},\xi} \subset \mathcal{R}_{\mathrm{b}}$, $\mathcal{W}_{\mathrm{b},\xi} \subset \mathcal{W}_{\mathrm{b}}$, $\mathcal{T}_{\mathrm{b},\xi} \subset \mathcal{T}_{\mathrm{b}}$ are subset of bird's-eye-view metrics for the model ξ.

Finally, $\boldsymbol{a}_{\xi}(\boldsymbol{\eta}_{\mathrm{b},\xi})$ and $\boldsymbol{b}_{\xi}(\boldsymbol{\eta}_{\mathrm{b},\xi})$ represent lower and upper bounds for the vector-valued function $\boldsymbol{\Upsilon}_{\xi}(\cdot,\cdot)$ appearing in (3.1). In this context, it should be clarified that the inequalities (3.1) need to be interpreted element-wise. As briefly mentioned in Sect. 2.4.1, they postulate the existence of certain relationships which mathematically formalise the so-called operating classes. For example, it may be noticed that the inequality in Eq. (2.44) has the same form of that in Eq. (3.1), being moreover scalar.

Concerning the stochastic models detailed in Chap. 2, the complete derivation for the expressions describing the corresponding operating classes has been carried out in Paper B and, for the sake of brevity, is not repeated in this thesis. Instead, the analytical formulae are presented and explained in the following with emphasis on their physical interpretation. It should be noticed that the expressions reported in this chapter are less general than those obtained in Paper B. Moreover, although in paper B the attention was restricted to the road, weather and traffic categories, relationships formally equivalent to that in Eq. (3.1) may be derived concerning the mission models.

3.1.1 Road category

The bird's-eye view descriptions corresponding to the GTA and UFD systems specify relationships for the operating classes concerning the models for topography, curviness, speed bumps and stop signs, road roughness, and speed signs.

Road topography

The analytical expression describing the operating class for the topography parameter is the same according to both the GTA and UFD classification systems, and reads specifically

$$p_{y,\min} < p_{y}(y, \boldsymbol{\sigma}_{Y}, \mathbf{P}_{R}, \boldsymbol{L}_{R}) \leq p_{y,\max}, \tag{3.2}$$

[1] In Paper B, it was asserted that the set of sOC parameters for a given model, in a given OC category, is only related to the corresponding bird's-eye view metrics for the same model. This is true in the context of Paper B, where the relationship for the operating classes were derived concerning individual road segments. However, when considering individual missions and entire transport applications, the same result does not hold, since the stationary distributions for road type enter the definition of the above-mentioned relationships.

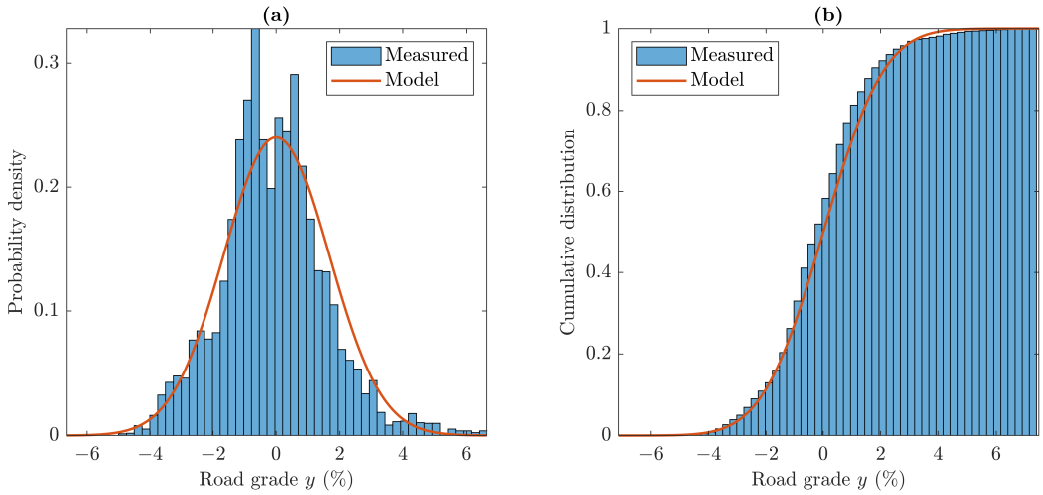

Figure 3.1: Comparison between the measured distribution and the analytical PDF and CDF of the road topography: **(a)** probability density; **(b)** cumulative distribution. The distribution refers to a random mission amongst those encompassing the Västra Götaland operating cycle of Paper C. Figure adapted from Paper B.

where the probability $p_y(y, \boldsymbol{\sigma}_Y, \mathbf{P}_R, \boldsymbol{L}_R)$ has been defined in Eq. (2.43). The expression is repeated here for the sake of readability:

$$p_y(y, \boldsymbol{\sigma}_Y, \mathbf{P}_R, \boldsymbol{L}_R) \triangleq \mathbb{P}\big(|Y| \leq y\big) = \sum_{i=1}^{n_r} \left[2\Phi\left(\frac{y}{\sigma_{Y|r_i}} \right) - 1 \right] \pi_{Ri}(\mathbf{P}_R, \boldsymbol{L}_R). \tag{3.3}$$

According to Eq. (3.3), the quantity $p_y(y, \boldsymbol{\sigma}_Y, \mathbf{P}_R, \boldsymbol{L}_R)$ in Eq. (3.2) should be interpreted as the proportion of the road for which the road grade, in absolute value, is less than a specified threshold y. In this context, it may be realised that $p_y(y, \boldsymbol{\sigma}_Y, \mathbf{P}_R, \boldsymbol{L}_R)$ in Eq. (3.2) represents, in fact, the CDF of the random variable $|Y|$. A comparison between the actual distribution of the topography measured along the vehicle's route and the analytical one obtained according to Eq. (3.2) is illustrated in Fig. 3.1.

It is worth observing that the mean hill lengths, conveniently collected here in a vector $\boldsymbol{L}_\mathrm{h} \triangleq [L_{\mathrm{h}|r_1} \ \ldots \ L_{\mathrm{h}|r_{n_r}}]^\mathrm{T}$, do not appear in Eqs. (3.2) and (3.3). Thus, according to the bird's-eye view representations inspired by the GTA and UFD systems, road missions characterised by the same process variance $\sigma^2_{Y|r_i}$, $i = 1, \ldots, n_r$, but different hill lengths are equivalent concerning the topography parameter. However, the mean hill length may also have a considerable influence upon the energy performance of road vehicles. To properly account for this effect, an additional criterion has been proposed in Papers B and C:

$$L_{\mathrm{h,min}} < L_\mathrm{h}(\boldsymbol{L}_\mathrm{h}, \mathbf{P}_R, \boldsymbol{L}_R) \leq L_{\mathrm{h,max}}, \tag{3.4}$$

where, with some abuse of notation,

$$L_{\mathrm{h}}(\boldsymbol{L}_{\mathrm{h}}, \mathbf{P}_R, \boldsymbol{L}_R) \triangleq \mathbb{E}(L_{\mathrm{h}}) = \sum_{i=1}^{n_r} L_{\mathrm{h}|r_i} \pi_{Ri}(\mathbf{P}_R, \boldsymbol{L}_R). \tag{3.5}$$

The interpretation of the above relationships is straightforward.

Road curviness

The criterion imposed on the road curviness differs according to the GTA and UFD descriptions. Indeed, the latter prescribes lower and upper bounds on the expected number of curves per unit of length for which the curvature is higher than a certain thresholds κ. The formula reads as follows:

$$\bar{n}'_{C,\min} < \bar{n}'_C(\kappa, \boldsymbol{\lambda}_C, \boldsymbol{\mu}_C, \boldsymbol{\sigma}_C, \mathbf{P}_R, \boldsymbol{L}_R) \leq \bar{n}'_{C,\max}, \tag{3.6}$$

in which, as usual, $\boldsymbol{\lambda}_C \triangleq [\lambda_{C|r_1} \ \dots \ \lambda_{C|r_{n_r}}]^{\mathrm{T}}$, $\boldsymbol{\mu}_C \triangleq [\mu_{C|r_1} \ \dots \ \mu_{C|r_{n_r}}]^{\mathrm{T}}$, $\boldsymbol{\sigma}_C \triangleq [\sigma_{C|r_1} \ \dots \ \sigma_{C|r_{n_r}}]^{\mathrm{T}}$, and $\bar{n}'_C(\kappa, \boldsymbol{\lambda}_C, \boldsymbol{\mu}_C, \boldsymbol{\sigma}_C, \mathbf{P}_R, \boldsymbol{L}_R)$ may be deduced to have the form

$$\begin{aligned}\bar{n}'_C(\kappa, \boldsymbol{\lambda}_C, \boldsymbol{\mu}_C, \boldsymbol{\sigma}_C, \mathbf{P}_R, \boldsymbol{L}_R) &\triangleq \mathbb{E}\left(\frac{N'_C}{L_{\mathrm{tot}}}\right) \\ &= \sum_{i=1}^{n_r} \frac{\lambda_{C|r_i}}{2} \left[1 + \operatorname{erf}\left(\frac{\ln(1/\kappa - r_{\mathrm{turn}}) - \mu_{C|r_i}}{\sqrt{2}\sigma_{C|r_i}}\right)\right] \pi_{Ri}(\mathbf{P}_R, \boldsymbol{L}_R),\end{aligned} \tag{3.7}$$

where N'_C represents a binomial random variable describing the number of curves for which the curvature exceeds the above-mentioned limit κ, and L_{tot} denotes the total length of the road.

Conversely, the GTA codification regards the road curvature K (clearly interpreted as a random variable) as a continuous function of the position along the vehicle's route, i.e., $K = K(X)$. Therefore, the corresponding expression for the operating class targets the proportion of road length for which the curvature is below a certain value κ, according to

$$p_{\kappa,\min} < p_\kappa(\kappa, \boldsymbol{\lambda}_C, \boldsymbol{\mu}_C, \boldsymbol{\sigma}_C, \boldsymbol{\mu}_L, \boldsymbol{\sigma}_L, \mathbf{P}_R, \boldsymbol{L}_R) \leq p_{\kappa,\max}, \tag{3.8}$$

being by definition $\boldsymbol{\mu}_L \triangleq [\mu_{L|r_1} \ \dots \ \mu_{L|r_{n_r}}]^{\mathrm{T}}$, $\boldsymbol{\sigma}_L \triangleq [\sigma_{L|r_1} \ \dots \ \sigma_{L|r_{n_r}}]^{\mathrm{T}}$, and

$$\begin{aligned}p_\kappa(\kappa, \boldsymbol{\lambda}_C, \boldsymbol{\mu}_C, \boldsymbol{\sigma}_C, \boldsymbol{\mu}_L, \boldsymbol{\sigma}_L, \mathbf{P}_R, \boldsymbol{L}_R) \triangleq \mathbb{P}(K \leq \kappa) = 1 - \sum_{i=1}^{n_r} \frac{\lambda_{C|r_i}}{2} \exp\left(\mu_{L|r_i} + \frac{\sigma^2_{L|r_i}}{2}\right) \\ \times \left[1 + \operatorname{erf}\left(\frac{\ln(1/\kappa - r_{\mathrm{turn}}) - \mu_{C|r_i}}{\sqrt{2}\sigma_{C|r_i}}\right)\right] \pi_{Ri}(\mathbf{P}_R, \boldsymbol{L}_R).\end{aligned} \tag{3.9}$$

Comparing the functions appearing in Eqs. (3.7) and (3.9), respectively, it may be inferred that the criterion imposed by the GTA system is more refined than that adopted by the UFD description, since the probability $p_\kappa(\kappa, \boldsymbol{\lambda}_C, \boldsymbol{\mu}_C, \boldsymbol{\sigma}_C, \boldsymbol{\mu}_L, \boldsymbol{\sigma}_L, \mathbf{P}_R, \boldsymbol{L}_R)$ involves all the sOC parameters connected with the model for road curviness, whereas the expression $\bar{n}'_C(\kappa, \boldsymbol{\lambda}_C, \boldsymbol{\mu}_C, \boldsymbol{\sigma}_C, \mathbf{P}_R, \boldsymbol{L}_R)$ neglects the contribution of the quantities related to the curve length. This may be intuitively explained by recalling that, according to the GTA representation, the curves along the road are treated as isolated events. In this context, it should also be emphasised that Eq. (3.9) represents indeed the CDF for the random variable K.

Speed bumps and stop signs

Only the UFD includes a system of classes for the speed bumps and stop signs. The criteria specified on both parameters prescribe upper and lower bounds on the expected number of events per unit of length along the vehicle's route. The corresponding analytical expressions are particularly simple and read

$$\bar{n}'_{\mathrm{b,min}} < \bar{N}_{\mathrm{b}}(\boldsymbol{\lambda}_{\mathrm{b}}, \mathbf{P}_R, \boldsymbol{L}_R) \leq \bar{n}'_{\mathrm{b,max}}, \tag{3.10a}$$

$$\bar{n}'_{\mathrm{s,min}} < \bar{N}_{\mathrm{s}}(\boldsymbol{\lambda}_{\mathrm{s}}, \mathbf{P}_R, \boldsymbol{L}_R) \leq \bar{n}'_{\mathrm{s,max}}, \tag{3.10b}$$

where, with the conventional notation, $\boldsymbol{\lambda}_{\mathrm{b}} \triangleq [\lambda_{\mathrm{s}|r_1} \ \dots \ \lambda_{\mathrm{b}|r_{nr}}]^{\mathrm{T}}$, $\boldsymbol{\lambda}_{\mathrm{s}} \triangleq [\lambda_{\mathrm{s}|r_1} \ \dots \ \lambda_{\mathrm{s}|r_{nr}}]^{\mathrm{T}}$, and the expectations $\lambda_{\mathrm{b}}(\boldsymbol{\lambda}_{\mathrm{b}}, \mathbf{P}_R, \boldsymbol{L}_R)$ and $\lambda_{\mathrm{s}}(\boldsymbol{\lambda}_{\mathrm{s}}, \mathbf{P}_R, \boldsymbol{L}_R)$ are given respectively by

$$\bar{N}_{\mathrm{b}}(\boldsymbol{\lambda}_{\mathrm{b}}, \mathbf{P}_R, \boldsymbol{L}_R) \triangleq \mathbb{E}\left(\frac{N_{\mathrm{b}}}{L_{\mathrm{tot}}}\right) = \sum_{i=1}^{n_r} \lambda_{\mathrm{b}|r_i} \pi_{Ri}(\mathbf{P}_R, \boldsymbol{L}_R), \tag{3.11a}$$

$$\bar{N}_{\mathrm{s}}(\boldsymbol{\lambda}_{\mathrm{s}}, \mathbf{P}_R, \boldsymbol{L}_R) \triangleq \mathbb{E}\left(\frac{N_{\mathrm{s}}}{L_{\mathrm{tot}}}\right) = \sum_{i=1}^{n_r} \lambda_{\mathrm{s}|r_i} \pi_{Ri}(\mathbf{P}_R, \boldsymbol{L}_R), \tag{3.11b}$$

in which N_{b} and N_{s} are random variables describing the number of speed bumps and stop signs along the vehicle's route. It is worth mentioning that the sOC parameters $t_{\mathrm{min}|r_i}$, $t_{\mathrm{max}|r_i}$, $v_{\mathrm{min}|r_i}$, and $v_{\mathrm{max}|r_i}$, $i = 1, \dots, n_r$, have deliberately not included in the definition of the relationships for the operating classes for the speed bumps and stop signs models. A more refined criterion may be instead found in Paper B.

Road roughness

Taking inspiration from the ISO classification [107], a road transport mission may be labelled in respect to the roughness depending on the degree of unevenness C_{r}:

$$C_{\mathrm{r,min}} < C_{\mathrm{r}}(\boldsymbol{C}_{\mathrm{r}}, \mathbf{P}_R, \boldsymbol{L}_R) \leq C_{\mathrm{r,max}}, \tag{3.12}$$

clearly with

$$C_{\mathrm{r}}(\boldsymbol{C}_{\mathrm{r}}, \mathbf{P}_R, \boldsymbol{L}_R) \triangleq \mathbb{E}(Z) = \sum_{i=1}^{n_r} C_{\mathrm{r}|r_i} \pi_{Ri}(\mathbf{P}_R, \boldsymbol{L}_R), \tag{3.13}$$

where $\boldsymbol{C}_{\mathrm{r}} = [C_{\mathrm{r}|r_1} \ \dots \ C_{\mathrm{r}|r_{n_r}}]^{\mathrm{T}}$ collects the conditional mean roughnesses $C_{\mathrm{r}|r_i}$, $i = 1, \dots, n_r$.

In particular, the ISO standard [107] specifies eight different road levels, ranging from class A to H in increasing roughness order. Amongst these, however, only the first five are important for automotive applications [101]. A similar criterion is adopted in Paper B. Accordingly, only Eq. (3.12) is required to establish a relationship between the set of sOC parameters and the two limits prescribed by the bird's-eye view description. It should be noticed that the proposed criterion systematically neglects the effect of variability between sections, since the conditional shape parameters $\nu_{\mathrm{r}|r_i}$, $i = 1, \dots, n_r$ does not appear in the inequality of Eq. (3.12). By contrast, a more refined classification approach would prescribe an additional relationship including the shape parameters. To this end, further details on generalised Laplace distributions may be found in [104, 105].

Speed signs

The speed signs represent perhaps the most delicate parameter when dealing with the operation of specifying a mathematical relationship for the operating class. The criteria set by the GTA and UFD codifications are rather vague and may eventually fail to build a univocal system of classes. The approach reported in this thesis is instead analogous to that proposed in Papers B and C, which has been in turn adapted from [25]. The criterion, which is also extremely intuitive, targets the mean legal speed along the road, on which upper and lower bounds are opportunely imposed, i.e.,

$$\hat{v}_{\min} < \hat{v}\big(\mathbf{P}_{V|r_1}, \dots, \mathbf{P}_{V|r_{n_r}}, \boldsymbol{L}_{V|r_1}, \dots, \boldsymbol{L}_{V|r_{n_r}}\mathbf{P}_R, \boldsymbol{L}_R\big) \leq \hat{v}_{\max}, \tag{3.14}$$

with

$$\begin{aligned}\hat{v}\big(\mathbf{P}_{V|r_1}, \dots, \mathbf{P}_{V|r_{n_r}}, \boldsymbol{L}_{V|r_1}, \dots, \boldsymbol{L}_{V|r_{n_r}}\mathbf{P}_R, \boldsymbol{L}_R\big) &= \mathbb{E}(V) \\ &= \sum_{i=1}^{n_r}\sum_{j=1}^{n_{v|r_i}} v_{j|r_i}\pi_{Vj|r_i}\big(\mathbf{P}_{V|r_i}, \boldsymbol{L}_{V|r_i}\big)\pi_{Ri}(\mathbf{P}_R, \boldsymbol{L}_R).\end{aligned} \tag{3.15}$$

Together, Eqs. (3.14) and (3.15) conclude the collection of relationships for the operating classes related to the road category.

3.1.2 Weather category

The weather parameters considered by the GTA and UFD classification systems include ambient temperature, relative humidity, and precipitation intensity, for which stochastic models have been introduced in Chap 2. Criteria on the wind speed and direction, and on the atmospheric pressure, are not explicitly specified.

Ambient temperature and relative humidity

The ambient temperature and relative humidity parameters are introduced simultaneously since the criteria specified on both, as well as the corresponding stochastic models, are similar. More specifically, they are both interpretable as limits imposed on the corresponding probabilities, according to

$$p_{T^*_{\mathrm{air}},\mathrm{min}} < p_{T_{\mathrm{air}}}\big(\mu_T, T_{\mathrm{d}}, T_{\mathrm{y}}, \varphi_{T_{\mathrm{d}}}, \varphi_{T_{\mathrm{y}}}, \boldsymbol{\sigma}_{\tilde{T}}\big) \leq p_{T^*_{\mathrm{air}},\mathrm{max}}, \tag{3.16a}$$

$$p_{\Psi^*_{\mathrm{RH}},\mathrm{min}} < p_{\Psi_{\mathrm{RH}}}\big(\mu_\Psi, \Psi_{\mathrm{d}}, \Psi_{\mathrm{y}}, \varphi_{\Psi_{\mathrm{d}}}, \varphi_{\Psi_{\mathrm{y}}}, \boldsymbol{\sigma}_{\tilde{\Psi}}\big) \leq p_{\Psi^*_{\mathrm{RH}},\mathrm{max}}, \tag{3.16b}$$

clearly with $\boldsymbol{\sigma}_{\tilde{T}} \triangleq [\sigma_{\tilde{T}|s_1}\ \sigma_{\tilde{T}|s_2}\ \sigma_{\tilde{T}|s_3}\ \sigma_{\tilde{T}|s_4}]^{\mathrm{T}}$, $\boldsymbol{\sigma}_{\tilde{\Psi}} \triangleq [\sigma_{\tilde{\Psi}|s_1}\ \sigma_{\tilde{\Psi}|s_2}\ \sigma_{\tilde{\Psi}|s_3}\ \sigma_{\tilde{\Psi}|s_4}]^{\mathrm{T}}$. The probability $p_{T_{\mathrm{air}}}(\mu_T, T_{\mathrm{d}}, T_{\mathrm{y}}, \varphi_{T_{\mathrm{d}}}, \varphi_{T_{\mathrm{y}}}, \boldsymbol{\sigma}_{\tilde{T}})$ appearing in the inequality displayed in Eq. (3.16a) has the form

$$\begin{aligned} p_{T_{\mathrm{air}}}\big(\mu_T, T_{\mathrm{d}}, T_{\mathrm{y}}, \varphi_{T_{\mathrm{d}}}, \varphi_{T_{\mathrm{y}}}, \boldsymbol{\sigma}_{\tilde{T}}\big) &\triangleq \mathbb{P}\big(T^*_{\mathrm{min}} < T_{\mathrm{air}} \leq T^*_{\mathrm{max}}\big) \\ &= \sum_{i=1}^{4} \sum_{\bar{T}_k \in \mathcal{S}_{\bar{T}|s_i}} p_{\bar{T}_k|s_i} p_{s_i} \mathbb{1}_{T^*_{\mathrm{max}} \in [T_0,\infty)} \\ &\quad \times \Phi\left(\frac{T^*_{\mathrm{max}} - \bar{T}_k\big(\mu_T, T_{\mathrm{d}}, T_{\mathrm{y}}, \varphi_{T_{\mathrm{d}}}, \varphi_{T_{\mathrm{y}}}\big)}{\sigma_{\tilde{T}|s_i}}\right) \\ &\quad - \sum_{i=1}^{4} \sum_{\bar{T}_k \in \mathcal{S}_{\bar{T}|s_i}} p_{\bar{T}_k|s_i} p_{s_i} \mathbb{1}_{T^*_{\mathrm{min}} \in [T_0,\infty)} \\ &\quad \times \Phi\left(\frac{T^*_{\mathrm{min}} - \bar{T}_k\big(\mu_T, T_{\mathrm{d}}, T_{\mathrm{y}}, \varphi_{T_{\mathrm{d}}}, \varphi_{T_{\mathrm{y}}}\big)}{\sigma_{\tilde{T}|s_i}}\right), \end{aligned} \tag{3.17}$$

where T_0 denotes the zero point for thermodynamic temperature, $\mathcal{S}_{\bar{T}|s_i}$, $i = 1, \ldots, 4$, represent the seasonal subsets collecting the values for the deterministic component of the ambient temperature, and $p_{\bar{T}_k|s_i}$ the probabilities associated to those values. Similarly, the probability

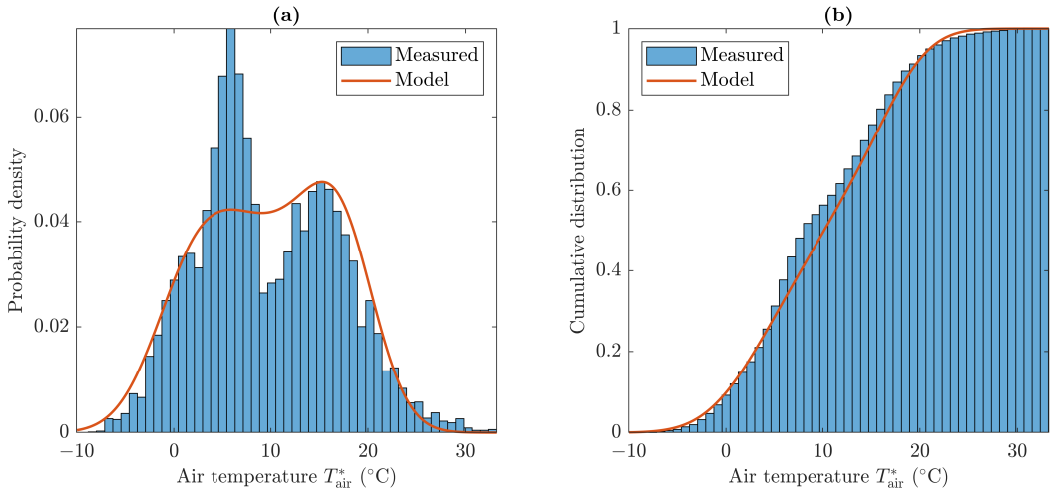

Figure 3.2: Comparison between the measured and analytical temperature distributions for the city of Gothenburg, Sweden, in 2019: **(a)** probability density; **(b)** cumulative distribution. Figure adapted from Paper B.

$p_{\Psi_{\text{RH}}}(\mu_\Psi, \Psi_{\text{d}}, \Psi_{\text{y}}, \varphi_{\Psi_{\text{d}}}, \varphi_{\Psi_{\text{y}}}, \boldsymbol{\sigma}_{\tilde{\Psi}})$ in Eq. (3.16b) may be deduced as follows:

$$
\begin{aligned}
p_{\Psi_{\text{RH}}}\left(\mu_\Psi, \Psi_{\text{d}}, \Psi_{\text{y}}, \varphi_{\Psi_{\text{d}}}, \varphi_{\Psi_{\text{y}}}, \boldsymbol{\sigma}_{\tilde{\Psi}}\right) &\triangleq \mathbb{P}\left(\Psi^*_{\min} < \Psi_{\text{RH}} \leq \Psi^*_{\max}\right) \\
&= \mathbb{1}_{\Psi^*_{\max}\in[1,\infty)} + \sum_{i=1}^{4} \sum_{\bar{\Psi}_k \in \mathcal{S}_{\bar{\Psi}|s_i}} p_{\bar{\Psi}_k|s_i} p_{s_i} \mathbb{1}_{\Psi^*_{\max}\in[0,1)} \\
&\quad \times \Phi\left(\frac{\Psi^*_{\max} - \bar{\Psi}_k\left(\mu_\Psi, \Psi_{\text{d}}, \Psi_{\text{y}}, \varphi_{\Psi_{\text{d}}}, \varphi_{\Psi_{\text{y}}}\right)}{\sigma_{\tilde{\Psi}|s_i}}\right) \\
&\quad - \sum_{i=1}^{4} \sum_{\bar{\Psi}_k \in \mathcal{S}_{\bar{\Psi}|s_i}} p_{\bar{\Psi}_k|s_i} p_{s_i} \mathbb{1}_{\Psi^*_{\min}\in[0,1)} \\
&\quad \times \Phi\left(\frac{\Psi^*_{\min} - \bar{\Psi}_k\left(\mu_\Psi, \Psi_{\text{d}}, \Psi_{\text{y}}, \varphi_{\Psi_{\text{d}}}, \varphi_{\Psi_{\text{y}}}\right)}{\sigma_{\tilde{\Psi}|s_i}}\right) - \mathbb{1}_{\Psi^*_{\max}\in[1,\infty)},
\end{aligned}
\tag{3.18}
$$

where the definition for $\mathcal{S}_{\bar{\Psi}|s_i}$, $i = 1, \ldots, 4$, and $p_{\bar{\Psi}_k|s_i}$ is analogous to that given for the ambient temperature. Equations (3.17) and (3.18) may be interpreted as CDFs by setting opportunely the values for the minimum thresholds $T^*_{\min}$ and $\Psi^*_{\min}$, respectively. As an example, the temperature distributions for the city of Gothenburg, Sweden, in 2019, obtained using data collected from the SMHI, are compared to the analytical PDF and CDF derived according to Eqs. (2.21), (2.22a) and (2.24a) in Fig. 3.2. The relative humidity exhibits a similar trend.

Precipitation intensity

Concerning the precipitation intensity, the criterion specified by the UFD representation is formulated in terms of probability, which translates in a formula as

$$p_{\lambda_\mathrm{p},\min} < p_{\lambda_\mathrm{p}}\big(\boldsymbol{\alpha}_{\Lambda_\mathrm{p}}, \boldsymbol{\beta}_{\Lambda_\mathrm{p}}, \mathbf{P}_{H|s_1}, \ldots, \mathbf{P}_{H|s_4}\big) \leq p_{\lambda_\mathrm{p},\max}, \tag{3.19}$$

as usual with $\boldsymbol{\alpha}_{\Lambda_\mathrm{p}} \triangleq [\alpha_{\Lambda_\mathrm{p}|s_1}\ \alpha_{\Lambda_\mathrm{p}|s_2}\ \alpha_{\Lambda_\mathrm{p}|s_3}\ \alpha_{\Lambda_\mathrm{p}|s_4}]^\mathrm{T}$, $\boldsymbol{\beta}_{\Lambda_\mathrm{p}} \triangleq [\beta_{\Lambda_\mathrm{p}|s_1}\ \beta_{\Lambda_\mathrm{p}|s_2}\ \beta_{\Lambda_\mathrm{p}|s_3}\ \beta_{\Lambda_\mathrm{p}|s_4}]^\mathrm{T}$, and the probability $p_{\lambda_\mathrm{p}}(\boldsymbol{\alpha}_{\Lambda_\mathrm{p}}, \boldsymbol{\beta}_{\Lambda_\mathrm{p}}, \mathbf{P}_{H|s_1}, \ldots, \mathbf{P}_{H|s_4})$ reading

$$\begin{aligned}
p_{\lambda_\mathrm{p}}\big(\boldsymbol{\alpha}_{\Lambda_\mathrm{p}}, \boldsymbol{\beta}_{\Lambda_\mathrm{p}}, \mathbf{P}_{H|s_1}, \ldots, \mathbf{P}_{H|s_4}\big) &\triangleq \mathbb{P}\big(\lambda_{\mathrm{p},\min} < \Lambda_\mathrm{p} \leq \lambda_{\mathrm{p},\max}\big) \\
&= \sum_{i=1}^{4} \pi_{H1|s_i}\Big(\mathbf{P}_{H|s_i}\Big) p_{s_i}\big[\mathbb{1}_{\lambda_{\mathrm{p},\max}\in\mathbb{R}_{\geq 0}} - \mathbb{1}_{\lambda_{\mathrm{p},\min}\in\mathbb{R}_{\geq 0}}\big] \\
&\quad + \sum_{i=1}^{4} \frac{1}{\Gamma\Big(\alpha_{\Lambda_\mathrm{p}|s_i}\Big)} \gamma\Big(\alpha_{\Lambda_\mathrm{p}|s_i}, \beta_{\Lambda_\mathrm{p}|s_i}\lambda_{\mathrm{p},\max}\Big) \\
&\quad \times \pi_{H2|s_i}\Big(\mathbf{P}_{H|s_i}\Big) p_{s_i} \mathbb{1}_{\lambda_{\mathrm{p},\max}\in\mathbb{R}_{>0}} \\
&\quad - \sum_{i=1}^{4} \frac{1}{\Gamma\Big(\alpha_{\Lambda_\mathrm{p}|s_i}\Big)} \gamma\Big(\alpha_{\Lambda_\mathrm{p}|s_i}, \beta_{\Lambda_\mathrm{p}|s_i}\lambda_{\mathrm{p},\min}\Big) \\
&\quad \times \pi_{H2|s_i}\Big(\mathbf{P}_{H|s_i}\Big) p_{s_i} \mathbb{1}_{\lambda_{\mathrm{p},\min}\in\mathbb{R}_{>0}}.
\end{aligned} \tag{3.20}$$

The above Eq. (3.20) yields again the CDF for the precipitation intensity, provided that the lower bound $\lambda_{\mathrm{p},\min}$ is specified correctly.

3.1.3 Traffic category

The traffic category only includes a stochastic model for the density. The equivalent interpretation from the perspective of the bird's-eye view description is detailed below.

Traffic density

No criterion is explicitly specified by the GTA and UFD classification systems concerning the traffic density parameter. However, the latter is included here since, similar to what done for the ambient temperature and relative humidity, a relationship for the corresponding operating class may be stated mathematically in terms of probability, on which upper and lower limits are imposed, that is,

$$p_{\rho_\mathrm{t}^*,\min} < p_{\rho_\mathrm{t}}\big(\rho^*_{\min}, \rho^*_{\max}, \boldsymbol{\mu}_\rho, \boldsymbol{\rho}_\mathrm{d}, \boldsymbol{\varphi}_{\rho_\mathrm{d}}, \boldsymbol{\sigma}_{\tilde{\rho}}, \mathbf{P}_{V|r_1}, \ldots, \mathbf{P}_{V|r_{n_r}}, \boldsymbol{L}_{V|r_1}, \ldots, \boldsymbol{L}_{V|r_{n_r}}, \mathbf{P}_r, \boldsymbol{L}_R\big) \leq p_{\rho_\mathrm{t}^*,\max}. \tag{3.21}$$

In the above Eq. (3.21), the vector-valued parameters have been defined respectively as $\boldsymbol{\mu}_{\rho} \triangleq [\mu_{\rho|v_{1|r_1}\cap s_1} \ \cdots \ \mu_{\rho|v_{n_{v|r_1}|r_1}\cap s_1} \ \cdots \ \mu_{\rho|v_{1|r_{n_r}}\cap s_4} \ \cdots \ \mu_{\rho|v_{n_{v|r_{n_r}}|r_{n_r}}\cap s_4}]^{\mathrm{T}}$ for the means, $\boldsymbol{\rho}_{\mathrm{d}} \triangleq [\rho_{\mathrm{d}|v_{1|r_1}\cap s_1} \ \cdots \ \rho_{\mathrm{d}|v_{n_{v|r_1}|r_1}\cap s_1} \ \cdots \ \rho_{\mathrm{d}|v_{1|r_{n_r}}\cap s_4} \ \cdots \ \rho_{\mathrm{d}|v_{n_{v|r_{n_r}}|r_{n_r}}\cap s_4}]^{\mathrm{T}}$ for the daily amplitudes, $\boldsymbol{\varphi}_{\rho_{\mathrm{d}}} \triangleq [\varphi_{\rho_{\mathrm{d}}|v_{1|r_1}\cap s_1} \ \cdots \ \varphi_{\rho_{\mathrm{d}}|v_{n_{v|r_1}|r_1}\cap s_1} \ \cdots \ \varphi_{\rho_{\mathrm{d}}|v_{1|r_{n_r}}\cap s_4} \ \cdots \ \varphi_{\rho_{\mathrm{d}}|v_{n_{v|r_{n_r}}|r_{n_r}}\cap s_4}]^{\mathrm{T}}$ for the phases, and $\boldsymbol{\sigma}_{\tilde{\rho}} \triangleq [\sigma_{\tilde{\rho}|v_{1|r_1}\cap s_1} \ \cdots \ \sigma_{\tilde{\rho}|v_{n_{v|r_1}|r_1}\cap s_1} \ \cdots \ \sigma_{\tilde{\rho}|v_{1|r_{n_r}}\cap s_4} \ \cdots \ \sigma_{\tilde{\rho}|v_{n_{v|r_{n_r}}|r_{n_r}}\cap s_4}]^{\mathrm{T}}$ for the standard deviations. The probability $p_{\rho_{\mathrm{t}}}(\boldsymbol{\mu}_{\rho}, \boldsymbol{\rho}_{\mathrm{d}}, \boldsymbol{\varphi}_{\rho_{\mathrm{d}}}, \boldsymbol{\sigma}_{\tilde{\rho}}, \mathbf{P}_{V|r_1}, \ldots, \mathbf{P}_{V|r_{n_r}}, \boldsymbol{L}_{V|r_1}, \ldots, \boldsymbol{L}_{V|r_{n_r}}, \mathbf{P}_r, \boldsymbol{L}_R)$ may be derived as

$$
\begin{aligned}
&p_{\rho_{\mathrm{t}}}\left(\rho^*_{\min}, \rho^*_{\max}, \boldsymbol{\mu}_{\rho}, \boldsymbol{\rho}_{\mathrm{d}}, \boldsymbol{\varphi}_{\rho_{\mathrm{d}}}, \boldsymbol{\sigma}_{\tilde{\rho}}, \mathbf{P}_{V|r_1}, \ldots, \mathbf{P}_{V|r_{n_r}}, \boldsymbol{L}_{V|r_1}, \ldots, \boldsymbol{L}_{V|r_{n_r}}, \mathbf{P}_r, \boldsymbol{L}_R\right) \\
&\quad \triangleq \mathbb{P}(\rho^*_{\min} < \rho_{\mathrm{t}} \leq \rho^*_{\max}) \\
&\quad = \sum_{l=1}^{n_r}\sum_{j=1}^{n_{v|r_l}} \mathbb{1}_{\rho^*_{\max}\in[\rho_{\mathrm{c}|v_{j|r_l}},\infty)} + \sum_{l=1}^{n_r}\sum_{j=1}^{n_{v|r_l}}\sum_{i=1}^{4}\sum_{\bar{\rho}_k\in\mathcal{S}_{\bar{\rho}|v_{j|r_l}\cap s_i}} p_{\bar{\rho}_k|v_{j|r_l}\cap s_i} p_{s_i} \mathbb{1}_{\rho^*_{\max}\in[0,\rho_{\mathrm{c}|v_{j|r_l}})} \\
&\qquad \times \Phi\left(\frac{\rho^*_{\max} - \bar{\rho}_k\left(\mu_{\rho|v_{j|r_l}\cap s_i}, \rho_{\mathrm{d}|v_{j|r_l}\cap s_i}, \varphi_{\rho_{\mathrm{d}}|v_{j|r_l}\cap s_i}\right)}{\sigma_{\tilde{\rho}|v_{j|r_l}\cap s_i}}\right) \pi_{Vj|r_l}\left(\mathbf{P}_{V|r_l}, \boldsymbol{L}_{V|r_l}\right)\pi_{Rl}(\mathbf{P}_R, \boldsymbol{L}_R) \\
&\qquad - \sum_{l=1}^{n_r}\sum_{j=1}^{n_{v|r_l}}\sum_{i=1}^{4}\sum_{\bar{\rho}_k\in\mathcal{S}_{\bar{\rho}|v_{j|r_l}\cap s_i}} p_{\bar{\rho}_k|v_{j|r_l}\cap s_i} p_{s_i} \mathbb{1}_{\rho^*_{\min}\in[0,\rho_{\mathrm{c}|v_{j|r_l}})} \\
&\qquad \times \Phi\left(\frac{\rho^*_{\min} - \bar{\rho}_k\left(\mu_{\rho|v_{j|r_l}\cap s_i}, \rho_{\mathrm{d}|v_{j|r_l}\cap s_i}, \varphi_{\rho_{\mathrm{d}}|v_{j|r_l}\cap s_i}\right)}{\sigma_{\tilde{\rho}|v_{j|r_l}\cap s_i}}\right) \pi_{Vj|r_l}\left(\mathbf{P}_{V|r_l}, \boldsymbol{L}_{V|r_l}\right)\pi_{Rl}(\mathbf{P}_R, \boldsymbol{L}_R) \\
&\qquad - \sum_{l=1}^{n_r}\sum_{j=1}^{n_{v|r_l}} \mathbb{1}_{\rho^*_{\min}\in[\rho_{\mathrm{c}|v_{j|r_l}},\infty)} \leq p_{\rho^*_{\mathrm{t}},\max},
\end{aligned}
\tag{3.22}
$$

where $\rho_{\mathrm{c}|v_{j|r_l}}$ is a threshold specified for the maximum allowable density on a generic segment for a given combination of speed signs and road types (see, e.g., Eq. (A.4) in Appendix A), $\mathcal{S}_{\bar{\rho}|v_{j|r_l}\cap s_i}$ are subsets corresponding to given combinations of speed signs and road types in which the deterministic component of the traffic density is allowed to take values, and $p_{\bar{\rho}_k|v_{j|r_l}\cap s_i}$ are the associated probabilities. The function in Eq. (3.22) provides an analytical expression for the CDF of the traffic density by fixing appropriate values of $\rho^*_{\min}$.

3.1.4 Mission category

The mission category only includes a stochastic model for the cargo weight. The equivalent interpretation from the perspective of the bird's-eye view description is formalised in terms of

expectation.

Cargo weight

An expression for the operating class concerning the cargo weight is not explicitly specified by the GTA and UFD codifications. Nonetheless, the expectation may be conveniently adopted, that is,

$$\hat{w}_{\min} < \hat{w}(\boldsymbol{\mu}_W, \boldsymbol{\sigma}_W, \boldsymbol{w}_{\max}, \mathbf{P}_\Xi, \boldsymbol{L}_\Xi) \leq \hat{w}_{\max}, \tag{3.23}$$

where

$$\begin{aligned}\hat{w}(\boldsymbol{\mu}_W, \boldsymbol{\sigma}_W, \boldsymbol{w}_{\max}, \mathbf{P}_\Xi, \boldsymbol{L}_\Xi) &= \mathbb{E}(W) \\ &= \sum_{i=1}^{n_\xi} \frac{1}{2} \Bigg[\sqrt{\frac{2}{\pi}} \sigma_{W|\xi_i} \left(\mathrm{e}^{-\mu_{W|\xi_i}^2/(2\sigma_{w|\xi_i}^2)} - \mathrm{e}^{-(w_{\max|\xi_i} - \mu_{W|\xi_i})^2/(2\sigma_{w|\xi_i}^2)} \right) \\ &\quad + \left(\mu_{W|\xi_i} - w_{\max|\xi_i} \right) \operatorname{erf}\left(\frac{w_{\max|\xi_i} - \mu_{W|\xi_i}}{\sqrt{2}\sigma_{W|\xi_i}} \right) \\ &\quad + \mu_{W|\xi_i} \operatorname{erf}\left(\frac{\mu_{W|\xi_i}}{\sqrt{2}\sigma_{W|\xi_i}} \right) + w_{\max|\xi_i} \Bigg] \pi_{\Xi i}(\mathbf{P}_\Xi, \boldsymbol{L}_\Xi),\end{aligned} \tag{3.24}$$

and, for convenience of notation, the conditional mean, variance, and maximum parameters have been be collected into vectors by defining $\boldsymbol{\mu}_W \triangleq [\mu_{W|\xi_1} \ \dots \ \mu_{W|\xi_{n_\xi}}]^{\mathrm{T}}$, $\boldsymbol{\sigma}_W \triangleq [\sigma_{W|\xi_1} \ \dots \ \sigma_{W|\xi_{n_\xi}}]^{\mathrm{T}}$, and $\boldsymbol{w}_{\max} \triangleq [w_{\max|\xi_1} \ \dots \ w_{\mathrm{w}|\xi_{n_\xi}}]^{\mathrm{T}}$, respectively.

All the relationships for the operating classes, together with their interpretation in terms of probability or expectation, are summarised in Table 3.1.

3.2 Composite random variables

In the derivation of the mathematical relationships defining the operating classes, attention has been restricted to individual road missions. When considering an entire transport application, the sOC parameters for the stochastic road and mission models may be allowed to vary over the population of missions. In this case, the probabilities and expectations computed in Sect. 3.1 become evidently random variables. Since they are functions of simpler random variables, i.e., the stochastic counterparts of the sOC parameters, in this thesis, and also in Paper C, they are generally referred to as composite variables. The present section reports for completeness the expressions for their analytical formulae. The only categories considered here are those for road, traffic (since the traffic density depends upon the speed signs and indirectly on the road types) and mission. By contrast, the weather models are deliberately

Model	Mathematical interpretation	Operating class relationships	sOC parameters $\mathcal{OC}_\mathrm{s}$	Bird's-eye view metrics $\mathcal{OC}_\mathrm{b}$
		Road category		
Topography	$p_{y,\min} < \mathbb{P}(\lvert Y\rvert \leq y) \leq p_{y,\max}$ $L_{\mathrm{h},\min} < L_\mathrm{h} \leq L_{\mathrm{h},\max}$	Eq. (3.3) Eq. (3.5)	$\boldsymbol{\sigma}_Y$, $\boldsymbol{L}_\mathrm{h}$, $\mathbf{P}_R$, $\boldsymbol{L}_R$	y, $p_{y,\min}$, $p_{y,\max}$ $L_{\mathrm{h},\min}$, $L_{\mathrm{h},\max}$
Curviness	$\bar{n}'_{C,\min} < \mathbb{E}\left(\frac{N'_C}{L_\mathrm{tot}}\right) \leq \bar{n}'_{C,\max}$, $p_{\kappa,\min} < \mathbb{P}(K \leq \kappa_\max) \leq p_{\kappa,\max}$	Eq. (3.7) Eq. (3.9)	$\boldsymbol{\lambda}_C$, $\boldsymbol{\mu}_C$, $\boldsymbol{\sigma}_C$, $\boldsymbol{\mu}_L$, $\boldsymbol{\sigma}_L$, $\mathbf{P}_R$, $\boldsymbol{L}_R$	$\bar{n}'_{C,\min}$, $\bar{n}'_{C,\max}$, κ, $p_{\kappa,\min}$, $p_{\kappa,\max}$
Speed bumps	$\bar{n}'_{\mathrm{b},\min} < \mathbb{E}\left(\frac{N_\mathrm{b}}{L_\mathrm{tot}}\right) \leq \bar{n}'_{\mathrm{b},\max}$	Eq. (3.11a)	$\boldsymbol{\lambda}_\mathrm{b}$, $\mathbf{P}_R$, $\boldsymbol{L}_R$	$\bar{n}'_{\mathrm{b},\min}$, $\bar{n}'_{\mathrm{b},\max}$
Stop signs	$\bar{n}'_{\mathrm{s},\min} < \mathbb{E}\left(\frac{N_\mathrm{s}}{L_\mathrm{tot}}\right) \leq \bar{n}'_{\mathrm{s},\max}$	Eq. (3.11b)	$\boldsymbol{\lambda}_\mathrm{s}$, $\mathbf{P}_R$, $\boldsymbol{L}_R$	$\bar{n}'_{\mathrm{s},\min}$, $\bar{n}'_{\mathrm{s},\max}$
Road roughness	$C_{\mathrm{r},\min} < \mathbb{E}(Z) \leq C_{\mathrm{r},\max}$	Eq. (3.13)	$\boldsymbol{C}_\mathrm{r}$, $\mathbf{P}_R$, $\boldsymbol{L}_R$	$C_{\mathrm{r},\min}$, $C_{\mathrm{r},\max}$
Speed signs	$\hat{v}_\min < \mathbb{E}(V) \leq \hat{v}_\max$	Eq. (3.15)	$\mathbf{P}_{V\vert r_i}$, $\boldsymbol{L}_{V\vert r_i}$, $\mathbf{P}_R$, $\boldsymbol{L}_R$	$\hat{v}_\min$, $\hat{v}_\max$
		Weather category		
Air temperature	$p_{T^*_\mathrm{air},\min} < \mathbb{P}(T^*_\min < T_\mathrm{air} \leq T^*_\max) \leq p_{T^*_\mathrm{air},\max}$	Eq. (3.17)	μ_T, T_d, T_y, φ_{T_d}, φ_{T_y}, $\boldsymbol{\sigma}_{\tilde{T}}$,	$T^*_\min$, $T^*_\max$, $p_{T^*_\mathrm{air},\min}$, $p_{T^*_\mathrm{air},\max}$
Atm. humidity	$p_{\Psi^*_\mathrm{RH},\min} < \mathbb{P}(\Psi^*_\min < \Psi_\mathrm{RH} \leq \Psi^*_\max) \leq p_{\Psi^*_\mathrm{RH},\max}$	Eq. (3.18)	μ_Ψ, Ψ_d, Ψ_y, $\varphi_{\Psi_\mathrm{d}}$, $\varphi_{\Psi_\mathrm{y}}$, $\boldsymbol{\sigma}_{\tilde{\Psi}}$,	$\Psi^*_\min$, $\Psi^*_\max$, $p_{\Psi^*_\mathrm{RH},\min}$, $p_{\Psi^*_\mathrm{RH},\max}$
Precipitation	$p_{\lambda_\mathrm{p},\min} < \mathbb{P}(\lambda_{\mathrm{p},\max} < \Lambda_\mathrm{p} \leq \lambda_{\mathrm{p},\max}) \leq p_{\lambda_\mathrm{p},\max}$	Eq. (3.20)	$\mathbf{P}_{H\vert s_i}$, $\boldsymbol{\alpha}_{\Lambda_\mathrm{p}}$, $\boldsymbol{\beta}_{\Lambda_\mathrm{p}}$	$\lambda_{\mathrm{p},\min}$, $\lambda_{\mathrm{p},\max}$ $p_{\lambda_\mathrm{p},\min}$, $p_{\lambda_\mathrm{p},\max}$
		Traffic category		
Traffic density	$p_{\rho^*_\mathrm{t},\min} < \mathbb{P}(\rho^*_\min < \rho_\mathrm{t} \leq \rho^*_\max) \leq p_{\rho^*_\mathrm{t},\max}$	Eq. (3.22)	$\boldsymbol{\mu}_\rho$, $\boldsymbol{\rho}_\mathrm{d}$, $\boldsymbol{\varphi}_{\rho_\mathrm{d}}$, $\boldsymbol{\sigma}_{\tilde{\rho}}$, $\mathbf{P}_{V\vert r_i}$, $\boldsymbol{L}_{V\vert r_i}$, $\mathbf{P}_R$, $\boldsymbol{L}_R$	$\rho^*_\min$, $\rho^*_\max$ $p_{\rho^*_\mathrm{t},\min}$, $p_{\rho^*_\mathrm{t},\max}$
		Mission category		
Cargo weight	$\hat{w}_\min < \hat{w}(\boldsymbol{\mu}_W, \boldsymbol{\sigma}_W, \boldsymbol{w}_\max, \mathbf{P}_\Xi, \boldsymbol{L}_\Xi) \leq \hat{w}_\max$	Eq. (3.24)	$\boldsymbol{\mu}_W$, $\boldsymbol{\sigma}_W$, $\boldsymbol{w}_\max$, $\mathbf{P}_\Xi$, $\boldsymbol{L}_\Xi$	$\hat{w}_\min$, $\hat{w}_\max$

Table 3.1: Summary of the relationships for the operating classes, with corresponding interpretation in terms of probabilities and expectations.

disregarded, being implicitly assumed that their parameters are already averaged concerning a certain geographical region. With respect to the mission category, the analytical expression for the composite variable is derived considering the mean cargo weight; additionally, a stochastic model is proposed to capture the variation of the mission length over the transport application. In this context, it should be mentioned that, whilst the exact form for the distributions of the original sOC parameters in the road category, treated as random variables, is irrelevant to the results advocated in the following, the same does not hold true for the mission length.

3.2.1 Road category

The composite variables in the road category include those for road topography, curviness, speed bumps and stop signs, and speed signs.

Road topography

Departing from Eq. (3.3), the composite random variable corresponding to the road grade length ratio may be deduced as follows:

$$P_y\Big(y, \boldsymbol{\Sigma}_Y, \tilde{\mathbf{P}}_R, \tilde{\boldsymbol{L}}_R\Big) \triangleq \sum_{i=1}^{n_r} \left[2\Phi\left(\frac{y}{\Sigma_{Y|r_i}}\right) - 1\right] \mathit{\Pi}_{Ri}\Big(\tilde{\mathbf{P}}_R, \tilde{\boldsymbol{L}}_R\Big), \tag{3.25}$$

where the vector $\boldsymbol{\Sigma}_Y \triangleq [\Sigma_{Y|r_1} \ \dots \ \Sigma_{Y|r_{n_r}}]^{\mathrm{T}}$ collects the conditional stochastic standard deviations $\Sigma_{Y|r_i}$, $i = 1, \dots, n_r$, and $\tilde{\mathbf{P}}_R$ and $\tilde{\boldsymbol{L}}_R$ denote the stochastic counterparts of the single-step transition matrix $\mathbf{P}_R$ and mean length vector $\boldsymbol{L}_R$, respectively, and the generic $\mathit{\Pi}_{Ri}(\tilde{\mathbf{P}}_R, \tilde{\boldsymbol{L}}_R)$, $i = 1, \dots, n_r$, is the stochastic version of the stationary probability $\pi_{Ri}(\mathbf{P}_R, \boldsymbol{L}_R)$ for the road type. The relationship for the random mean hill length may be instead derived by starting from Eq. (3.5):

$$\tilde{L}_{\mathrm{h}}\Big(\tilde{\boldsymbol{L}}_{\mathrm{h}}, \tilde{\mathbf{P}}_R, \tilde{\boldsymbol{L}}_R\Big) \triangleq \sum_{i=1}^{n_r} \tilde{L}_{\mathrm{h}|r_i} \mathit{\Pi}_{Ri}\Big(\tilde{\mathbf{P}}_R, \tilde{\boldsymbol{L}}_R\Big), \tag{3.26}$$

in which $\tilde{\boldsymbol{L}}_{\mathrm{h}} \triangleq [\tilde{L}_{\mathrm{h}|r_1} \ \dots \ \tilde{L}_{\mathrm{h}|r_{n_r}}]^{\mathrm{T}}$ is a vector collecting the stochastic mean hill lengths $\tilde{L}_{\mathrm{h}|r_i}$, $i = 1, \dots, n_r$.

Road curviness

For the curviness model, two different composite variables may be introduced based on Eqs. (3.7) and (3.9), respectively. These would correspond to the relationships derived by considering the criterion imposed by the UFD and GTA codifications, in turn. For the

expected number of curves, the stochastic variable describing the variation over the mission population may be expressed as

$$\bar{N}'_C\Big(\kappa, \boldsymbol{\Lambda}_C, \boldsymbol{M}_C, \boldsymbol{\Sigma}_C, \tilde{\mathbf{P}}_R, \tilde{\boldsymbol{L}}_R\Big) \triangleq \sum_{i=1}^{n_r} \frac{\Lambda_{C|r_i}}{2}\left[1 + \operatorname{erf}\left(\frac{\ln(1/\kappa - r_{\text{turn}}) - M_{C|r_i}}{\sqrt{2}\Sigma_{C|r_i}}\right)\right] \times \Pi_{Ri}\Big(\tilde{\mathbf{P}}_R, \tilde{\boldsymbol{L}}_R\Big), \tag{3.27}$$

being this time $\boldsymbol{\Lambda}_C \triangleq [\Lambda_{C|r_1} \ \dots \ \Lambda_{C|r_{n_r}}]^{\mathrm{T}}$, $\boldsymbol{M}_C \triangleq [M_{C|r_1} \ \dots \ M_{C|r_{n_r}}]^{\mathrm{T}}$, $\boldsymbol{\Sigma}_C \triangleq [\Sigma_{C|r_1} \ \dots \ \Sigma_{C|r_{n_r}}]^{\mathrm{T}}$ the vectors collecting the variables $\Lambda_{C|r_i}$, $M_{C|r_i}$, $\Sigma_{C|r_i}$, $i = 1, \dots, n_r$, which represent the stochastic counterparts of the sOC parameters $\lambda_{C|r_i}$, $\mu_{C|r_i}$, $\sigma_{C|r_i}$.

On the other hand, combining Eqs. (2.8) and (3.9) yields

$$P_\kappa\Big(\kappa, \boldsymbol{\Lambda}_C, \boldsymbol{M}_C, \boldsymbol{\Sigma}_C, \boldsymbol{M}_L, \boldsymbol{\Sigma}_L, \tilde{\mathbf{P}}_R, \tilde{\boldsymbol{L}}_R\Big) \triangleq 1 - \sum_{i=1}^{n_r} \frac{\Lambda_{C|r_i}}{2} \exp\left(M_{L|r_i} + \frac{\Sigma^2_{L|r_i}}{2}\right) \times \left[1 + \operatorname{erf}\left(\frac{\ln(1/\kappa - r_{\text{turn}}) - M_{C|r_i}}{\sqrt{2}\Sigma_{C|r_i}}\right)\right] \times \Pi_{Ri}\Big(\tilde{\mathbf{P}}_R, \tilde{\boldsymbol{L}}_R\Big), \tag{3.28}$$

with, as usual, $\boldsymbol{M}_L \triangleq [M_{L|r_1} \ \dots \ M_{L|r_{n_r}}]^{\mathrm{T}}$, and $\boldsymbol{\Sigma}_L \triangleq [\Sigma_{L|r_1} \ \dots \ \Sigma_{L|r_{n_r}}]^{\mathrm{T}}$ collecting the variables $M_{L|r_i}$, $\Sigma_{L|r_i}$, $i = 1, \dots, n_r$, which are the stochastic versions of the parameters $\mu_{L|r_i}$, $\sigma_{L|r_i}$. Comparing Eq. (3.28) to (3.27), it may be clearly noticed that the former relationship is more complete, and involves all the characteristic parameters of the curviness model. Indeed, the analytical expression for $\bar{N}'_C = \bar{N}'_C(\boldsymbol{\Lambda}_C, \boldsymbol{M}_C, \boldsymbol{\Sigma}_C, \tilde{\mathbf{P}}_R, \tilde{\boldsymbol{L}}_R)$ in Eq. (3.27) does not depend upon the stochastic mean lenghts $M_{L|r_i}$ and standard deviations $\Sigma_{L|r_i}$, $i = 1, \dots, n_r$.

The variable in Eq. (3.28) is sometimes referred to as *curviness length ratio* (Paper C).

Speed bumps and stop signs

The composite variables corresponding to the expectations in Eqs. (3.11a) and (3.11b) may immediately be deduced as follows:

$$\bar{N}_{\mathrm{b}}\Big(\boldsymbol{\Lambda}_{\mathrm{s}}, \tilde{\mathbf{P}}_R, \tilde{\boldsymbol{L}}_R\Big) \triangleq \sum_{i=1}^{n_r} \Lambda_{\mathrm{b}|r_i} \Pi_{Ri}\Big(\tilde{\mathbf{P}}_R, \tilde{\boldsymbol{L}}_R\Big), \tag{3.29a}$$

$$\bar{N}_{\mathrm{s}}\Big(\boldsymbol{\Lambda}_{\mathrm{s}}, \tilde{\mathbf{P}}_R, \tilde{\boldsymbol{L}}_R\Big) \triangleq \sum_{i=1}^{n_r} \Lambda_{\mathrm{s}|r_i} \Pi_{Ri}\Big(\tilde{\mathbf{P}}_R, \tilde{\boldsymbol{L}}_R\Big), \tag{3.29b}$$

where the vectors $\boldsymbol{\Lambda}_{\mathrm{b}} \triangleq [\Lambda_{\mathrm{b}|r_1} \ \dots \ \Lambda_{\mathrm{b}|r_{n_r}}]^{\mathrm{T}}$, $\boldsymbol{\Lambda}_{\mathrm{s}} \triangleq [\Lambda_{\mathrm{s}|r_1} \ \dots \ \Lambda_{\mathrm{s}|r_{n_r}}]^{\mathrm{T}}$ have been defined whose elements $\Lambda_{\mathrm{b}|r_i}$, $\Lambda_{\mathrm{s}|r_i}$, $i = 1, \dots, n_r$, represent the stochastic counterpart of the intensities $\lambda_{\mathrm{b}|r_i}$, $\lambda_{\mathrm{s}|r_i}$.

Road roughness

The composite value for the road roughness may be derived starting directly with Eq. (3.13):

$$\tilde{C}_{\mathrm{r}}\left(\tilde{\boldsymbol{C}}_{\mathrm{r}}, \tilde{\mathbf{P}}_R, \tilde{\boldsymbol{L}}_R\right) \triangleq \sum_{i=1}^{n_r} \tilde{C}_{\mathrm{r}|r_i} \Pi_{Ri}\left(\tilde{\mathbf{P}}_R, \tilde{\boldsymbol{L}}_R\right), \tag{3.30}$$

where $\tilde{\boldsymbol{C}}_{\mathrm{r}} = [\tilde{C}_{\mathrm{r}|r_1} \ \dots \ \tilde{C}_{\mathrm{r}|r_{n_r}}]^{\mathrm{T}}$ collects the stochastic conditional mean roughnesses $\tilde{C}_{\mathrm{r}|r_i}$, $i = 1, \dots, n_r$.

Speed signs

The composite variable describing the distribution of the mean legal speed over the population of missions encompassing an application may be derived from Eq. (3.15) and reads specifically

$$\begin{aligned}\hat{V}\left(\tilde{\mathbf{P}}_{V|r_1}, \dots, \tilde{\mathbf{P}}_{V|r_{n_r}}, \tilde{\boldsymbol{L}}_{V|r_1}, \dots, \tilde{\boldsymbol{L}}_{V|r_{n_r}}, \tilde{\mathbf{P}}_R, \tilde{\boldsymbol{L}}_R\right) \triangleq \sum_{i=1}^{n_r} \sum_{j=1}^{n_{v|r_i}} v_{j|r_i} \Pi_{Vj|r_i}\left(\tilde{\mathbf{P}}_{V|r_i}, \tilde{\boldsymbol{L}}_{V|r_i}\right) \\ \times \Pi_{Ri}\left(\tilde{\mathbf{P}}_R, \tilde{\boldsymbol{L}}_R\right),\end{aligned} \tag{3.31}$$

where the variables $\Pi_{Vj|r_i}(\tilde{\mathbf{P}}_R, \tilde{\boldsymbol{L}}_R)$, $j = 1, \dots, n_{v|r_i}$, represent the stochastic counterparts of the conditional stationary probabilities $\pi_{Vj|r_i}(\mathbf{P}_R, \boldsymbol{L}_R)$ for the speed signs.

Figure 3.3 illustrates the PDFs of the composite random variables for the road category, concerning the Västra Götaland operating cycle parametrised in Paper C. In particular, it is interesting to notice that the variables $P_y(y, \boldsymbol{\Sigma}_Y, \tilde{\mathbf{P}}_R, \tilde{\boldsymbol{L}}_R)$ and $P_\kappa(\kappa, \boldsymbol{\Lambda}_C, \boldsymbol{M}_C, \boldsymbol{\Sigma}_C, \boldsymbol{M}_L, \boldsymbol{\Sigma}_L, \tilde{\mathbf{P}}_R, \tilde{\boldsymbol{L}}_R)$ in Eqs. (3.25) and (3.28) only assume value in the range $[0, 1]$. This may be easily explained by recalling that they should be interpreted as stochastic CDFs. Along with the actual distributions, the mean value is also reported, computed both numerically (solid grey lines), and estimated using a first-order approximation[2] (dashed yellow lines).

Before moving to the treatment of the composite variable for the traffic density, it is essential to realise that all the composite variables in the road category are correlated through the stationary probabilities $\Pi_{Ri}(\tilde{\mathbf{P}}_R, \tilde{\boldsymbol{L}}_R)$, $i = 1, \dots, n_r$ for any value of $n_r > 1$.

3.2.2 Traffic category

The traffic category includes a single model for the density. All the sOC parameters of such a model are supposed to depend explicitly upon a given combination of speed signs and season. However, since these parameters are usually estimated concerning certain geographical regions, they may already be interpreted as averaged values over the application. Hence, the only contribution to the traffic density variation over the population of missions is assumed to come from those for speed signs and, consequently, road types.

[2]For a generic vector-valued function $\boldsymbol{f}(\cdot)$ of random variables $\boldsymbol{X} = [X_1 \ \dots \ X_n]^{\mathrm{T}}$, its expectation may be approximated as $\mathbb{E}(\boldsymbol{f}(\boldsymbol{X})) \approx \boldsymbol{f}(\mathbb{E}(\boldsymbol{X}))$ using the propagation of the uncertainty technique.

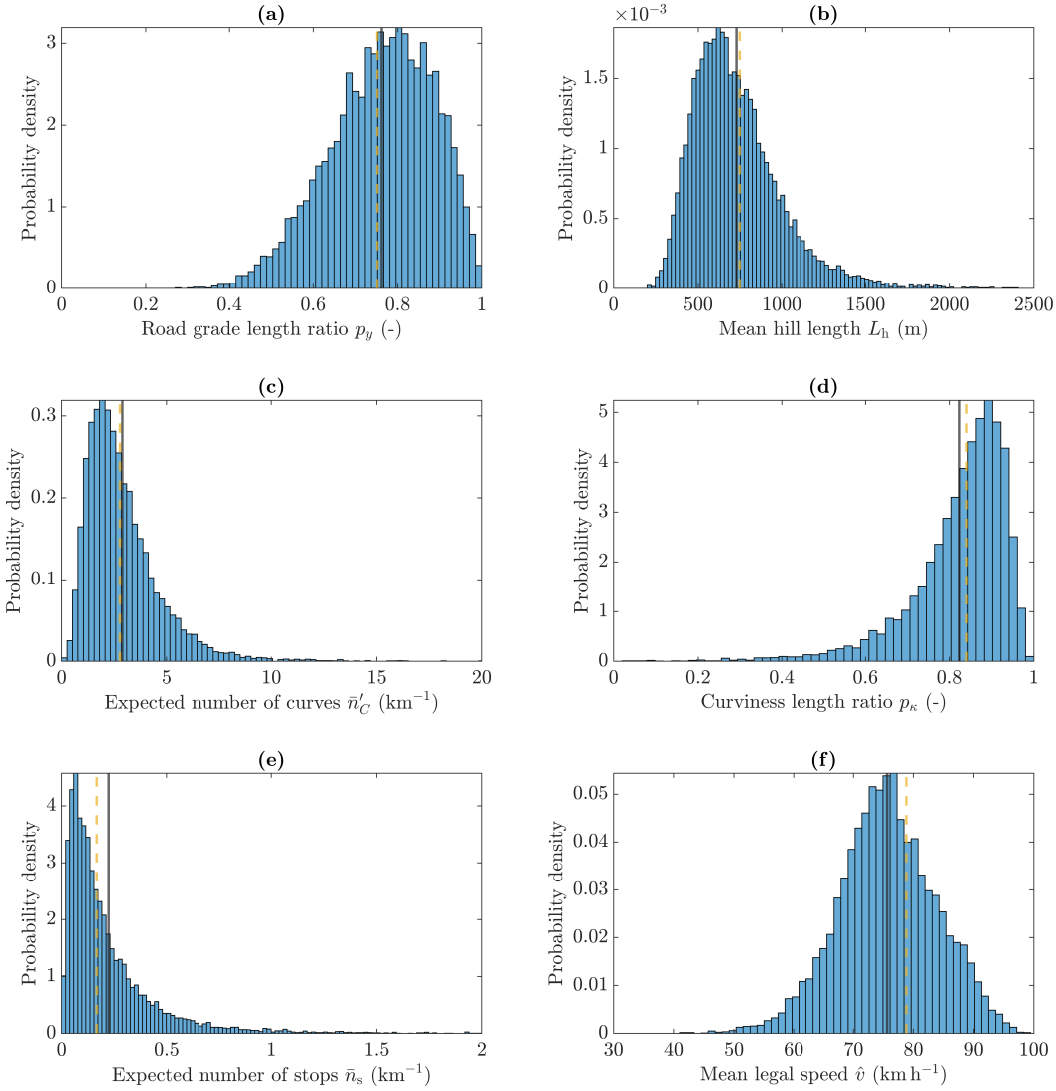

Figure 3.3: Distributions of the composite variables, with estimated (solid grey lines) and approximated (dashed yellow lines) mean values, concerning the Västra Götaland operating cycle: **(a)** road grade length ration; **(b)** mean hill length; **(c)** expected number of curves; **(d)** curviness length ratio; **(e)** expected number of stops; **(f)** mean legal speed. Figure adapted from Paper C.

Traffic density

Owing to the premises above, the analytical expression for the composite variable corresponding to Eq. (3.22) may be deduced to have the form

$$
\begin{aligned}
&P_{\rho_{\mathrm{t}}}\Big(\rho^*_{\min},\rho^*_{\max},\boldsymbol{\mu}_{\rho},\boldsymbol{\rho}_{\mathrm{d}},\boldsymbol{\varphi}_{\rho_{\mathrm{d}}},\boldsymbol{\sigma}_{\tilde{\rho}},\tilde{\mathbf{P}}_{V|r_1},\ldots,\tilde{\mathbf{P}}_{V|r_{n_r}},\tilde{\boldsymbol{L}}_{V|r_1},\ldots,\tilde{\boldsymbol{L}}_{V|r_{n_r}},\tilde{\mathbf{P}}_r,\tilde{\boldsymbol{L}}_R\Big)\\
&\quad\triangleq\sum_{l=1}^{n_r}\sum_{j=1}^{n_{v|r_l}}\mathbb{1}_{\rho^*_{\max}\in[\rho_{\mathrm{c}|v_{j|r_l}},\infty)}+\sum_{l=1}^{n_r}\sum_{j=1}^{n_{v|r_l}}\sum_{i=1}^{4}\sum_{\bar{\rho}_k\in\mathcal{S}_{\bar{\rho}|v_{j|r_l}\cap s_i}}p_{\bar{\rho}_k|v_{j|r_l}\cap s_i}p_{s_i}\mathbb{1}_{\rho^*_{\max}\in[0,\rho_{\mathrm{c}|v_{j|r_l}})}\\
&\qquad\times\Phi\left(\frac{\rho^*_{\max}-\bar{\rho}_k\Big(\mu_{\rho|v_{j|r_l}\cap s_i},\rho_{\mathrm{d}|v_{j|r_l}\cap s_i},\varphi_{\rho_{\mathrm{d}}|v_{j|r_l}\cap s_i}\Big)}{\sigma_{\tilde{\rho}|v_{j|r_l}\cap s_i}}\right)\Pi_{Vj|r_i}\Big(\tilde{\mathbf{P}}_{V|r_i},\tilde{\boldsymbol{L}}_{V|r_i}\Big)\Pi_{Ri}\Big(\tilde{\mathbf{P}}_R,\tilde{\boldsymbol{L}}_R\Big)\\
&\qquad-\sum_{l=1}^{n_r}\sum_{j=1}^{n_{v|r_l}}\sum_{i=1}^{4}\sum_{\bar{\rho}_k\in\mathcal{S}_{\bar{\rho}|v_{j|r_l}\cap s_i}}p_{\bar{\rho}_k|v_{j|r_l}\cap s_i}p_{s_i}\mathbb{1}_{\rho^*_{\min}\in[0,\rho_{\mathrm{c}|v_{j|r_l}})}\\
&\qquad\times\Phi\left(\frac{\rho^*_{\min}-\bar{\rho}_k\Big(\mu_{\rho|v_{j|r_l}\cap s_i},\rho_{\mathrm{d}|v_{j|r_l}\cap s_i},\varphi_{\rho_{\mathrm{d}}|v_{j|r_l}\cap s_i}\Big)}{\sigma_{\tilde{\rho}|v_{j|r_l}\cap s_i}}\right)\Pi_{Vj|r_i}\Big(\tilde{\mathbf{P}}_{V|r_i},\tilde{\boldsymbol{L}}_{V|r_i}\Big)\Pi_{Ri}\Big(\tilde{\mathbf{P}}_R,\tilde{\boldsymbol{L}}_R\Big)\\
&\qquad-\sum_{l=1}^{n_r}\sum_{j=1}^{n_{v|r_l}}\mathbb{1}_{\rho^*_{\min}\in[\rho_{\mathrm{c}|v_{j|r_l}},\infty)}\leq p_{\rho^*_{\mathrm{t}},\max}.
\end{aligned}
\tag{3.32}
$$

It should be observed that, even though it belongs to another category, the composite variable for the traffic density is also correlated to those in the road section, again via the stationary stochastic distributions $\Pi_{Ri}(\tilde{\mathbf{P}}_R,\tilde{\boldsymbol{L}}_R)$, $i=1,\ldots,n_r$, and possibly also via the random terms $\Pi_{Vj|r_i}(\tilde{\mathbf{P}}_{V|r_i},\tilde{\boldsymbol{L}}_{V|r_i})$, $j=1,\ldots,n_{v|r_i}$.

3.2.3 Mission category

Apart from the cargo weight already considered, an additional stochastic model for the mission length is introduced in the following, concerning entire transport applications.

Cargo weight

The analytical formula for the composite variable corresponding to the mean cargo weight in Eq. (3.24) may be deduced as

$$\hat{W}\left(\boldsymbol{M}_W, \boldsymbol{\Sigma}_W, \boldsymbol{w}_{\max}, \tilde{\mathbf{P}}_\Xi, \tilde{\boldsymbol{L}}_\Xi\right) \triangleq \sum_{i=1}^{n_\xi} \frac{1}{2} \Bigg[\sqrt{\frac{2}{\pi}} \Sigma_{W|\xi_i} \left(\mathrm{e}^{-M_{W|\xi_i}^2/(2\Sigma_{w|\xi_i}^2)} - \mathrm{e}^{-(w_{\max|\xi_i} - M_{W|\xi_i})^2/(2\Sigma_{w|\xi_i}^2)} \right) + \left(M_{W|\xi_i} - w_{\max|\xi_i} \right) \operatorname{erf}\left(\frac{w_{\max|\xi_i} - M_{W|\xi_i}}{\sqrt{2}\Sigma_{W|\xi_i}} \right) + M_{W|\xi_i} \operatorname{erf}\left(\frac{M_{W|\xi_i}}{\sqrt{2}\Sigma_{W|\xi_i}} \right) + w_{\max|\xi_i} \Bigg] \Pi_{\Xi i}\left(\tilde{\mathbf{P}}_\Xi, \tilde{\boldsymbol{L}}_\Xi\right), \tag{3.33}$$

where the variables $\boldsymbol{M}_W \triangleq [M_{W|\xi_1} \ \dots \ M_{W|\xi_{n_\xi}}]^{\mathrm{T}}$ and $\boldsymbol{\Sigma}_W \triangleq [\Sigma_{W|\xi_1} \ \dots \ \Sigma_{W|\xi_{n_\xi}}]^{\mathrm{T}}$ have been defined, whose components represent the stochastic counterparts of the parameters $\mu_{W|\xi_i}$ and $\sigma_{W|\xi_i}$, $i = 1, \dots, n_\xi$. Similarly, $\tilde{\mathbf{P}}_\Xi$, $\tilde{\boldsymbol{L}}_\Xi$ denote the random version of the transition matrix and mean length vector $\mathbf{P}_\Xi$, $\boldsymbol{L}_\Xi$, respectively. Finally, the generic $\Pi_{\Xi i}(\tilde{\mathbf{P}}_\Xi, \tilde{\boldsymbol{L}}_\Xi)$ represents the stochastic counterpart of the stationary probability $\pi_{\Xi i}(\mathbf{P}_\Xi, \boldsymbol{L}_\Xi)$.

Mission length

A stochastic variable for the mission length is not technically a composite random variable; nonetheless, it is discussed in this thesis since the mission length parameter is included in both the GTA and UFD representations. In this context, it should be observed that it refers to a population of missions, that is, a transport application. Indeed, no stochastic model is required when considering road operations in isolation. The model presented here is based on that developed in Paper C, and assumes that the mission length follows a Gamma distribution, i.e., $\tilde{L}_{\mathrm{m}} \sim \mathrm{Ga}(\alpha_{\tilde{L}_{\mathrm{m}}}, \beta_{\tilde{L}_{\mathrm{m}}})$, with $L_{\mathrm{m}} \in \mathcal{S}_{\tilde{L}_{\mathrm{m}}} \equiv \mathbb{R}_{>0}$. This specific choice is motivated by the fact that the sum of Gamma variables with the same rate parameter is still a Gamma variable. For the case of mission length, all the realisations for a certain transport application would be generated from a unique distribution, and thus any sequence of consecutive missions would also obey the same law. This introduces some freedom in the definition of a mission itself, which could be interpreted as a single trip associated with a specific task, as well as a collection of trips or subtasks.

Actually, if a transport mission is defined as a single pick-up/delivery operation, then the cargo weight model is already sufficient to describe the mission length if it is parametrised concerning the whole transport application. Indeed, by assuming the same intensity parameter for each operating state, every sequence of mission becomes may be modelled using a gamma distribution, which is simply the generalisation of an exponential random variable. However, if

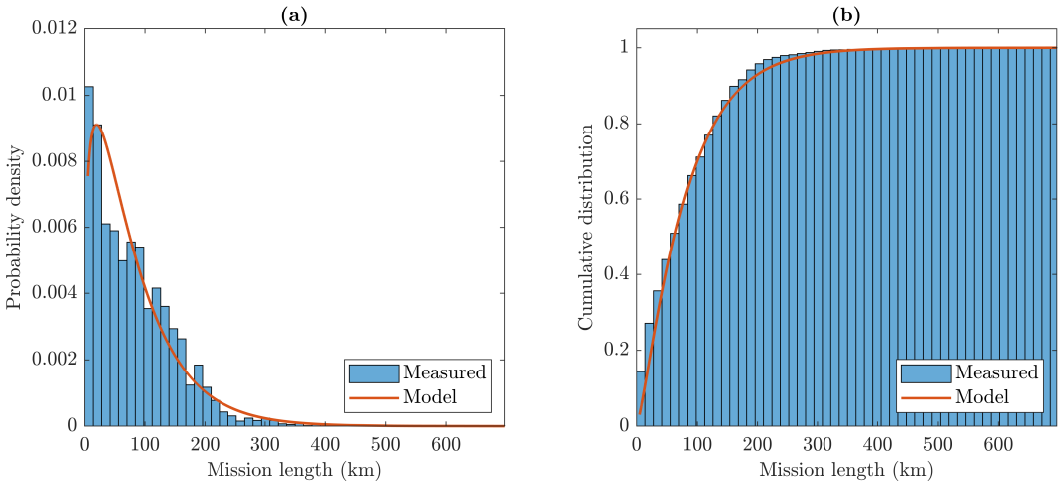

Figure 3.4: Measured distribution and the analytical PDF and CDF of the mission length for the Västra Götaland operating cycle: **(a)** probability density; **(b)** cumulative distribution. Figure adapted from Paper C.

different intensities are employed for each operating state, this is not true anymore, and then the notion of a road mission should be specified *a priori* depending on the specific application.

Concerning the Västra Götaland operating cycle parametrised in Paper C, the comparison between the empirical and analytical distributions for the mission length is shown in Fig. 3.4.

3.3 Specifying limits and thresholds

In Sect. 3.1, the notion of an operating class has been introduced based on the intrinsic relationship existing between the sOC and bird's-eye view descriptions. This concept has been formalised by deriving analytical expressions connecting several subsets of sOC parameters to the metrics and thresholds imposed by the bird's-eye view representation. However, nothing has been said about how to specify limits and bounds in an effective way. This is a rather intriguing dilemma, that has been conventionally addressed by vehicle manufacturers by simply relying on experience. Ideally, the bird's-eye view thresholds should be instead prescribed so as to yield a classification system that is optimally representative of the usage from the perspective of energy efficiency, that is, an *energy-metric-optimal (EMO) classification system*, as referred to as in Paper D.

To illustrate the general idea behind Paper D, a simple example may be adduced concerning only the topography parameter, and in particular the road grade length ratio. Owing to the additional simplification of having a unique road type, i.e., $\sigma_{Y|r_1} \equiv \sigma_Y$, the expression in Eq. (3.3) simplifies to

$$\mathbb{P}\big(|Y| \leq y\big) = 2\Phi\left(\frac{y}{\sigma_Y}\right) - 1 \tag{3.34}$$

and hence the inequality in Eq. (3.2) may be recast directly in terms of standard deviation

$$\sigma_{Y,\min} \leq \sigma_Y < \sigma_{Y,\max}, \tag{3.35}$$

where it has been defined

$$\sigma_{Y,\min} \triangleq \frac{y}{\Phi^{-1}\left(\dfrac{p_{y,\max}+1}{2}\right)}, \qquad \text{and} \qquad \sigma_{Y,\max} \triangleq \frac{y}{\Phi^{-1}\left(\dfrac{p_{y,\min}+1}{2}\right)}, \tag{3.36}$$

being y fixed. Considering then a sequence of $\tilde{n}_Y$ intermediate limits between minimum and maximum values $\tilde{\sigma}_{Y,0}$ and $\tilde{\sigma}_{Y,\tilde{n}_Y+1}$, collected opportunely into a vector $\tilde{\boldsymbol{\sigma}}_Y \triangleq [\tilde{\sigma}_{Y,1} \ \dots \ \tilde{\sigma}_{Y,\tilde{n}_Y}]^{\mathrm{T}}$, a system of $\tilde{n}_Y + 1$ classes may be specified similarly by setting

$$\tilde{\sigma}_{Y,i} \leq \sigma_Y < \tilde{\sigma}_{Y,i+1}, \quad i = 0, \dots, \tilde{n}_Y, \tag{3.37a}$$

where $\tilde{\sigma}_{Y,0} = \tilde{\sigma}_Y^0$ and $\tilde{\sigma}_{Y,\tilde{n}_Y+1} = \tilde{\sigma}_Y^{\tilde{n}_Y+1}$ are assigned.

The objective would then consists in optimising the values of the intermediate thresholds $\tilde{\sigma}_{Y,i}$, $i = 1, \dots, \tilde{n}_Y$ so as to minimise the variation of a certain metric inside each class, whilst maximising that between the different classes. This may be done systematically by computing an appropriate function, and then evaluating its variation over the given intervals. Since the OC format targets explicitly energy performance, the obvious choice would be to consider a vehicle-independent mean energy function $\mu_{E_Y}(\cdot)$ that, for a given transport application, exhibits an explicit dependency solely upon σ_Y. Assuming reasonably $\mu_{E_Y} \in C^1([\sigma_{Y,0}, \sigma_{Y,\tilde{n}_Y+1}]; \mathbb{R})$, its total variation over the interval i may thus be computed as [133–136]

$$\mathrm{TV}_{\mu_{E_Y},i}\big(\tilde{\boldsymbol{\sigma}}_Y\big) = \int_{\tilde{\sigma}_{Y,i-1}}^{\tilde{\sigma}_{Y,i}} \left| \frac{\partial \mu_{E_Y}(\sigma_Y)}{\partial \sigma_Y} \right| \mathrm{d}\sigma_Y, \quad i = 1, \dots, \tilde{n}_Y + 1. \tag{3.38}$$

Consequently, the problem of building an EMO classification system may be formulated as follows in minimisation form:

$$\begin{aligned} &\underset{\tilde{\boldsymbol{\sigma}}_Y \in \mathbb{R}^{\tilde{n}_Y}}{\text{minimise}} \quad \boldsymbol{f}_Y\big(\tilde{\boldsymbol{\sigma}}_Y\big), \\ &\text{subject to} \quad \boldsymbol{g}_Y\big(\tilde{\boldsymbol{\sigma}}_Y\big) \leq \mathbf{0}, \end{aligned} \tag{3.39}$$

where $\boldsymbol{f}_Y(\cdot) = [f_{Y,1}(\cdot) \ \dots \ f_{Y,\tilde{n}_Y+1}(\cdot)]^{\mathrm{T}} \triangleq [\mathrm{TV}_{\mu_{E_Y},1}(\cdot) \ \dots \ \mathrm{TV}_{\mu_{E_Y},\tilde{n}_Y+1}(\cdot)]^{\mathrm{T}}$, and the functions $\boldsymbol{g}_Y(\cdot) = [g_{Y,1}(\cdot) \ \dots \ g_{Y,\tilde{n}_Y+1}(\cdot)]^{\mathrm{T}}$ describing the inequality constraints are of the type

$$g_{Y,i}\big(\tilde{\boldsymbol{\sigma}}_Y\big) = \tilde{\sigma}_{Y,i} - \tilde{\sigma}_{Y,i-1}, \qquad i = 1, \dots, \tilde{n}_\xi + 1. \tag{3.40a}$$

In Eq. (3.39), the the inequality constraints $\boldsymbol{g}_Y(\cdot) \leq \mathbf{0}$ ensure that any optimal (and, in fact, feasible[3]) solution $\tilde{\boldsymbol{\sigma}}_Y^*$ to (3.39) yields an ordered sequence $\{\tilde{\sigma}_{Y,i}^*\}_{i=1}^{\tilde{n}_Y}$ of limits $\tilde{\sigma}_{Y,i}^* \in [\tilde{\sigma}_Y^0, \tilde{\sigma}_Y^{\tilde{n}_Y+1}]$.

[3]It should be noticed that the set $S_Y \triangleq \{\tilde{\boldsymbol{\sigma}}_Y \in \mathbb{R}^{\tilde{n}_Y} \mid \boldsymbol{g}_Y(\tilde{\boldsymbol{\sigma}}_Y) \leq \mathbf{0}\}$ is polyhedral and bounded, which implies that the problem described by Eq. (3.39) is feasible [137].

Hence, the minimisation problem described by Eq. (3.39) provides a useful method for building an EMO classification system for road transport missions, concerning a fixed number of classes $\tilde{n}_Y + 1$.

For a multi-objective optimisation problem like that in Eq. (3.39), however, it is often impossible to find a unique solution which would be simultaneously optimal for all the objective functions, due to their inherently conflicting natures and their possible incommensurability [78]. Therefore, the notion of optimality is usually replaced by those of Pareto-optimality or efficiency. In this context, a common approach to recover Pareto-optimal solutions consists in simplifying the original formulation, which is then reduced to a single-objective optimisation problem by resorting, for example, to ε-constraint or weighting methods [78]. The latter approach has been followed in Paper D, where the formulation above has been extended to most of the road models discussed in Sect. 3.1. It is also important to clarify that, in Paper D, the mean energy functions were deduced by generating virtual environments for different values of the sOC parameters, and then performing complete vehicle dynamics simulations in VehProp. The corresponding energy functions were then parametrised by considering different vehicle configurations, for which the same trend could be observed. For example, a quadratic trend with the standard deviation could be deduced[4], i.e., $\mu_{E_Y} \propto \sigma_Y^2$, under the assumption that the contributions relating to different sOC parameters were simply additive.

The optimised bird's-eye view thresholds obtained by solving the minimisation problem in Eq. (3.39) are compared in Table 3.2 to those imposed by the GTA and UFD representations, considering the same extremal values $\tilde{\sigma}_Y^{\tilde{n}_Y+1} = 3.87$ and 2.38, respectively. It may be noticed that the intermediate limits differ considerably from those prescribed originally by the two classification systems. In particular, the GTA description subdivides the interval $[0, 3.87]$ into segments of equal lengths, whereas some unprecise criterion is adopted by the UFD codification. Instead, for a generic $\tilde{n}_Y$, the optimal thresholds are specified according to the progression $\sqrt{i/(\tilde{n}_Y+1)}\tilde{\sigma}_Y^{\tilde{n}_Y+1}$, $i = 1, \ldots, \tilde{n}_Y$.

[4]It may be realised that any function of the type $f(x) = ax^2 + b$ would yield the same sequence of thresholds according to Eq. (3.39), provided that the same strategy is used to solve the original multi-objective optimisation problem.

Class	Original UFD	Optimised UFD
FLAT	$\sigma_Y < 1.56$	$\sigma_Y < 1.69$
HILLY	$1.56 \leq \sigma_Y \leq 2.38$	$1.69 \leq \sigma_Y \leq 2.38$
V-HILLY	$2.38 < \sigma_Y$	$2.38 < \sigma_Y$
Class	**Original GTA**	**Optimised GTA**
FLAT	$\sigma_Y < 1.29$	$\sigma_Y < 2.23$
P-FLAT	$1.29 \leq \sigma_Y < 2.58$	$2.23 \leq \sigma_Y < 3.16$
HILLY	$2.58 \leq \sigma_Y < 3.87$	$3.16 \leq \sigma_Y < 3.87$
V-HILLY	$3.87 \leq \sigma_Y$	$3.87 \leq \sigma_Y$

Table 3.2: Comparison between the original and optimised thresholds for the UFD and GTA classification systems. The classes for both descriptions may be obtained by specifying $\tilde{\sigma}_Y^{\tilde{n}_Y+1} = 2.38$ and 3.87, with $\tilde{n}_Y = 1$ and 2, respectively.

Chapter 4

Applications: from design optimisation to virtual testing

In the previous Chaps. 2 and 3, the mathematical foundation of the operating cycle format was outlined, and the relationships existing between the three levels of representation were analysed in detail. In spite of the appearances, the construction of such a theoretical edifice is not a sterile exercise and is in fact propaedeutic to more conventional studies concerning the energy efficiency of road vehicles. Indeed, the applicability of the OC description extends to a wide variety of applications, spacing from theoretical investigations, like pure optimisation, to more practical situations requiring a strict interaction between the stakeholders. In this context, the aim of the present chapter is to briefly comment on how the OC framework can be used in practice concerning the entire process of optimal design and selection, and virtual testing of commercial vehicles, with particular emphasis on the classification problem.

4.1 Vehicle design optimisation

The first phase concerns vehicle design optimisation, depending on the characteristics of the transport application. This operation may be conducted by taking into account a number of different factors, including road properties, weather and traffic conditions. Specifically, vehicle manufacturers may optimise individual configurations by considering a combination of classes, defined according to their internal bird's-eye view descriptions, like, e.g., the GTA and UFD systems adopted by Volvo and Scania[1]. Building upon the relationship between the bird's-eye view and sOC representations illustrated in Chap. 3, an sOC may be parametrised that corresponds uniquely to each combination of classes. Moreover, the resulting sOCs may be simulated to yield an equivalent description in terms of a dOC. In turn, the latter may be

[1]The very starting point would be the development of a suitable classification system, the existence of which is not really questioned here. Possible methods to address this problem would be based on iterative processes or similar arguments to that presented in Paper D and Sect. 3.3.

added with a simple model for longitudinal vehicle dynamics to enable classic optimisation routines. This would ultimately allow tailoring the vehicle design based on the characteristics of the transport application, for which a representation is available concerning all three levels of the OC format. For example, referring to the road and mission parameters listed in Table B.1 in Appendix B, a total of 9216 different vehicle configurations may be obtained depending on how the different classes interact, concerning both the GTA and UFD descriptions. A similar procedure has been followed, for instance, in [25].

In the process outlined above, the most delicate step consists perhaps in the parametrisation of a representative sOC concerning every combination of classes. Vehicle manufacturers may easily succeed in such an operation using their internal datasets, which are usually assembled from log data. Statistical indicators may be calculated for road missions translated into the dOC and sOC formalisms, and then their representativeness may be evaluated based on such indicators. For example, if the sOC parameters are treated as random variables and their probability distribution is known, their conditional expectations (restricted, i.e., to a certain transport application interpreted as a given combination of bird's-eye view classes) may be estimated to parametrise a unique sOC. This expedient would assure the mean performance to be optimised over any population of missions defining the application itself, as corroborated by the findings in Paper C. To illustrate this concept, it may be beneficial to introduce a vector $\boldsymbol{X}_{\mathcal{OC}_\mathrm{s}}$ collecting the relevant stochastic sOC parameters entering the mathematical expressions for the composite variables that define the operating classes. For example, restricting the attention to the road and mission parameters listed again in Table B.1, for which specific values are available concerning the bird's-eye view metrics imposed by the GTA and UFD descriptions, such a vector may be constructed as $\boldsymbol{X}_{\mathcal{OC}_\mathrm{s}} \triangleq [\tilde{\mathbf{P}}_R \ \tilde{\boldsymbol{L}}_R \ \boldsymbol{\Sigma}_y \ \dots \ \tilde{\mathbf{P}}_{V|r_1} \ \dots \ \tilde{\mathbf{P}}_{V|r_{n_r}} \ \tilde{\boldsymbol{L}}_{V|r_1} \ \dots \ \tilde{\boldsymbol{L}}_{V|r_{n_r}} \ \tilde{L}_\mathrm{m}]^\mathrm{T}$. Assuming that the distributions for the random sOC parameters collected in $\boldsymbol{X}_{\mathcal{OC}_\mathrm{s}}$ may be estimated, e.g., from log data or external sources, the conditional distributions of the composite variables are also known, at least numerically. Consequently, the mathematical mean of the vector $\boldsymbol{X}_{\mathcal{OC}_\mathrm{s}}$, conditioned to a certain transport application, may be defined as $\boldsymbol{\mu}^{\mathrm{TC}}_{\boldsymbol{X}_{\mathcal{OC}_\mathrm{s}}} \triangleq \mathbb{E}_{\mathrm{TC}}(\boldsymbol{X}_{\mathcal{OC}_\mathrm{s}})$.

The problem of designing an energy-efficient vehicle translates then into minimising the mean energy consumption calculated over the population of missions encompassing the transport application. In this context, the existence of a function $f_E(\cdot)$ may be postulated describing the mean energy consumption (i.e., averaged concerning a given set of sOC parameters) for a certain vehicle configuration. In general, the mathematical expression for such a function may not be known analytically, but it might reasonably be expected to be deterministic, and dependent solely upon the sOC parameters, the vehicle's specifications, and possibly the driver's behaviour. Then, treating the sOC parameters as random variables as already done in Sect. 3.2, its conditional expectation over the relevant population of missions may be approximated as $\mathbb{E}_{\mathrm{TC}}(f_E(\boldsymbol{X}_{\mathcal{OC}_\mathrm{s}})) \approx f_E(\mathbb{E}_{\mathrm{TC}}(\boldsymbol{X}_{\mathcal{OC}_\mathrm{s}})) \equiv f_E(\boldsymbol{\mu}^{\mathrm{TC}}_{\boldsymbol{X}_{\mathcal{OC}_\mathrm{s}}})$ using the propagation of the uncertainty technique. This result, which may perhaps appear trivial, asserts that the average energy performance may be estimated simply by simulating an

adequately large number[2] of dOCs generated from a single representative sOC, parametrised by the conditional mean vector $\boldsymbol{\mu}^{\mathrm{TC}}_{\boldsymbol{X}_{\mathcal{OC}_\mathrm{s}}}$. Hence, a vehicle configuration whose consumption is minimised over a set of missions generated from such a unique sOC would also be optimally designed (at least on average) concerning the whole transport application. This observation allows to considerably reduce the number of required simulations which need to be run during the optimisation phase, with obvious advantages in terms of computational cost, whilst at the same time avoiding overfitting. Moreover, since the approximation discussed above is valid for any other function, it may be conjectured that, in order to estimate the mean value of a quantity in interest, simulating an appropriate number of dOCs originating from such a unique representative sOC may always be sufficient. Except for the advantage of minimising the risk of overfitting, another aspect justifies this strategy: individual dOCs synthesised stochastically may not be completely realistic. Instead, simulating a large number of dOCs would smoothen, on average, the effect of unlikely scenarios on the predicted energy performance.

In this context, is also worth mentioning that the dimension of the optimisation problem may be reduced even further by considering a few (possibly a single) representative dOCs instead of an entire population. However, since dOCs generated from the same sOC are statistically equivalent, the selection of a typical dOC would require measuring representativeness in terms of energy performance instead. This may be done by first simulating different vehicle configurations considering the given population of missions, and evaluating the statistical distributions of their energy performance. Then, a few dOCs may be designated corresponding to energy performances that are sufficiently close to the mean value. In this process, there is again no guarantee that such dOCs would be completely realistic. An alternative possibility would then consist in constructing dOCs starting directly from log data, thus avoiding the intermediate step of parametrising an equivalent description in terms of an sOC.

4.2 Optimal selection

The second phase concerns the optimal selection of single vehicles or entire fleets, based on the available information about the intended usage, possibly integrated with other criteria specified by the customer. This operations heavily relies on the relationship between the bird's-eye view and sOC levels of representation. In fact, if a large optimisation problem has been solved as described in Sect. 4.1, it merely reduces to that of classifying a certain transport application, and should hence be addressed concerning individual road operators. To this end, two complementary strategies are envisioned.

I. If log data are available for a specific customer, individual missions may be converted into the dOC and sOC formalisms. In this way, the stochastic parameters needed to properly classify the transport application would be estimated directly without the need of interacting explicitly with the stakeholders.

[2] Typically, around 300.

II. If log data are not available, a preliminary understanding of the intended application may be gained by resorting to questionnaires, to be answered either online or physically. The questions should be formulated so as to allow a conversion from the bird's-eye view to the sOC representation, and *vice versa*. The process should ideally involve active participation from the stakeholders, which may include not only the final customer but also, e.g., drivers.

There are numerous advantages connected with the availability of log data. The first one is that the procedure for extracting the sOC parameters may be easily automatised. Indeed, for most of the road models presented in Sect. 2.2.1, the estimation may be carried out starting from available signals measured by onboard sensors. In this process, standard open-access tools may be used, like the WAFO[3] package implemented in MATLAB®. On the other hand, detailed information about weather and traffic conditions is often not available directly from log data and must be supplemented using external sources. This can be certainly done if the GPS coordinates and the exact daytime of the mission are known. The most intuitive and simple choice is perhaps to resort to external databases which offer data free to download. Some examples are the SMHI service and Trafikverket database, which collect weather and traffic data at a fixed time resolution (usually one hour). This is particularly practical when it comes to analysing transport operations taking place within a well-defined geographical area, for which the weather parameters can be assumed to remain approximately constant in space. If the road operations extend into a larger area, an option is to build a weather map by combining information collected from several stations. The interaction with third actors like Here and Klimator may be also desirable since they would be able to integrate quantities deducible from log data with additional information required to estimate the sOC parameters for the weather and traffic models.

The relationships derived in Sect. 3.2 provide the analytical expressions for the stochastic variables involved in the characterisation of an entire transport application. In particular, to properly address the classification problem, the definition of a random vector is required that should condense all the information (in terms of composite variables) necessary to qualify the transport application according to the specific bird's-eye view description in use. This is necessary since the composite variables are usually correlated via the simple stochastic counterparts of the sOC parameters. For example, concerning the GTA codification for the

[3]Available from: http://www.maths.lth.se/matstat/wafo/.

parameters specified in Table B.1, such a vector may be defined as

$$\boldsymbol{X}_{\mathrm{GTA}}(\boldsymbol{X}_{\mathcal{OC}_{\mathrm{s}}}) \triangleq \begin{bmatrix} P_y\Big(3, \boldsymbol{\Sigma}_Y, \tilde{\mathbf{P}}_R, \tilde{\boldsymbol{L}}_R\Big) \\ P_y\Big(6, \boldsymbol{\Sigma}_Y, \tilde{\mathbf{P}}_R, \tilde{\boldsymbol{L}}_R\Big) \\ P_y\Big(9, \boldsymbol{\Sigma}_Y, \tilde{\mathbf{P}}_R, \tilde{\boldsymbol{L}}_R\Big) \\ \tilde{L}_{\mathrm{h}}\Big(\tilde{\boldsymbol{L}}_{\mathrm{h}}, \tilde{\mathbf{P}}_R, \tilde{\boldsymbol{L}}_R\Big) \\ P_\kappa\Big(0.008, \boldsymbol{\Lambda}_C, \boldsymbol{M}_C, \boldsymbol{\Sigma}_C, \boldsymbol{M}_L, \boldsymbol{\Sigma}_L, \tilde{\mathbf{P}}_R, \tilde{\boldsymbol{L}}_R\Big) \\ \bar{N}_{\mathrm{s}}\Big(\boldsymbol{\Lambda}_{\mathrm{s}}, \tilde{\mathbf{P}}_R, \tilde{\boldsymbol{L}}_R\Big) \\ \tilde{C}_{\mathrm{r}}\Big(\tilde{\boldsymbol{C}}_{\mathrm{r}}, \tilde{\mathbf{P}}_R, \tilde{\boldsymbol{L}}_R\Big) \\ \hat{V}\Big(\tilde{\mathbf{P}}_{V|r_1}, \ldots, \tilde{\mathbf{P}}_{V|r_{n_r}}, \tilde{\boldsymbol{L}}_{V|r_1}, \ldots, \tilde{\boldsymbol{L}}_{V|r_{n_r}}, \tilde{\mathbf{P}}_R, \tilde{\boldsymbol{L}}_R\Big) \\ \tilde{L}_{\mathrm{m}} \end{bmatrix}, \tag{4.1}$$

whereas for the UFD representation it may be constructed as

$$\boldsymbol{X}_{\mathrm{UFD}}(\boldsymbol{X}_{\mathcal{OC}_{\mathrm{s}}}) \triangleq \begin{bmatrix} P_y\Big(2, \boldsymbol{\Sigma}_Y, \tilde{\mathbf{P}}_R, \tilde{\boldsymbol{L}}_R\Big) \\ \tilde{L}_{\mathrm{h}}\Big(\tilde{\boldsymbol{L}}_{\mathrm{h}}, \tilde{\mathbf{P}}_R, \tilde{\boldsymbol{L}}_R\Big) \\ \bar{N}'_C\Big(0.008, \boldsymbol{\Lambda}_C, \boldsymbol{M}_C, \boldsymbol{\Sigma}_C, \tilde{\mathbf{P}}_R, \tilde{\boldsymbol{L}}_R\Big) \\ \bar{N}_{\mathrm{s}}\Big(\boldsymbol{\Lambda}_{\mathrm{s}}, \tilde{\mathbf{P}}_R, \tilde{\boldsymbol{L}}_R\Big) \\ \hat{V}\Big(\tilde{\mathbf{P}}_{V|r_1}, \ldots, \tilde{\mathbf{P}}_{V|r_{n_r}}, \tilde{\boldsymbol{L}}_{V|r_1}, \ldots, \tilde{\boldsymbol{L}}_{V|r_{n_r}}, \tilde{\mathbf{P}}_R, \tilde{\boldsymbol{L}}_R\Big) \\ \tilde{L}_{\mathrm{m}} \end{bmatrix}, \tag{4.2}$$

where $\boldsymbol{X}_{\mathcal{OC}_{\mathrm{s}}}$ has already been introduced in Sect 4.1.

Departing from Eqs. (4.1) and (4.2), a transport application may be classified either by computing numerically the expectations of the random vectors $\boldsymbol{X}_{\mathrm{GTA}}$ and $\boldsymbol{X}_{\mathrm{UFD}}$, or alternatively by resorting again to a first-order approximation based on the propagation of uncertainty method[4], i.e., $\mathbb{E}(\boldsymbol{X}_{\mathrm{GTA}}(\boldsymbol{X}_{\mathcal{OC}_{\mathrm{s}}})) \approx \boldsymbol{X}_{\mathrm{GTA}}(\mathbb{E}(\boldsymbol{X}_{\mathcal{OC}_{\mathrm{s}}})) \equiv \boldsymbol{X}_{\mathrm{UFD}}(\boldsymbol{\mu}_{\boldsymbol{X}_{\mathcal{OC}_{\mathrm{s}}}})$ and $\mathbb{E}(\boldsymbol{X}_{\mathrm{UFD}}(\boldsymbol{X}_{\mathcal{OC}_{\mathrm{s}}})) \approx \boldsymbol{X}_{\mathrm{UFD}}(\mathbb{E}(\boldsymbol{X}_{\mathcal{OC}_{\mathrm{s}}})) \equiv \boldsymbol{X}_{\mathrm{UFD}}(\boldsymbol{\mu}_{\boldsymbol{X}_{\mathcal{OC}_{\mathrm{s}}}})$. The latter approach may be eventually preferred to avoid performing large Monte-Carlo simulations, and would moreover enable the synthesis of a unique representative sOC describing the entire application. In this context, the main reason to consider the mathematical expectation resides in the semplicity of such a choice[5]; however, there are also other strong arguments that support the adoption

[4]Here the expectation is calculated over the population of missions concerning a given road operator or customer, so it is not interpreted as conditioned to a certain transport application.

[5]For example, it is relatively easy to estimate numerically, or by resorting to some analytical approximation, the expectation of a vector-valued composite variable collecting a combination of the composite variables introduced in Sect. 3.2. Additional difficulties could be encountered if other functionals for the individual composite variables were instead considered, given that most of them are correlated.

Description	Composite variable	Estimated expectation	Approximated expectation	Relative error	Unit
Road grade length ratio	$P_y(2, \boldsymbol{\Sigma}_Y, \tilde{\mathbf{P}}_R, \tilde{\boldsymbol{L}}_R)$ $P_y(3, \boldsymbol{\Sigma}_Y, \tilde{\mathbf{P}}_R, \tilde{\boldsymbol{L}}_R)$ $P_y(6, \boldsymbol{\Sigma}_Y, \tilde{\mathbf{P}}_R, \tilde{\boldsymbol{L}}_R)$ $P_y(9, \boldsymbol{\Sigma}_Y, \tilde{\mathbf{P}}_R, \tilde{\boldsymbol{L}}_R)$	0.761 0.893 0.989 0.998	0.720 0.887 0.996 0.999	5.39% 0.68% 0.71% 0.10%	-
Mean hill length	$\tilde{L}_{\mathrm{h}}(\tilde{\boldsymbol{L}}_{\mathrm{h}}, \tilde{\mathbf{P}}_R, \tilde{\boldsymbol{L}}_R)$	728	748	2.75%	m
Number of curves	$\bar{N}'_C(0.008, \boldsymbol{\Lambda}_C, \boldsymbol{M}_C, \boldsymbol{\Sigma}_C, \tilde{\mathbf{P}}_R, \tilde{\boldsymbol{L}}_R)$	2.892	2.780	5.57%	km^{-1}
Curviness length ratio	$P_\kappa(0.008, \boldsymbol{\Lambda}_C, \boldsymbol{M}_C, \boldsymbol{\Sigma}_C, \boldsymbol{M}_L, \boldsymbol{\Sigma}_L, \tilde{\mathbf{P}}_R, \tilde{\boldsymbol{L}}_R)$	0.823	0.840	2.07%	-
Number of stops	$\bar{N}_{\mathrm{s}}(\boldsymbol{\Lambda}_{\mathrm{s}}, \tilde{\mathbf{P}}_R, \tilde{\boldsymbol{L}}_R)$	0.224	0.168	25.00%	km^{-1}
Mean legal speed	$\hat{V}(\tilde{\mathbf{P}}_{V\|r_1}, \ldots, \tilde{\mathbf{P}}_{V\|r_{n_r}}, \tilde{\boldsymbol{L}}_{V\|r_1}, \ldots, \tilde{\boldsymbol{L}}_{V\|r_{n_r}}, \tilde{\mathbf{P}}_R, \tilde{\boldsymbol{L}}_R)$	75.61	79.65	5.34%	$\mathrm{km\,h}^{-1}$

Table 4.1: Estimated and approximated expectations for the composite variables of Sect. 3.2.

of such a criterion, like that already presented in Sect. 4.1 and in Paper D.

As an example, Table 4.1 reports the error committed by the first-order approximation concerning the Västra Götaland operating cycle developed in Paper C, whereas Table 4.2 lists the set of sOC parameters for the single representative sOC parametrised using the mean vector $\boldsymbol{\mu}_{\boldsymbol{X}_{\mathcal{OC}_{\mathrm{s}}}}$. Moreover, considering both the GTA and UFD classification systems, the marginal PMFs for the road transport missions comprised in the Västra Götaland application, concerning the legal speed, mission length, and topography (only via the road grade length ratio) parameters is illustrated in Fig. 4.1. According to both the approaches outlined above, the entire transport application is labelled as `MEDIUM/L-DISTANCE/P-FLAT` by the GTA, and as `HIGH/L-DISTANCE/HILLY` by the UFD, with respect to the speed signs, mission length, and topography parameters (see Table B.1). Clearly, by visual inspection, it may be realised the overall application spans also other combinations of classes than those which is assigned to. In the very same context, the discrepancy between the labels assigned by the GTA and UFD representations is symptomatic of the fact that a non-unified interpretation of the operating environment may yield completely different results in terms of classification, and indirectly of optimal vehicle design to be selected concerning a certain application. This aspect intimately relates to the notion of representativeness discussed exhaustively in Paper C.

Another advantage connected with the availability of log data is that the conversion of information between the bird's-eye view and sOC representations is not required when dealing with the stakeholders. This aspect is particularly important since it eliminates the additional uncertainty deriving from the perception of individual drivers and road operators, which may not share the same interpretation of the external surroundings. Moreover, recalling that the relationship between the bird's-eye view and sOC descriptions is not bijective and that the resolution of the former is much lower than that of the latter, small discrepancies between the customers' perception and the actuality would potentially lead to misclassifying the transport application. In turn, this may obviously have detrimental implications concerning the selection of the optimal vehicles or fleets. By contrast, if the sOC parameters are known for all the road missions defining a certain application, the operating classes defined according to the

Model	**Parameter**	**Value (per road type)**			**Unit**
		Urban	*Rural*	*Highway*	
Road type	L_{Ri}	1.38	6.77	7.57	km
	p_{Rij}	$\begin{bmatrix}0 & 0.89 & 0.11\end{bmatrix}$	$\begin{bmatrix}0.55 & 0 & 0.45\end{bmatrix}$	$\begin{bmatrix}0.11 & 0.89 & 0\end{bmatrix}$	-
Speed signs	$v_{i\|r_k}$	$\begin{bmatrix}30 & 40 & 50\end{bmatrix}^{\mathrm{T}}$	$\begin{bmatrix}60 & 70 & 80\end{bmatrix}^{\mathrm{T}}$	$\begin{bmatrix}90 & 100\end{bmatrix}^{\mathrm{T}}$	$\mathrm{km\,h^{-1}}$
	$L_{Vi\|r_k}$	$\begin{bmatrix}0.54 & 0.49 & 1.44\end{bmatrix}^{\mathrm{T}}$	$\begin{bmatrix}0.97 & 1.36 & 6.47\end{bmatrix}^{\mathrm{T}}$	$\begin{bmatrix}7.00 & 1.83\end{bmatrix}^{\mathrm{T}}$	km
	$p_{Vij\|r_k}$	$\begin{bmatrix}0 & 0.48 & 0.52\\ 0.49 & 0 & 0.51\\ 0.45 & 0.55 & 0\end{bmatrix}$	$\begin{bmatrix}0 & 0.54 & 0.46\\ 0.32 & 0 & 0.68\\ 0.22 & 0.78 & 0\end{bmatrix}$	$\begin{bmatrix}0 & 1\\ 1 & 0\end{bmatrix}$	-
Stop signs	$\lambda_{\mathrm{s}\|r_i}$	1.18	0.10	0.06	$\mathrm{km^{-1}}$
	$t_{\mathrm{min}\|r_i}$	21.00	19.75	34.50	s
	$t_{\mathrm{max}\|r_i}$	277.00	95.19	64.79	s
Curviness	$\lambda_{C\|r_i}$	6.59	1.92	0.89	$\mathrm{km^{-1}}$
	$\mu_{C\|r_i}$	4.27	4.86	5.07	ln m
	$\sigma_{C\|r_i}$	1.03	0.92	0.82	ln m
	r_{turn}	12.5	12.5	12.5	m
	$\mu_{L\|r_i}$	3.92	3.91	3.79	ln m
	$\sigma_{L\|r_i}$	0.65	0.59	0.54	ln m
Topography	$L_{\mathrm{h}\|r_i}$	291	811	739	m
	$\sigma_{Y\|r_i}$	2.30	1.76	1.58	%

Table 4.2: Parameters for a single representative sOC, parametrised by the vector-valued mean $\boldsymbol{\mu}_{\boldsymbol{X}_{\mathcal{OC}_{\mathrm{s}}}}$.

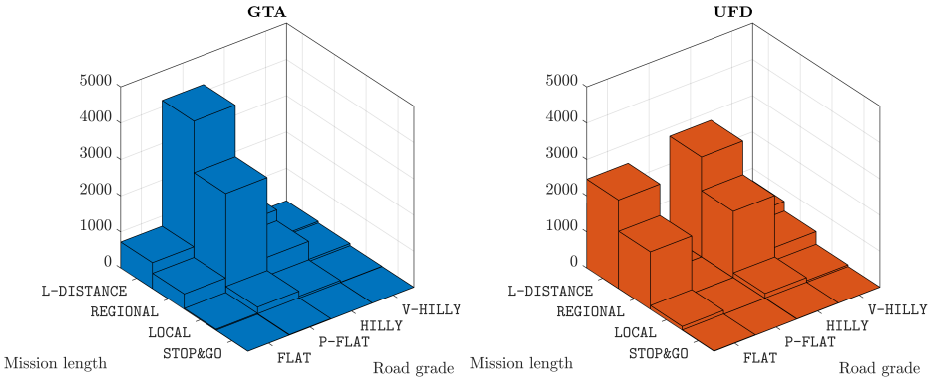

(a) Joint PMF for the mission length and road grade parameters, according to the GTA (left) and UFD (right) classification systems.

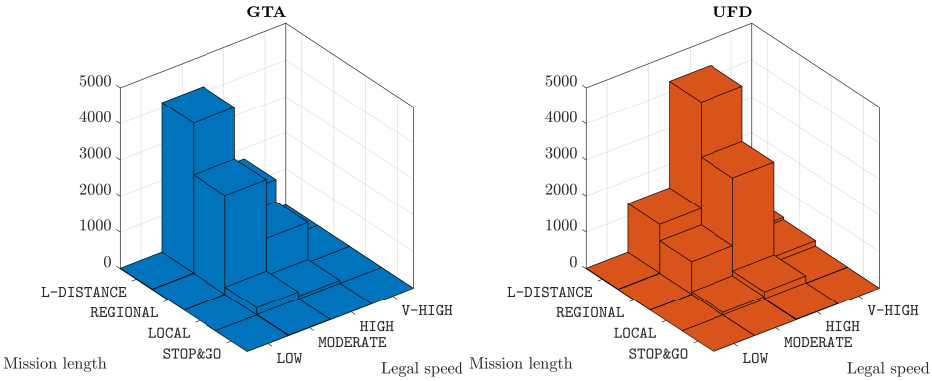

(b) Joint PMF for the mission length and legal speed parameters, according to the GTA (left) and UFD (right) classification systems.

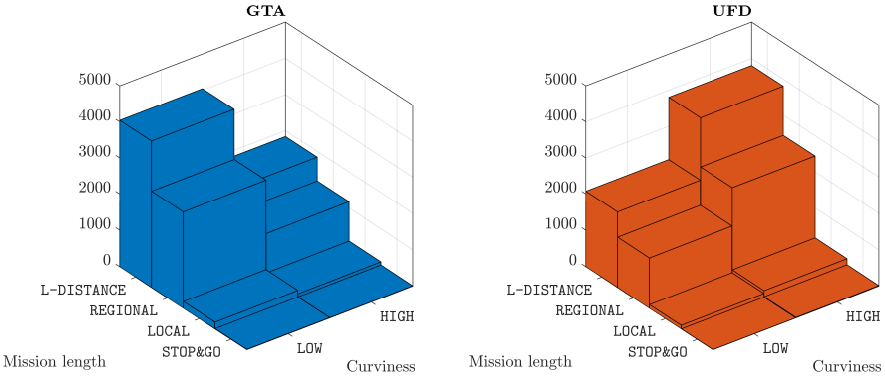

(c) Joint PMF for the mission length and curviness parameters, according to the GTA (left) and UFD (right) classification systems.

Figure 4.1: Joint PMFs for different combination of parameters according to the GTA (left) and UFD (right) bird's-eye view representations: **(a)** mission length and road grade; **(b)** mission length and legal speed; **(c)** mission length and curviness. The distributions refer to the Västra Götaland operating cycle. Figure adapted from Paper C.

bird's-eye view description may be uniquely deduced as explained in Sect 2.4.1, without any loss of information.

Finally, once an optimal vehicle or fleet has been selected for a given transport application, the energy performance may be tested in a virtual environment considering a population of missions.

4.3 Virtual testing

The last phase concerns virtual testing of optimised configurations or prototypes, considering a more accurate description of the transport application that explicitly accounts for the inherent variation between individual missions. This process exploits the connection between the sOC and dOC descriptions. In particular, similar to what was discussed in the previous Sect. 4.2, two different possibilities may be identified:

I. If log data are available from a specific customer or operator, the performance of an optimally selected vehicle or fleet, according to the processes outlined in Sects. 4.1 and 4.2, may be assessed considering the real distribution of road missions for that specific application, starting from a fully-parametrised population of sOCs.

II. In absence of log data from a specific customer, vehicle and fleet may be tested considering virtual representations of a typical transport application (described in terms of a single or multiple sOCs) for, e.g., a certain geographical area, parametrised starting from other sources.

Clearly, the first option would provide a customer with more accurate information about how much the performance can deviate from the optimal target. Concerning instead the second option, typical transport applications tailored to specific markets or geographical areas may be parametrised, for instance, starting from data logged from other road operators active in the same region. Additional information about the characteristics of the intended usage may also be supplemented by external sources, including services similar to the above-mentioned SMHI and Trafikverket. Generally speaking, vehicle manufacturers such as Volvo and Scania do have access to large databases that enable them to parametrise regional applications in terms of sOCs. In the context of the present thesis, the Västra Götaland operating cycle developed in Paper C may be adduced as an emblematic example of such a description.

Starting from a fully parameterised sOC, a virtually infinite number of dOCs may be synthesised and integrated with dynamic models for the vehicle and the driver. In this way, performance may be assessed by exploiting the natural connection between the two levels of representation. Remarking again that two dOCs originating from the sOC are only statistically equivalent, it is worth observing that simulating a complete vehicle model would then produce a distribution in performance rather than a scalar metric. This is represented graphically in Fig. 4.2.

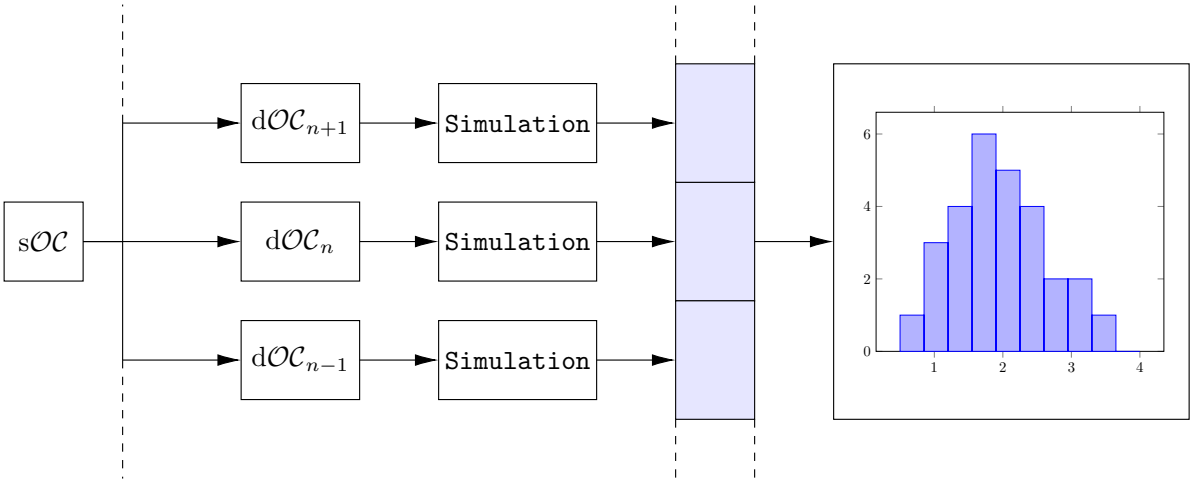

Figure 4.2: A stochastic operating cycle (sOC) may be used to synthesise different deterministic realisations (dOCs) which share the same statistical properties. The distribution in performance produced by a specific combination of sOC parameters and vehicle's specification may be evaluated by simulating each dOC and clustering the output data. Figure adapted from Paper A.

In the same context, it should be mentioned that virtual testing may be performed concerning either an entire population of sOCs or a single parametrisation, built opportunely so as to be representative of the whole application. This may again be done by estimating numerically or analytically the mean values for the sOC parameters interpreted as random variables. If the objective consists in predicting the mean performance for a certain application, both options are viable and ultimately equivalent, according to the discussion in Sect. 4.1 and Paper C. Indeed, simulating a unique sOC parametrised using the expected values for the sOC parameters would again ensure the consistency of the estimated mean performance according to both methods. A proper assessment of the variation in performance would instead require considering all the individual missions that define the application. Concerning the Västra Götaland application developed in Paper C, an example of the discrepancy between the two strategies is illustrated in Fig. 4.3, where the distribution of CO_2 emissions obtained by considering a unique reference sOC, parametrised according to the values reported in Table 4.2, is compared to that produced by simulating the complete population of missions. Unfortunately, whilst the mean emissions almost coincide, analogous considerations cannot be extended to other statistical indicators like the variance. However, it should be clarified that, in the context of virtual testing, reducing the dimension of the problem, particularly the number of simulations to be run, is not as crucial as in the optimisation phase.

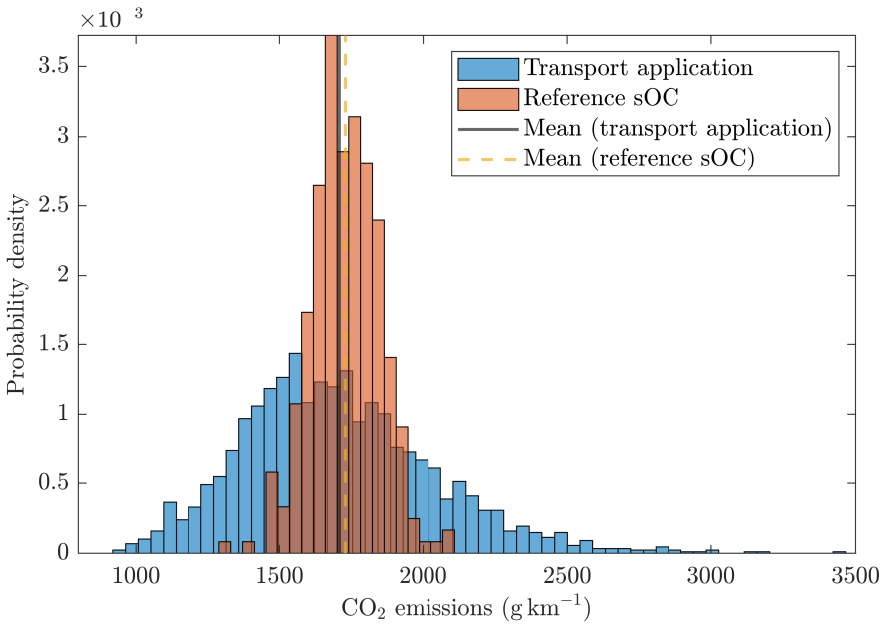

Figure 4.3: Distribution of CO_2 emissions estimated in simulation by generating dOCs according to both the entire transport application (blue histogram) and the reference sOC (orange histogram). Figure adapted from Paper C.

Chapter 5

Discussion, conclusions and future research

The present chapter summarises the main results of the thesis, also providing an outlook on future research.

5.1 Discussion and conclusions

In the introducory chapter, four main research objectives were identified. The first three were related to the representation, variation, and classification problems and were mainly theoretical in nature; the fourth concerned the practical usefulness of the OC description, in conjunction with its concrete applicability. The formulation of these four problems was motivated by the necessity of developing more energy-efficient vehicles, in order to contrast the threat posed by climate change and support the development of a sustainable transportation system.

To address the representation and variation problems, the OC format has been extended to include new stochastic models and parameters for the weather, traffic and mission categories. These have been introduced in Paper A and E, respectively, and discussed in more general terms in Chap. 2. To establish a continuity with the original sOC formulation, relatively simple descriptions, based, e.g., on Markovian and autoregressive processes, have been preferred. The outcome is an enriched collection of stochastic models and parameters, which can be used to describe the statistical properties of a transport mission. The enhanced framework has been conceived to allow for modularity and to preserve the mutual independence between the preexisting road models and the new ones. At the same time, parsimony has been achieved by defining a new primary model for the weather category: seasonality. In this way, it has been possible to introduce a high level of diversification without resorting to complicated multivariate distributions. Starting from the novel sOC description, synthetic operating cycles may be generated which are able to reproduce dynamically the weather

and traffic characteristics. These may be used as a virtual environment for detailed vehicle dynamics simulations. For example, an investigation of the effect of the weather and traffic settings on the vehicle's performance has been presented in Paper A. More specifically, a categorical analysis has been made to assess the influence of seasonality and traffic regime (free or congested) on CO_2 emissions. It has been shown that both factors play a major role in determining the vehicle's response, but simulation results have not been corroborated experimentally. The principal reason why the study has been limited to the theoretical domain is that information about weather and traffic conditions is generally not available from log data and needs to be supplemented by external databases. In any case, similar studies to that conducted in Paper A may be carried out concerning other performance indicators than energy efficiency.

The classification and variation problems have been simultaneously addressed in Paper B, where the connection between the bird's-eye view and sOC representations has been explored in detail. By taking inspiration from two existing descriptions in use by vehicle manufacturers, namely the GTA and UFD systems, a method to statistically analyse and classify road transport missions and applications has been proposed. The suggested approach exploits the non-bijective relationship between the two above-mentioned levels of the OC format and allows one to qualify road missions based on physical quantities that are easy to estimate and interpret. More specifically, the notion of an operating class has been introduced in Paper B, which consists of a mathematical relationship connecting the sOC parameters to the bird's-eye view metrics and thresholds. The method has been exemplified considering a number of individual road operations, as well as entire transport applications. In the same context outlined above, it is worth observing that the limits imposed by the GTA and UFD systems are sometimes ambiguous, and it is also unclear how they have been specified. Therefore, concerning the pure classification problem, a technique to optimally prescribe thresholds for certain classes of parameters, summarised concisely in Chap. 3, has been first proposed in Paper D. The envisioned method departs from the definition of some vehicle-independent energy metrics to maximise the variation in performance amongst a target number of classes and relies again on the relationship existing between the bird's-eye view and the sOC.

The representation, variation and classification problems have also been dealt with in Paper C, in which an OC complete with all the stochastic road models discussed in Sect. 2.2.1 has been parametrised starting from log data collected from vehicles operating in the region of Västra Götaland, Sweden. In Paper C, the potential of the OC has also been exemplified concerning real applications, including certification of early prototypes and production planning. These aspects relate to the fourth research question formulated in the present thesis and formalised in the so-called application problem. The discussion initiated in Paper C has been further extended in Chap. 4, considering the applicability of the OC machinery to the entire process of product development, optimal selection, and virtual testing of commercial vehicles, depending on the characteristics of the intended application. In particular, it was argued that the three levels of description comprised in the OC format, namely the bird's-eye view, the sOC and the dOC, can cooperate synergically to assist

vehicle manufacturers in the design of more energy-efficient vehicles. In this context, the preliminary optimisation phase outlined in Sect. 4.1 requires an accurate description of the entire application to which the vehicle should be tailored. It has been shown, using a simple mathematical argument, that the dimension of the problem may be enormously reduced by considering a mean sOC in place than the actual distribution of missions encompassing the application. Even resorting to this expedient, the optimisation process may be expected to be computationally expensive. The recent trend towards quantum computing may offer an adequate solution to tackle the problem in a few years.

5.2 Future research

Thus far, this thesis may appear to be an apology for the operating cycle description. Quite the contrary, it should be regarded instead as a constructive criticism of the OC concept. Indeed, there are still numerous issues to tackle, and enormous margins for improvement.

To start, one of the greatest limitations of this work is connected with the difficulty to provide a unique, scientific method to classify road transport missions. Taking inspiration from the GTA and UFD representations, the duality between the bird's-eye view and the sOC has been explored to a large extent, but it is still unclear whether this approach is generally good, or can be significantly improved. The metrics and labels used so far have been demonstrated to be representative of variations in usage, but this is not necessarily reflected in variations in performance. Moreover, it would be amenable for all the interacting stakeholders who take part in the development, selection, testing and certification processes to share a unique classification system. This aspect intimately relates to the notion of representativeness introduced in Paper D, and highlights the need for a unified description of a transport mission. Whilst there is no current scientific evidence that the GTA and UFD descriptions may effectively support the internal processes of vehicle manufacturers, empirical findings may eventually corroborate this hypothesis.

How to choose metrics and thresholds is an open and interesting question. As shown in Paper D, one choice could be to formalise it as an optimisation problem and then solve it analytically or numerically. This however implies the need to identify vehicle-independent metrics. Alternative approaches may reveal to be more suited for this purpose. Currently, vehicle manufacturers like Volvo and Scania have access to an enormous database that provides detailed information about the distribution of sOC parameters amongst different transport applications. In fact, understanding how the sOC parameters vary over entire populations of missions is crucial when it comes to specifying metrics and thresholds in a way that is independent of the vehicle's design, in accordance with the very fundamental philosophy animating the OC framework.

Descending the hierarchical ordering of OC representations, another intriguing option concerns the stochastic modelling of the mission properties. So far, statistical models have been introduced almost exclusively for the road, weather and traffic categories. A first attempt

to develop an equivalent description for the mission properties has been made in Paper E, limitedly to the cargo weight parameter. With few exceptions [64, 65], stochastic approaches are not common in this context, and therefore this could potentially represent a research topic even in isolation. Furthermore, there is the tangible risk that stochastic models for the mission might not be developed to be completely independent of the vehicle itself. This was also evident concerning the stochastic model for proposed in Paper E, which was developed based on a specific vehicle topology. Indeed, whilst the road, the weather and the traffic are separate entities which exist before the transport operation, vehicles are developed with a specific purpose in mind. From this perspective, the problem is soon complicated when considering that the mission properties should probably be estimated from log data, implying unavoidably some sort of contamination. The question seems to be rather delicate, and dedicated approaches may be required to overcome these difficulties. Eventually, the same building principles of the OC description might contrast with the need for stochastic modelling of the mission. Another important add-on to the current version of the framework would include the external infrastructure, *in primis* fuel and charging stations. Whether to include these features amongst the road parameters is debatable, but the need for stochastic models is quite obvious, especially in conjunction with the possibility of using the OC format for optimisation analyses online (see, e.g., [23–25, 87]). Furthermore, in this thesis, as well as in the appended paper, the weather models have been consistently assumed to be independent of the road type. This simplification may be removed to improve the accuracy of the description, for example considering that in urban areas the air temperature may increase due to the presence of conditioning systems, or using different parameters for the logarithmic speed profile of the wind.

Finally, by exploiting the inherent uncertainty of the sOC representation, the methods of stochastic calculus may be applied to model the longitudinal dynamics of vehicles stochastically, specifically using a system of stochastic differential equations (SDEs) [138, 139]. This approach, very innovative and peculiar concerning the context explored in this thesis, would eventually not be dissimilar to those adopted in some branches of physics, like molecular dynamics and quantum mechanics. From this perspective, a particularly interesting opportunity would reside in the fact that, starting from an SDE-based formalism, a Fokker-Planck equation may be derived describing the PDF of the required power output along the vehicle's trajectory [140], depending on the stochastic behaviour of the road and traffic parameters[1]. This information may be then converted into a certain distribution concerning the total energy consumption, enabling faster estimation than simulating a large number of sOCs and dOCs, as well as the synthesis of a refined classification system according to the principles discussed in Sect. 3.3. This research line, combining methods and analytical tools from PDE and SDE theories with the theoretical foundation of the sOC, has recently started and is currently ongoing.

Concerning the dOC description, there are several chances for improvement. All the vehicle models used in this thesis are in fact very simple, with a reduced number of components.

[1]For example, the simple AR(1) model used for topography may be approximated exactly by a continuous Ornstein-Uhlenbeck process for any value of the sampling length L_s.

There is nothing really new in this direction, however, and the development of more realistic models should definitely not represent the true core of future research. The driver constitutes perhaps the unique exception. At present, the model is split into a tactical and operational part, as detailed in Appendix A.2. The former interprets the external stimuli coming from the environment and translates them into the desired speed input. Mathematical relationships have been derived only for some dOC parameters (curviness, speed bumps, legal speed, traffic density), but other factors might be influential as well. This is the case, for example, of precipitation amount: a driver may prefer to travel slower in case of heavy rain. Understanding the correlation existing especially between some weather parameters and the speed set by the driver is an involving task. It may be anticipated that some relationships will need to be established starting from empirical evidence rather than deductive principles. In this context, it would be crucial to collect a large amount of data to make a statistical inference, or to perform dedicated experiments. Virtual settings built in a driver simulator are mainly effective to study the influence of road parameters, but other approaches could be advantageous when it comes to weather or traffic. A preliminary effort has been already made in this sense, but both aspects need to be explored more in detail. The operational module of the driver is instead based on a simple PID controller, which tries to replicate human behaviour during normal driving conditions. A possible direction for future research would be to account for different driving styles. In fact, several studies have shown that it is possible to distinguish amongst different driver categories (aggressive, mild, etc.), but at present only one generic set of parameters is used.

The last direction which should be indicated is more broadly connected with the overall idea behind the OC concept. As remarked throughout the whole thesis, the format has been conceived to assist vehicles manufacturer in product development, from the early stage to the sale phases. Possible applications in the context of product development, selection, and testing have been extensively discussed. However, the applicability of the OC format should not be limited to virtual models of physical products. Algorithms and control strategies may be effectively tested and validated in simulation environments. An opportunity for future research resides therefore in the possibility of using the OC description (or some methods and tools borrowed from it) for online estimation. The idea has only been formulated in embryonic form, but can be worthy of further investigations.

Appendix A

VehProp

VehProp is a modular, open platform for simulations of longitudinal vehicle dynamics. It classifies as a simplified version of the virtual environments adopted internally by vehicle manufacturers and consists of three main modules that interact dynamically: the operating cycle, the driver, and the vehicle itself. It was originally developed to conduct studies on powertrain efficiency and has been gradually improved over the years to allow more extensive investigations concerning longitudinal motion. The present appendix provides an introduction to VehProp to the extent that is necessary to understand the thesis, as well as the findings of the appended papers.

A schematic of the three models included in VehProp, along with a typical workflow of signals, is illustrated in Fig. A.1.

A.1 Operating cycle model

The first model discussed here is that of an OC. By acting in cooperation with the vehicle and driver models, this should be able to translate the static information encoded in the dOC into dynamic signals. This operation is executed by interpolating between the sequences of values for each physical quantity, based on either time, position, or both. More formally, denoting the dynamic values of the dOC parameters by $\mathcal{OC}_{\mathrm{dyn}}$, an interpolator operator may be defined as $I_{\mathrm{dyn}} : \mathcal{OC}_{\mathrm{d}} \mapsto \mathcal{OC}_{\mathrm{dyn}}$. The parameters relating to the road category only depend on the position of the vehicle along the route, whereas the quantities in the weather category are assumed to only vary with time for the sake of simplicity. Conversely, the parameters labelled as traffic and mission may exhibit strong dependencies on time and position and hence require both as input.

In addition, concerning the mission category, the current value of the vehicle's speed is necessary to separate the two opposite situations of standstill and motion, which are handled via a state machine. This separates the two behaviours by scanning through the dOC mission parameters and extracting all the standstill events in a sequence of action matrices. The action matrices describe the actions to execute whilst at standstill. The resulting lean

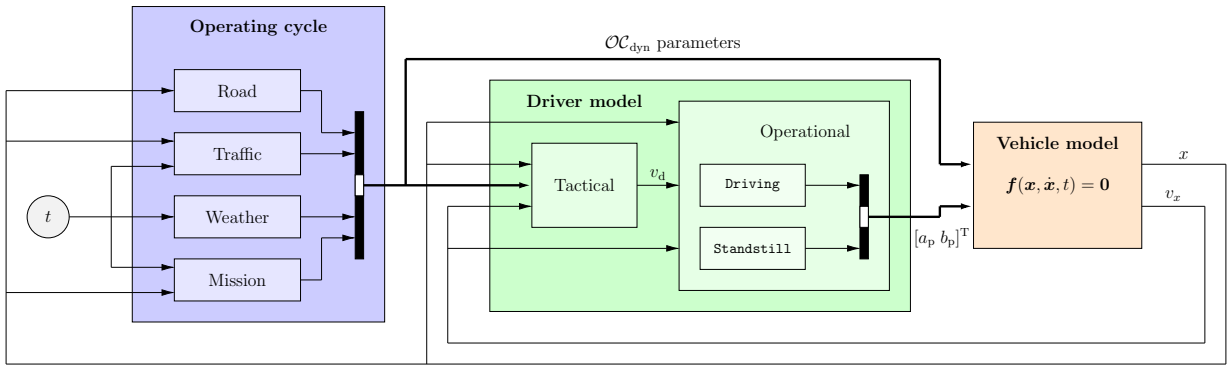

Figure A.1: Schematic representation of the three main modules comprised in VehProp, with a typical workflow. Figure adapted from Paper A.

mission parameters depend explicitly only upon the position along the trajectory, whereas the information encoded in the action matrices is only made dependent on time. The current implementation of VehProp involves two different modules for motion and standstill. The state machine deliberates which one should be active and keeps track of which action matrix to use. The standstill time consists of the total duration of all the actions that need to be executed during the stops, whereas the stop zone defines the effective length of the site. Additional details are given in [18].

A.2 Driver model

In VehProp, the driver model mainly serves as a connection between the dynamic OC model and the vehicle. It must interpret the information concerning the operating environment, originally encoded in the dOC format and then opportunely translated into dynamic parameters, into control actuator signals. To this end, it is split into a tactical and an operational part. The former interprets the OC parameters based on simplified physical models and converts them into a desired speed input for the operational driver. The underlying assumption is that the driver wants to travel as fast as possible, in compliance with legal and comfort criteria. Therefore, at each time step and position, the final desired speed v_{d} is chosen as:

$$v_{\text{d}} = \min\Big(v_{\text{sign}}, v'_{\text{sign}}, v_{\kappa}, v'_{\kappa}, v_{\text{b}}, v'_{\text{b}}, v_{\text{stop}}, v'_{\text{stop}}, v_{\text{t}}, v'_{\text{t}}\Big), \tag{A.1}$$

where the generic v_p is function of the dynamic OC parameters, i.e., $v_p = f_p(\mathcal{OC}_{\text{dyn}})$. More specifically, the speeds v_{sign}, v_{κ}, v_{b} and v_{stop} correlate with the legal speed limit, road curvature κ, speed bumps and stops, respectively. Concerning the stop signs, the corresponding desired speed is automatically set to zero, i.e., $v_{\text{sign}} = 0$. The functions $f_p(\cdot)$ corresponding to the desired speeds for curvature and speed bumps are given in [75] and reported here for completeness.

Starting with the curvature, it is assumed that the driver has a maximum lateral acceleration limit, $|a_y| \leq a_y^{\max}$, above which they are not comfortable driving. A simple kinematical relationship implies

$$v_\kappa(\kappa) = \sqrt{\frac{a_y^{\max}}{\kappa}}. \tag{A.2}$$

Concerning the speed bumps, an empirical formula is used based on the results reported in [141], in which was found that a mean speed $\bar{V}_\mathrm{b}$ may be observed for a a certain bump type with given height, length and geometry. Accordingly, the equation is postulated as follows:

$$v_\mathrm{b}(\beta) = C_1 \frac{\pi/2 - \beta}{\beta} + C_2, \tag{A.3}$$

where β denotes the angle describing the bump deflection, and C_1 and C_2 are two constants chosen such that $v_\mathrm{b}(\beta_0) = \bar{V}_\mathrm{b}$ and $v_\mathrm{b}(\pi/2) = V_\mathrm{b}^{\min}$.

An expression for the traffic speed v_t has been introduced in Paper A and is based on an equilibrium equation relating the traffic density and the flow speed, according to

$$v_\mathrm{t}(\rho_\mathrm{t}) = v_\mathrm{f}\left(1 - \frac{\rho_\mathrm{t}}{\rho_\mathrm{c}}\right), \tag{A.4}$$

where v_f represents the *free-flow* speed, i.e., the traffic speed corresponding to have almost no vehicle on the road, and ρ_c is the *critical density*.

Furthermore, for each speed v_p, a corresponding *dynamic* value is calculated as

$$v_p' = \sqrt{v_{p,i+1} - 2a_x^{\max}(x_{i+1} - x)}, \tag{A.5}$$

where x is the current position, x_{i+1} the next (discrete) position at which the speed v_p changes value, and $a_x^{\max}$ denotes the maximum lateral acceleration threshold. Once the desired speed has been set, the operational part of the driver computes the difference between the desired and the actual speed to produce the pedal outputs $a_\mathrm{p}, b_\mathrm{p} \in [0, 1]$. In paper A, as well as in the current implementation of VehProp, the operational part of the driver is modelled using a PID controller. Specifically, the expressions for a_p and b_p read as follows:

$$a_\mathrm{p} = \frac{1}{2} f_\mathrm{PID}(v_\mathrm{d} - v_x)\Big[1 + \mathrm{sgn}\big(f_\mathrm{PID}(v_\mathrm{d} - v_x)\big)\Big], \tag{A.6a}$$

$$b_\mathrm{p} = -\frac{1}{2} f_\mathrm{PID}(v_\mathrm{d} - v_x)\Big[1 - \mathrm{sgn}\big(f_\mathrm{PID}(v_\mathrm{d} - v_x)\big)\Big], \tag{A.6b}$$

where $f_\mathrm{PID}(\cdot)$ is the function describing the PID control law.

A graphical illustration of the driver module, together with the input and output quantities, is given in Fig. A.2.

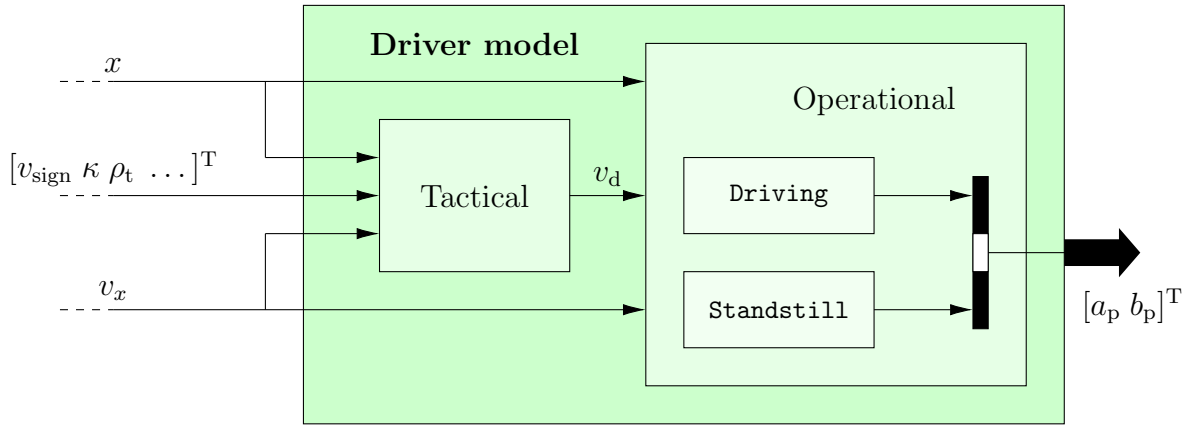

Figure A.2: Schematic representation of the driver model. The inputs to the module are the vehicle's longitudinal speed and position $[v_x\ x]^{\text{T}}$ and the dynamic OC parameters $\mathcal{OC}_{\text{dyn}}$ which determine the speeds in Eq. (A.1). The outputs are the acceleration and brake pedal positions $[a_{\text{p}}\ b_{\text{p}}]^{\text{T}}$. Figure adapted from Paper A.

A.3 Vehicle model

The model used in the current implementation of VehProp approximates the vehicle with a point-mass and neglects the tyre slip. Owing to these assumptions, the total longitudinal force acting at the tyres' contact patch may be deduced as $F_x = (T_{\text{d}} - T_{\text{b}}\,\text{sgn}(v_x))/R_{\text{w}}$, where T_{d} and T_{b} are the total driving torque reported at the wheels and the braking torque, respectively. Therefore, the governing equations for the longitudinal vehicle dynamics can be derived as follows:

$$m^*\dot{v}_x = \frac{T_{\text{d}} - T_{\text{b}}\,\text{sgn}(v_x)}{R_{\text{w}}} - F_{\text{grade}} - F_{\text{roll}} - F_{\text{air}}, \qquad v_x \neq 0, \tag{A.7a}$$

$$F_{\text{b}} = F_{\text{grade}} + F_{\text{roll}} + F_{\text{air}} - \frac{T_{\text{d}}}{R_{\text{w}}}, \qquad |F_{\text{b}}| \leq \frac{T_{\text{b}}}{R_{\text{w}}}, \tag{A.7b}$$

where $m^* = m + J_{\text{w}}/R_{\text{w}}^2$ is given by the total mass of the vehicle plus the sum of the reduced rotational inertias J_{w}, R_{w} is the wheel radius, v_x its longitudinal speed, F_{grade} is the longitudinal projection of the gravitational force in the vehicle reference frame, F_{roll} is the rolling resistance, and F_{air} the drag force. The resistive forces appearing in Eq. (A.7a) read specifically

$$F_{\text{grade}} = -mg\sin\alpha, \tag{A.8a}$$

$$F_{\text{roll}} = f_{\text{r}}mg\cos\alpha, \tag{A.8b}$$

$$F_{\text{air}} = \frac{1}{2}\rho_{\text{air}}C_{\text{d}}A\left|v_x^{\text{rel}}\right|v_x^{\text{rel}}, \tag{A.8c}$$

where α is the road slope angle defined according to ISO 8855, f_r is the rolling resistance coefficient, ρ_air the air density, C_d the drag coefficient, A the effective frontal area and v_x^rel is the relative speed between the vehicle and the wind. Equations (A.7a) and (A.7b) are valid under normal driving conditions and at standstill.

The torques T_d and T_b in Eqs. (A.7) are calculated starting from the engine torque T_e and the output from the operational part of the driver as

$$T_\mathrm{d} = \eta_\mathrm{t} i_\mathrm{g} i_\mathrm{FD} \left(T_\mathrm{e} - \frac{P_\mathrm{PTO}}{\omega_\mathrm{e}} \right), \tag{A.9a}$$

$$T_\mathrm{b} = T_\mathrm{b}^\mathrm{max} b_\mathrm{p}, \tag{A.9b}$$

where i_g and i_FD are the gear ratio and final drive gear, and η_t is the overall efficiency of the transmission. In turn, the engine torque T_e is modelled using steady-state maps as a function of the engine speed ω_e and fuel injection q:

$$T_\mathrm{req} = T_\mathrm{e}^\mathrm{max} a_\mathrm{p}, \tag{A.10a}$$

$$q = f_q\big(\omega_\mathrm{e}, T_\mathrm{req}\big), \tag{A.10b}$$

$$T_\mathrm{e} = f_T\left(\omega_\mathrm{e}, q\right), \tag{A.10c}$$

where the mappings $f_T(\cdot,\cdot)$ and $f_q(\cdot,\cdot)$ are given in the form of look-up tables.

For a vehicle equipped with an internal combustion engine, the total mass of fuel may be calculated departing from Eqs. (A.10) as

$$m_\mathrm{f} = \int_{t_0}^{t_\mathrm{f}} \gamma \omega_\mathrm{e} q \, \mathrm{d}t, \tag{A.11}$$

in which t_0 and t_f are the initial and final times, and γ is a proportionality constant. The corresponding mass of CO_2 is then computed from Eq. (A.11) by multiplying for the factor c_f, expressed in grams of CO_2 per kilogram of fuel.

A graphical illustration of the vehicle module, together with the input and output quantities, is shown in Fig. A.3.

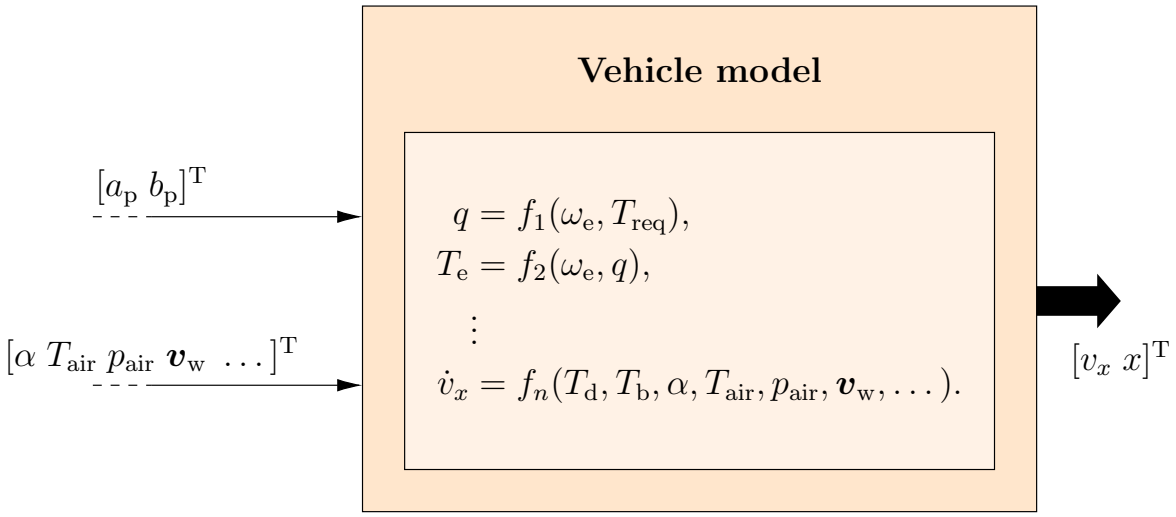

Figure A.3: Schematic representation of the vehicle, modelled as a system of DAEs. The inputs to the module are the acceleration and brake pedal positions $[a_\mathrm{p}\ b_\mathrm{p}]^\mathrm{T}$ and the dynamic OC parameters $\mathcal{OC}_\mathrm{dyn}$ in Eqs. (A.8). The outputs are the vehicle's longitudinal speed and position $[v_x\ x]^\mathrm{T}$. The functions $f_1(\cdot,\cdot)$ and $f_2(\cdot,\cdot)$ correspond specifically to the ones on the right-hand side of the last two Eqs. (A.10). Figure adapted from Paper A.

Appendix B

The GTA and UFD systems

The GTA and UFD classification systems developed by Volvo and Scania are conceived as high-level representations targeting individual road missions, as well as entire transport applications. They have been refined over the years in an iterative process, and are intended to facilitate the interaction with the customer during the selection and sales stages. To this end, they describe the operating environments using colloquial tones and statements, which may however be reformulated in terms of statistical indicators, including mathematical expectations and probabilities. Imposing limits and thresholds on these, the GTA and UFD systems build a discrete representation of the usage. Consequently, a transport application may be qualified by resorting to a countable number of labels, each of them relating to a certain operating class.

For the sake of brevity, the original formulation of each operating class is not discussed in this appendix, whereas Table B.1 lists the classes specified by both the GTA and UFD representations in mathematical form, with respect to the different relationships derived in Chap. 3 concerning the road and mission categories. In this context, the quantities appearing in Table B.1 should be interpreted as realisations of the composite variables introduced in Sects. 3.2.1 and 3.2.3. It is worth mentioning that the original classification systems are actually deficient in the mean hill length parameter and, concerning the topography, completely qualify a mission depending on the value of the road grade length ratio. Moreover, the GTA description does not include any indication about the mean speed. However, in this thesis, and also in Paper C, the latter parameters have been added to allow for a fair comparison with the UFD system. In this context, the values for the speed limits have been inspired by the stochastic model for the road type. Finally, the value $\kappa = 0.008\ \mathrm{m}^{-1}$ appearing in both the expressions for the expected number of curves and the curviness length ratio corresponds to a speed reduction of nearly 20% when driving at $70\ \mathrm{km\,h}^{-1}$ (Paper B).

Concerning the stochastic models falling in the weather and traffic categories reported in Sect. 2.2, the GTA and UFD do not explicitly specify thresholds for the relative humidity, precipitation intensities, and traffic density parameters. On the other hand, the ambient temperature is treated differently in the GTA and UFD classification systems and deserves

Model	Variable	Operating Class	GTA Relationship	UFD Relationship
Topography	Road grade length ratio	FLAT	$p_y(3, \boldsymbol{\sigma}_Y, \mathbf{P}_R, \boldsymbol{L}_R) > 0.98$	$p_y(2, \boldsymbol{\sigma}_Y, \mathbf{P}_R, \boldsymbol{L}_R) \geq 0.8$
		P-FLAT	$p_y(6, \boldsymbol{\sigma}_Y, \mathbf{P}_R, \boldsymbol{L}_R) > 0.98$	-
		HILLY	$p_y(9, \boldsymbol{\sigma}_Y, \mathbf{P}_R, \boldsymbol{L}_R) > 0.98$	$0.6 \leq p_y(2, \boldsymbol{\sigma}_Y, \mathbf{P}_R, \boldsymbol{L}_R) < 0.8$
		V-HILLY	else	else
	Mean hill length	SHORT	$L_\mathrm{h}(\boldsymbol{L}_\mathrm{h}, \mathbf{P}_R, \boldsymbol{L}_R) \leq 500$	$L_\mathrm{h}(\boldsymbol{L}_\mathrm{h}, \mathbf{P}_R, \boldsymbol{L}_R) \leq 500$
		MEDIUM	$500 < L_\mathrm{h}(\boldsymbol{L}_\mathrm{h}, \mathbf{P}_R, \boldsymbol{L}_R) \leq 1000$	$500 < L_\mathrm{h}(\boldsymbol{L}_\mathrm{h}, \mathbf{P}_R, \boldsymbol{L}_R) \leq 1000$
		LONG	$1000 < L_\mathrm{h}(\boldsymbol{L}_\mathrm{h}, \mathbf{P}_R, \boldsymbol{L}_R) \leq 1500$	$1000 < L_\mathrm{h}(\boldsymbol{L}_\mathrm{h}, \mathbf{P}_R, \boldsymbol{L}_R) \leq 1500$
		V-LONG	else	else
Curviness	Number of curves	LOW	-	$\bar{n}'_C(0.008, \boldsymbol{\lambda}_C, \boldsymbol{\mu}_C, \boldsymbol{\sigma}_C, \mathbf{P}_R, \boldsymbol{L}_R) \leq 2$
		HIGH	-	else
	Curviness length ratio	LOW	$p_\kappa(0.008, \boldsymbol{\lambda}_C, \boldsymbol{\mu}_C, \boldsymbol{\sigma}_C, \boldsymbol{\mu}_L, \boldsymbol{\sigma}_L, \mathbf{P}_R, \boldsymbol{L}_R) > 0.8$	-
		HIGH	else	-
Stop signs	Number of stops	FLUID	$\bar{n}_\mathrm{s}(\boldsymbol{\lambda}_\mathrm{s}, \mathbf{P}_R, \boldsymbol{L}_R) \leq 0.2$	$\bar{n}_\mathrm{s}(\boldsymbol{\lambda}_\mathrm{s}, \mathbf{P}_R, \boldsymbol{L}_R) \leq 0.2$
		LIGHT	$0.2 < \bar{n}_\mathrm{s}(\boldsymbol{\lambda}_\mathrm{s}, \mathbf{P}_R, \boldsymbol{L}_R) \leq 0.5$	$0.2 < \bar{n}_\mathrm{s}(\boldsymbol{\lambda}_\mathrm{s}, \mathbf{P}_R, \boldsymbol{L}_R) \leq 0.5$
		RESIDENTIAL	$0.5 < \bar{n}_\mathrm{s}(\boldsymbol{\lambda}_\mathrm{s}, \mathbf{P}_R, \boldsymbol{L}_R) \leq 1.5$	$0.5 < \bar{n}_\mathrm{s}(\boldsymbol{\lambda}_\mathrm{s}, \mathbf{P}_R, \boldsymbol{L}_R) \leq 1.5$
		DENSE	$1.5 < \bar{n}_\mathrm{s}(\boldsymbol{\lambda}_\mathrm{s}, \mathbf{P}_R, \boldsymbol{L}_R) \leq 2.5$	$1.5 < \bar{n}_\mathrm{s}(\boldsymbol{\lambda}_\mathrm{s}, \mathbf{P}_R, \boldsymbol{L}_R) \leq 2.5$
		START&STOP	$2.5 < \bar{n}_\mathrm{s}(\boldsymbol{\lambda}_\mathrm{s}, \mathbf{P}_R, \boldsymbol{L}_R) \leq 5$	$2.5 < \bar{n}_\mathrm{s}(\boldsymbol{\lambda}_\mathrm{s}, \mathbf{P}_R, \boldsymbol{L}_R) \leq 5$
		VF-START&STOP	else	else
Road roughness	Mean roughness	SMOOTH	$C_\mathrm{r}(\boldsymbol{C}_\mathrm{r}, \mathbf{P}_R, \boldsymbol{L}_R) \leq 16 \cdot 10^{-6}$	$C_\mathrm{r}(\boldsymbol{C}_\mathrm{r}, \mathbf{P}_R, \boldsymbol{L}_R) \leq 16 \cdot 10^{-6}$
		ROUGH	$16 \cdot 10^{-6} < C_\mathrm{r}(\boldsymbol{C}_\mathrm{r}, \mathbf{P}_R, \boldsymbol{L}_R) \leq 64 \cdot 10^{-6}$	$16 \cdot 10^{-6} < C_\mathrm{r}(\boldsymbol{C}_\mathrm{r}, \mathbf{P}_R, \boldsymbol{L}_R) \leq 64 \cdot 10^{-6}$
		V-ROUGH	$64 \cdot 10^{-6} < C_\mathrm{r}(\boldsymbol{C}_\mathrm{r}, \mathbf{P}_R, \boldsymbol{L}_R) \leq 256 \cdot 10^{-6}$	$64 \cdot 10^{-6} < C_\mathrm{r}(\boldsymbol{C}_\mathrm{r}, \mathbf{P}_R, \boldsymbol{L}_R) \leq 256 \cdot 10^{-6}$
		OFF-ROAD	else	else
Speed signs	Mean legal speed	LOW	$\hat{v}(\mathbf{P}_{V\|r_1}, \ldots, \boldsymbol{L}_{V\|r_1}, \ldots, \mathbf{P}_R, \boldsymbol{L}_R) \leq 50$	$\hat{v}(\mathbf{P}_{V\|r_1}, \ldots, \boldsymbol{L}_{V\|r_1}, \ldots, \mathbf{P}_R, \boldsymbol{L}_R) \leq 50$
		MEDIUM	$50 < \hat{v}(\mathbf{P}_{V\|r_1}, \ldots, \boldsymbol{L}_{V\|r_1}, \ldots, \mathbf{P}_R, \boldsymbol{L}_R) \leq 80$	$50 < \hat{v}(\mathbf{P}_{V\|r_1}, \ldots, \boldsymbol{L}_{V\|r_1}, \ldots, \mathbf{P}_R, \boldsymbol{L}_R) \leq 70$
		HIGH	else	$70 < \hat{v}(\mathbf{P}_{V\|r_1}, \ldots, \boldsymbol{L}_{V\|r_1}, \ldots, \mathbf{P}_R, \boldsymbol{L}_R) \leq 90$
		V-HIGH	-	else
Mission length	Mission length	STOP&GO	$L_\mathrm{m} < 0.5$	$L_\mathrm{m} < 0.5$
		LOCAL	$0.5 \leq L_\mathrm{m} < 5$	$0.5 \leq L_\mathrm{m} < 5$
		REGIONAL	$5 \leq L_\mathrm{m} < 50$	$5 \leq L_\mathrm{m} < 50$
		L-DISTANCE	else	else

Table B.1: Operating classes according to the GTA and UFD classification system. The limits on the mean hill length L_h are expressed in m; those for the expected number of curves and stop signs $\bar{n}'_C$ and $\bar{n}_\mathrm{s}$, respectively, in km^{-1}; the thresholds on the mean legal speed $\hat{v}$ are prescribed in $\mathrm{km\,h}^{-1}$; finally, the limits on the mission length L_m are specified in km.

special attention. In particular, the GTA description specifies the lower and upper bound on the thresholds T^*_{min} and T^*_{max} (Table B.2). From Table B.2, it may be understood there are eight possible combinations between the upper and lower limits, and therefore eight possible classes[1]. Accordingly, each operating class only needs one relationship to be completely determined.

Upper limit	**Lower limit**
$T^*_{\text{max}} = 40°\text{C}$	$T^*_{\text{min}} = -15°\text{C}$
$T^*_{\text{max}} > 40°\text{C}$	$T^*_{\text{min}} = -25°\text{C}$
	$T^*_{\text{min}} = -40°\text{C}$
	$T^*_{\text{min}} < -40°\text{C}$

Table B.2: Upper and lower limits on the air temperature according to the GTA classification system.

Instead, the UFD description uses a more sophisticated strategy. Five levels are specified as follows:

I. `V-COLD` if sometimes colder than $-30°\text{C}$, rarely warmer than $20°\text{C}$ and never warmer than $30°\text{C}$.

II. `COLD` if sometimes colder than $-15°\text{C}$, rarely warmer than $25°\text{C}$, and never warmer than $25°\text{C}$.

III. `MIXED` if rarely colder than $-15°\text{C}$ and rarely warmer than $30°\text{C}$.

IV. `WARM` if sometimes colder than $5°\text{C}$, never colder than $0°\text{C}$ and rarely warmer than $40°\text{C}$.

V. `V-WARM` if rarely colder than $15°\text{C}$, never colder than $0°\text{C}$ and sometimes warmer than $45°\text{C}$.

However, in the list above, the classes are formulated rather vaguely, since 'sometimes' and 'rarely' are not specified in terms of frequencies or probabilities. As a first interpretation, they may be assumed to indicate frequencies of around fifty and twenty percent, respectively, as done first in Paper B. Moreover, in the UFD system, each class is determined using multiple conditions on the limits T^*_{min}, T^*_{max} and the probabilities $p_{T^*_{\text{air, min}}}$ and $p_{T^*_{\text{air, max}}}$. Table B.3 summarises the operating classes for the air temperature parameter according to the UFD interpretation.

However, concerning of the operating classes defined using the values in Tables B.2 and B.3, it should be observed that the relationship (3.17) does not guarantee absolute lower and upper limits on the air temperature (apart from the zero point for thermodynamics).

[1]In each case, the corresponding probability $p_{T^*_{\text{air}},\text{max}}$ could be assumed to be close to the unity (for example $p_{T^*_{\text{air}},\text{max}} = 0.99$) when it is not possible to define a class using unit probabilities.

Air temperature classes in the UFD description					
Operating class	Number of relationship i	UFD thresholds			
		$T_{\min}^{*(i)}$	$T_{\max}^{*(i)}$	$p_{T_{\text{air}}^*,\min}^{(i)}$	$p_{T_{\text{air}}^*,\max}^{(i)}$
V-COLD	1	$-\infty$	$-30°C$	0	0.5
	2	$20°C$	∞	0	0.2
	3	$30°C$	∞	0	0
COLD	1	$-\infty$	$-15°C$	0	0.5
	2	$25°C$	∞	0	0.2
	3	$30°C$	∞	0	0
MIXED	1	$-\infty$	$-15°C$	0	0.2
	3	$30°C$	∞	0	0.2
WARM	1	$-\infty$	$5°C$	0	0.5
	2	$-\infty$	$0°C$	0	0
	3	$40°C$	∞	0	0.2
V-WARM	1	$-\infty$	$15°C$	0	0.2
	2	$-\infty$	$0°C$	0	0
	3	$45°C$	∞	0	0.5

Table B.3: The operating classes for the air temperature parameter in the UDF description. The V-COLD, COLD, WARM and V-WARM classes are defined by three relationships of the same type. On the other hand, the MIXED class only needs two inequalities to be completely defined.

Bibliography

[1] Z. Hausfather, "State of the climate: 2020 set to be the first ot second warmest year on record", 2020. Available: https://www.carbonbrief.org/state-of-the-climate-2020-set-to-be-first-or-second-warmest-year-on-record.

[2] J. Cook, D. Nuccitelli, S. A. Green et al., "Quantifying the consensus on anthropogenic global warming in the scientific literature", *Environmental Research Letters*, vol. 8, no. 2, pp. 024024, 2013. Available: https://doi.org/10.1088/1748-9326/8/2/024024.

[3] R. S. J. Tol, "Quantifying the consensus on anthropogenic global warming in the literature: A re-analysis", *Energy Policy*, vol. *73*, pp. *701-705*, 2014. Available: https://www.sciencedirect.com/science/article/pii/S0301421514002821.

[4] S. Callery, "Climate change: How do we know", 2019.

[5] Union of concerned scientists, "Global warming", Cambridge, MA, U.S, 2019.

[6] European Environmental Agency, "Greenhouse gas emissions from transport", 2019.

[7] C. C. C. Service, "Record-breaking temperatures for june!, 2019. Available: https://ucsusa.org/climate/science.

[8] U. S. E. P. Agency, "Overview of greenhouse gases", Environmental Protection Agency, Two independence square, Washington D.C., U.S.: United States, 2019.

[9] Eurostat, "Greenhouse gas emission statistics – emission inventories", 2019. Available: https://ec.europa.eu/eurostat/statistics-explained/index.php/Greenhouse_gas_emission_statistics.

[10] G. C. Project, "The global carbon atlas, co2 emissions", 2017. Available: http://www.globalcarbonatlas.org/en/CO2-emissions.

[11] European Commission, "Regulation (eu) no 333/2014 of the european parliament and of the council of 11 march 2014 amending regulation (ec) no 443/2009 to define modalities for reaching the 2020 target to reduce co2 emissions from new passenger cars", 2014. Available: https://eur-lex.europa.eu/legal-content/EN/TXT/?uri=OJ%3AL%3A2014%3A084%3ATOC.

[12] European Commission, "Regulation (eu) no 253/2014 of the european parliament and of the council of 26 february 2014 amending regulation (ec) no 510/2011 to define modalities for reaching the 2020 target to reduce co2 emissions from new light commercial vehicles", 2014. Available: https://eur-lex.europa.eu/legal-content/EN/TXT/?uri=OJ%3AL%3A2014%3A084%3ATOC.

[13] European Commission, "Commission regulation (eu) no 2017/2400. official journal of european union 60.l 247 (dec. 2017)", 2017. Available: https://eur-lex.europa.eu/legal-content/EN/TXT/?uri=OJ%3AL%3A2017%3A349%3ATOC.

[14] European Commission, "Vehicle Energy Consumption calculation Tool – VECTO", 2019. Available: https://ec.europa.eu/clima/policies/transport/vehicles/vecto_en.

[15] M. Xu, H. Yang and S. Wang, "Mitigate the range anxiety: Siting battery charging stations for electric vehicle drivers", *Transportation Research Part C: Emerging Technologies*, vol. *114*, 2020. DOI: 10.1016/j.trc.2020.02.001.

[16] J. Neubauer and E. Wood, "The impact of range anxiety and home, workplace, and public charging infrastructure on simulated battery electric vehicle lifetime utility", *Journal of Power Sources*, vol. *257*, 2014. DOI: 10.1016/j.jpowsour.2014.01.075.

[17] M. Esmaili, H. Shafiee and J. Aghaei, "Range anxiety of electric vehicles in energy management of microgrids with controllable loads", *Journal of Energy Storage*, vo. *20*, 2018. DOI: 10.1016/j.est.2018.08.023.

[18] P. Pettersson, "Operating cycle representation for road vehicles", Ph.D. dissertation, Chalmers University of Technology, Göteborg, Sweden, 2019.

[19] E. Silvas, "Integrated optimal design for hybrid electric vehicles", Ph.D. dissertation, Technische Universiteit Eindhoven, Eindhoven, the Netherlands, 2015.

[20] G. Fontaras, M. Rexeis, P. Dilara, S. Hausberger and K. Anagnostopoulos, "Development of a simulation tool for monitoring heavy-duty vehicle co2 emissions and fuel consumption in europe" in *11th International Conference on Engines and Vehicles*, 2013.

[21] R. Basso, B. Kulcsár, B. Egardt et al., "Energy consumption estimation integrated into the Electric Vehicle Routing Problem", *Transportation Research Part D: Transport and Environment*, vol. *69*, pp. *141-167*, 2019. Available: https://doi.org/10.1016/j.trd.2019.01.006.

[22] R. Basso, B. Kulcsár and I. Sanchez-Diaz, "Electric vehicle routing problem with machine learning for energy prediction", *Transportation Research Part B: Methodological*, vol. *145*, pp. *24-55*, 2021. Available: https://doi.org/10.1016/j.trb.2020.12.007.

[23] T. Ghandriz, J. Hellgren, M. Islam, L. Laine and B. Jacobson, "Optimization based design of heterogeneous truck fleet and electric propulsion", in *IEEE 19th International Conference on Intelligent Transportation Systems (ITSC)*, Rio de Janeiro, Brazil, 2016, pp. *328-335*.

[24] T. Ghandriz, "Transportation Mission Based Optimization of Heavy Vehicle Fleets including Propulsion Tailoring", Licentiate thesis, Chalmers University of Technology, Göteborg, Sweden, 2018.

[25] T. Ghandriz, B. Jacobson, L. Laine and J. Hellgren, "Impact of automated driving systems on road freight transport and electrified propulsion of heavy vehicles", *Transportation Research Part C: Emerging Technologies*, vol. *115*, 2020. DOI: 10.1016/j.trc.2020.102610.

[26] M. Åsbogård, L. Johannesson, D. Angervall and P. Johansson, "Improving system design of a hybrid powertrain using stochastic drive cycles and dynamic programming", in *SAE World Congress and Exhibition*, Detroit, MI, USA, 2007.

[27] T. Hofman, S. Ebbesen and L. Guzzella, "Topology Optimization for Hybrid Electric Vehicles With Automated Transmissions", *IEEE Transactions on Vehicular Technology*, vol. *61*, no. *6*, pp. *2442-2451*, 2012. DOI: 10.1109/TVT.2012.2196299.

[28] X. Hu, N. Murgovski, L. M. Johannesson and B. Egardt, "Optimal Dimensioning and Power Management of a Fuel Cell/Battery Hybrid Bus via Convex Programming", *IEEE/ASME Transactions on Mechatronics*, vol. *20*, no. *1*, pp. *457-468*, 2015. DOI: 10.1109/TMECH.2014.2336264.

[29] E. Silvas, T. Hofman, N. Murgovski, L. F. P. Etman and M. Steinbuch, "Review of Optimization Strategies for System-Level Design in Hybrid Electric Vehicles", *IEEE Transactions on Vehicular Technology*, vol. *66*, no. *1*, pp. *57-70*, 2015. DOI: 10.1109/TVT.2016.2547897.

[30] X. Hu, S. J. Moura, N. Murgovski, B. Egardt and D. Cao, "Integrated Optimization of Battery Sizing, Charging, and Power Management in Plug-In Hybrid Electric Vehicles", *IEEE Transactions on Control Systems Technology*, vol. *24*, no. *3*, pp. *1036-1043*, 2016. DOI: 10.1109/TCST.2015.2476799.

[31] M. Pourabdollah, N. Murgovski, A. Grauers and B. Egardt, "Optimal Sizing of a Parallel PHEV Powertrain", *IEEE Transactions on Vehicular Technology*, vol. *62*, no. *6*, pp. *2469-2480*, 2013. DOI: 10.1109/TVT.2013.2240326.

[32] D. W. Wyatt, H. Li. and J. E. Tate, "The impact of road grade on carbon dioxide (co2) emissions of passenger vehicle in real-world driving", *Transportation Research Part D: Transport and Environment*, vol. *32*, pp. *160-170*, 2014. DOI: 10.1016/j.trd.2014.07.015.

[33] K. Sentoff, L. Aultman-Hall and B. Holmé, "Implications of driving style on road grade for accurate vehicle data and emissions estimates", *Transportation Research Part D: Transport and Environment*, vol. *35*, pp. *175-188*, 2015. DOI: 10.1016/j.trd.2014.11.021.

[34] D. Llopis-Castelló, A. M. Pérez-Zuriaga, F. J. Camacho-Torregrosa and A. García, "Impact of horizontal geometric design of two-lane rural roads on vehicle co2 emissions", *Transportation Research Part D: Transport and Environment*, vol. *59*, pp. *46-57*, 2018. DOI: doi.org/10.1016/j.trd.2017.12.020.

[35] A. Sciarretta, "Energy-Efficient Driving of Road Vehicles", *1st* ed. Springer (Cham), Springer Nature Switzerland AG, 2020. Available: https://doi.org/10.1007/978-3-030-24127-8.

[36] H. Achour and A.G. Olabi, "Driving cycle developments and their impacts on energy consumption of transportation", *Journal of Cleaner Production*, vol. *112*, pp. *1778-1788*, 2016. DOI: 10.1016/j.jclepro.2015.08.007.

[37] J. Liu, X. Wang and A. Khattak, "Customizing driving cycles to support vehicle purchase and use decisions: Fuel economy estimation for alternative fuel vehicle users", *Transportation Research Part C: Emerging Technologies*, vol. *67*, pp. *280-298*, 2016. DOI: 10.1016/j.trc.2016.02.016.

[38] P. Shen, Z. Zhao, J. Li and X. Zhan, "Development of a typical driving cycle for an intra-city hybrid electric bus with a fixed route", *Transportation Research Part D: Transport and Environment*, vol. *59*, pp. *346-360*, 2018. DOI: 10.1016/j.trd.2018.01.032.

[39] X. Liu, J. Ma, X. Zhao, J. Du and Y. Xiong, "Study on Driving Cycle Synthesis Method for City Buses considering Random Passenger Load", *Journal of Advanced Transportation*, Hindawi, 2020. DOI: 10.1155/2020/3871703.

[40] S. Shi, S. Wei, H. Kui, L. Liu, C. Huang and M. Liu, "Improvements of the design method of transient driving cycle for passenger car", in *2009 IEEE Vehicle Power and Propulsion Conference*, 2009, pp. *1581-1586*. DOI: 10.1109/VPPC.2009.5289594.

[41] L. Liu, C. Huang, M. Liu and S. Shi, "Study on the Combined Design Method of Transient Driving Cycles for Passenger Car in Changchun", in *2009 IEEE Vehicle Power and Propulsion Conference*, 2009. Available: https://ieeexplore.ieee.org/stamp/stamp.jsp?arnumber=4677594.

[42] W.T. Hung, H.Y. Tong, C.P. Lee, K. Ha and L.Y. Pao, "Development of a practical driving cycle construction methodology: A case study in Hong Kong", *Transportation Research Part D: Transport and Environment*, vol. *12*, no. *2*, pp. *115-128*, 2007. DOI: 10.1016/j.trd.2007.01.002.

[43] K. S. Nesamani and K. P. Subramanian, "Development of a driving cycle for intra-city buses in Chennai, India", *Atmospheric Environment*, vol. *45*, no. *31*, pp. *5469-5476*, 2011. DOI: 10.1016/j.atmosenv.2011.06.067.

[44] S.-H. Ho, Y.-D. Wong and V. Wei-Chung Chang, "Developing Singapore Driving Cycle for passenger cars to estimate fuel consumption and vehicular emissions", *Atmospheric Environment*, vol. *97*, pp. *353-362*, 2014. DOI: 10.1016/j.atmosenv.2014.08.042.

[45] F. Guo and F. Zhang, "A study of driving cycle for electric cars on Beijing urban and suburban roads", in *2016 IEEE International Conference on Power and Renewable Energy (ICPRE)*, pp. *319-322*, 2016. DOI: 10.1109/ICPRE.2016.7871224.

[46] S. Ou, Y. Zhou, L. Lian, P. Jia and B. Tian, "Development of hybrid city bus's driving cycle", in *2011 International Conference on Electric Information and Control Engineering*, pp. *2112-2116*, 2011. DOI: 10.1109/ICEICE.2011.5777149.

[47] L. Berzi, M. Delogu and M. Pierini, "Development of driving cycles for electric vehicles in the context of the city of Florence", *Transportation Research Part D: Transport and Environment*, vol. *47*, pp. *299-322*, 2016. DOI: 10.1016/j.trd.2016.05.010.

[48] S. Shi, N. Lin, Y. Zhang, C. Huang, L. Liu, B. Lu and J. Cheng, "Research on Markov Property Analysis of Driving Cycle", in *2013 IEEE Vehicle Power and Propulsion Conference (VPPC)*, pp. *1-5*, 2013. DOI: 10.1109/VPPC.2013.6671737.

[49] Z. Jing, G. Wang, S. Zhang and C. Qiu, "Building Tianjin driving cycle based on linear discriminant analysis", *Transportation Research Part D: Transport and Environment*, vol. *53*, pp. *78-87*, 2017. DOI: 10.1016/j.trd.2017.04.005.

[50] Z. Zou, S. Davis, K. Beaty et al., "A New Composite Drive Cycle for Heavy-Duty Hybrid Electric Class 4-6 Vehicles", *SAE Technical Paper*, 2004. DOI: 10.4271/2004-01-1052.

[51] M. Naghizadeh, "Development oF Car Drive Cycle For Simulation of Emissions and Fuel Economy", 2003.

[52] P. Nyberg, "Evaluation, generation and transformation of driving cycles", Ph.D. dissertation, Linköping, Sweden, 2015.

[53] P. Nyberg, E. Frisk and L. Nielsen, "Using Real-World Driving Databases to Generate Driving Cycles With Equivalence Properties," *IEEE Transactions on Vehicular Technology*, vol. *65*, no. *6*, pp. *4095-4105*, 2016. DOI: 10.1109/TVT.2015.2502069.

[54] P. Nyberg, E. Frisk and L. Nielsen, "Driving Cycle Equivalence and Transformation", *IEEE Transactions on Vehicular Technology*, vol. *66*, no. *3*, pp. *1963-1974*. DOI: 10.1109/TVT.2016.2582079.

[55] A. Ashatari, E. Bibeau and S. Shahidinejad, "Using large driving record samples and a stochastic approach for real-world driving cycle construction: Winnipeg driving cycle", *Transportation Science*, vol. *48*, no. *2*, pp. *170-183*, 2014. DOI: 10.1287/trsc.1120.0447.

[56] E. Tazelaar, J. Bruinsma, B. Veenhuizen and P. Van den Bosch, "Driving cycle characterization and generation, for design and control of fuel cell buses", *World Electric Vehicle Journal*, vol. *3*, no. *4*, pp. *812–819*, 2009. DOI: 10.3390/wevj3040812.

[57] J. Lin and D. A. Niemeier, "An exploratory analysis comparing a stochastic driving cycle to California's regulatory cycle", *Atmospheric Environment*, vol. *36*, no. *38*, pp. *5759-5770*, 2002. DOI: 10.1016/S1352-2310(02)00695-7.

[58] J. Brady and M. O'Mahony, "Development of a driving cycle to evaluate the energy economy of electric vehicles in urban areas", *Applied Energy*, vol. *177*, pp. *165-178*, 2016. DOI: 10.1016/j.apenergy.2016.05.094.

[59] T. K. Lee and Z. S. Filipi, "Synthesis of real-world driving cycles using stochastic process and statistical methodology", *International Journal of Vehicle Design*, vol. *57*, no. *1*, pp. *17-36*, 2011. Available: http://www.inderscience.com/offer.php?id=43590.

[60] T. Lee, B. Adornato and Z. S. Filipi, "Synthesis of Real-World Driving Cycles and Their Use for Estimating PHEV Energy Consumption and Charging Opportunities: Case Study for Midwest/U.S.", *IEEE Transactions on Vehicular Technology*, vol. *60*, no. *9*, 2011. DOI: 10.1109/TVT.2011.2168251.

[61] G. Amirjamshidi and M. J. Roorda, "Development of simulated driving cycles for light, medium, and heavy duty trucks: Case of the Toronto Waterfront Area", *Transportation Research Part D: Transport and Environment*, vol. *34*, pp. *255-266*, 2015. DOI: 10.1016/j.trd.2014.11.010.

[62] S. H. Kamble, T. V. Mathew and G. K. Sharma, "Development of real-world driving cycle: Case study of Pune, India", *Transportation Research Part D: Transport and Environment*, vol. *14*, no. *2*, pp. *132-140*, 2009. DOI: 10.1016/j.trd.2008.11.008.

[63] E. Silvas, K. Hereijgers, H. Peng, T. Hofman and M. Steinbuch, "Synthesis of Realistic Driving Cycles With High Accuracy and Computational Speed, Including Slope Information", *IEEE Transactions on Vehicular Technology*, vol. *65*, no. *6*, pp. *4118-412*, 2016. DOI: 10.1109/TVT.2016.2546338.

[64] K. Kivekäs, J. Vepsäläinen and K. Tammi, "Stochastic Driving Cycle Synthesis for Analyzing the Energy Consumption of a Battery Electric Bus", *IEEE Access*, vol. *6*, pp. *55586-55598*, 2018. DOI: 10.1109/ACCESS.2018.2871574.

[65] K. Kivekäs, J. Vepsäläinen, K. Tammi and J. Anttila, "Influence of Driving Cycle Uncertainty on Electric City Bus Energy Consumption", in *2017 IEEE Vehicle Power*

and Propulsion Conference (VPPC), 2017. Available: DOI: 10.1109/VPPC.2017.8331014.

[66] J. Vepsäläinen, K. Kivekäs, K. Otto, A. Lajunen and K. Tammi, "Development and validation of energy demand uncertainty model for electric city buses", *Transportation Research Part D: Transport and Environment*, vol. *63*, pp. *347-361*, 2018. DOI: 10.1016/j.trd.2018.06.004.

[67] P. Johannesson, K. Podgórski, I. Rychlik and N. Shariati, "AR(1) time series with autoregressive gamma variance for road topography modeling", *Probabilistic Engineering Mechanics*, vol. *34*, pp. *106-116*, 2016. DOI: 10.1016/j.probengmech.2015.12.006.

[68] P. Johannesson, K. Podgórski and I. Rychlik, "Laplace distribution models for road topography and roughness", *International Journal of Vehicle Performance (IJVP)*, vol. *3*, no. *3*, 2017. Available: http://www.inderscience.com/offer.php?id=85032.

[69] A. Donkers, D. Yang and M. Viktorović, "Influence of driving style, infrastructure, weather and traffic on electric vehicle performance", *Transportation Research Part D: Transport and Environment*, vol. *88*, pp. *102569*, 2020. DOI: 10.1016/j.trd.2020.102569.

[70] D. Akin, V. P. Sisiopiku and A. Skabardonis, "Impacts of Weather on Traffic Flow Characteristics of Urban Freeways in Istanbul", *Procedia - Social and Behavioral Sciences*, vol. *16*, pp. *88-89*, 2011. DOI: 10.1016/j.sbspro.2011.04.432.

[71] E. Hooper, L. Chapman and A. Quinn, "The impact of precipitation on speed–flow relationships along a UK motorway corridor", *Theor Appl Climatol*, vol. *117*, pp. *303-316*, 2013. DOI: 10.1007/s00704-013-0999-5.

[72] O. Travesset-Baro. M. Rosas-Casals and E. Jover, "Transport energy consumption in mountainous roads. A comparative case study for internal combustion engines and electric vehicles in Andorra", *Transportation Research Part D: Transport and Environment*, vol. *34*, pp. *16-26*, 2020. DOI: 10.1016/j.trd.2014.09.006.

[73] B. Yazdani Boroujeni and H. C. Frey, "Road grade quantification based on global positioning system data obtained from real-world vehicle fuel use and emissions measurements", *Atmospheric Environment*, vol. *85*, pp. *179-186*, 2014. DOI: 10.1016/j.atmosenv.2013.12.025.

[74] P. Pettersson, P. Johannesson, B. Jacobson, F. Bruzelius, L. Fast and S. Berglund, "A statistical operating cycle description for prediction of road vehicles' energy consumption", *Transportation Research Part D: Transport and Environment*, vol. *73*, pp. *205-229*, 2013. DOI: 10.1016/j.trd.2019.07.006.

[75] P. Pettersson, S. Berglund, B. J. Jacobson, L. Fast, P. Johannesson and F. Santandrea, "A proposal for an operating cycle description format for road transport missions", *European Transport Research Review*, vol. *10*, no. *31*, pp. *1-19*, 2013. DOI: 10.1186/s12544-018-0298-4.

[76] G. Grimmett and D. Stirzaker, "Probability and random processes", *4th* ed. Oxford university press, Oxford, 2020.

[77] G. Box, G. Jenkins, G. Reinsel, G. Ljung and G. Ljung, "Time Series Analysis: Forecasting and Control", *5th* ed. John Wiley & Sons, San Francisco, Holden-Day, 2015.

[78] K. Miettinen, "Nonlinear Multiobjective Optimization", *1st* ed. Springer, Boston, MA,

1998.

[79] M. Guiggiani, "The Science of Vehicle Dynamics", *2nd* ed. Cham(Switzerland): Springer International; 2018.

[80] M. Guiggiani, "The Science of Vehicle Dynamics", *3rd* ed. Cham(Switzerland): Springer International; 2023.

[81] L. Romano, "Advanced Brush Tyre Modelling", Springer, Cham; 2022. DOI: 10.1007/978-3-030-98435-9.

[82] L. Guzzella and A. Sciarretta, "Vehicle propulsion systems: introduction to modeling and optimization", *3rd* ed. Springer (Cham), Berlin, Germany: Springer, 2013.

[83] L. Romano, F. Bruzelius and B. Jacobson, "A Brush Tyre Model with Standstill Handler for Energy Efficiency Studies", Commercial Vehicle Technology 2020/21, pp. *119-134*, 2021.

[84] L. Romano, F. Timpone, F. Bruzelius and B. Jacobson, "Transient Tire Slip Losses Using the Brush Theory", Tire Science and Technology, 2022.

[85] T. Ghandriz, B. Jacobson, L. Laine and J. Hellgren, "Optimization data on total cost of ownership for conventional and battery electric heavy vehicles driven by humans and by automated driving systems", *Data in Brief*, vol. *30*, pp. *105566*, 2020. DOI: 10.1016/j.dib.2020.105566.

[86] T. Ghandriz, B. Jacobson, M. Islam, J. Hellgren and L. Laine, "Transportation-Mission-Based Optimization of Heterogeneous Heavy-Vehicle Fleet Including Electrified Propulsion", *Energies*, vol. *14*, no. *11*, 2020. DOI: 10.3390/en14113221.

[87] T. Ghandriz, "Transportation Mission-Based Optimization of Heavy Combination Road Vehicles and Distributed Propulsion, Including Predictive Energy and Motion Contro", Ph.D. dissertation, Chalmers University of Technology, Göteborg, Sweden, 2020.

[88] U. Kiencke, L. Nielsen, "Automotive Control Systems", *2nd* ed. Springer Berlin, Heidelberg, 2005.

[89] L. Romano, "Mathematical modelling of operating cycles for road vehicles", Licentiate thesis, Chalmers University of Technology, Göteborg, Sweden, 2021.

[90] L. Romano, P. Johannesson, E. Nordström et al., "A classification method of road transport missions and applications using the operating cycle format", *IEEE Access*, vol. *10*, pp. *73087-73121*.

[91] S. Edlund and P.-O. Fryk, "The Right Truck for the Job with Global Truck Application Descriptions," *SAE Technical Paper*. 2004. DOI: 10.4271/2004-01-2645.

[92] L. Ntziachristos and Z. Samaras, "EMEP/EEA air pollutant emission inventory guidebook 2016 Part B.1.A.3.b.i-iv Road transport 2018", Copenhagen, Denmark: European Environment Agency, Chalmers University of Technology, Göteborg, Sweden, 2018.

[93] R. Griego and R. Hersh, "Theory of Random Evolutions with Applications to Partial Differential Equations", *Transactions of the American Mathematical Society*, vol. *156*, pp. *405-418*, 1971. DOI: 10.2307/1995620.

[94] K. L. Chungr, "Markov Chains With Stationary Transition Probabilities", *2nd* ed. Springer, Berlin, Berlin, Heidelberg, 1967. DOI: 10.1007/978-3-642-62015-7.

[95] C. J. J. Beckers, I. J. M. Besselink and H. Nijmeijer, "Modeling of Energy Losses During Cornering for Electric City Buses," 2019 IEEE Intelligent Transportation Systems Conference (ITSC), 2019, pp. 4164-4169, doi: 10.1109/ITSC.2019.8917232.

[96] C. Beckers, I. Besselink and H. Nijmeijer, "On-line Test of a Real-Time Velocity Prediction for E-bus Energy Consumption Estimation," 2021 IEEE Vehicle Power and Propulsion Conference (VPPC), 2021, pp. 1-5, doi: 10.1109/VPPC53923.2021.9699205.

[97] C. Beckers, I. Besselink and H. Nijmeijer, "Assessing the impact of cornering losses on the energy consumption of electric city buses", *Transportation Research Part D: Transport and Environment*, vol. *86*, no. *1361-9209*, 2021, doi: 10.1109/VPPC53923.2021.9699205.

[98] M. Karlsson, "Load Modelling for Fatigue Assessment of Vehicles – a Statistical Approach", Ph.D. dissertation, Chalmers University of Technology, Göteborg, Sweden, 2007.

[99] M. Karlsson, "Evaluation of Approximative Methods for Rainflow Damage of Broad-Banded Non-Gaussian Random Loads", *Proceedings of the ASME 2005 International Mechanical Engineering Congress and Exposition. Design Engineering, Parts A and B*, pp. *79-87*, 2005. DOI: 10.1115/IMECE2005-79868.

[100] M. Karlsson, "Evaluation of road load classification for fatigue assessments", *International Journal of Vehicle Design*, vol. *47*, no. *1/2/3/4*, pp. *250-268*, 2013. DOI: 10.1504/IJVD.2008.020890.

[101] F. Pellicano, Z. Li, W. Yu, and X. Cui, "Online Classification of Road Roughness Conditions with Vehicle Unsprung Mass Acceleration by Sliding Time Window", *Shock and Vibration*, vol. *10*, no. *3*, 2018. DOI: 10.1109/TVT.2012.2196299.

[102] K. Bogsjö, "Coherence of road roughness in left and right wheel-path", *Vehicle System Dynamics*, vol. *46*, no. *sup1*, pp. *599-609*, 2008. DOI: 10.1080/00423110802018289.

[103] P. Johannesson, K. Podgórski and I. Rychlik, "Modelling roughness of road profiles on parallel tracks using roughness indicators", *International Journal of Vehicle Design (IJVD)*, vol. *70*, no. *2*, 2016.

[104] K. Bogsjö, K. Podgórski and I. Rychlik, "Models for road surface roughness", *Vehicle System Dynamics*, vol. *50*, no. *5*, pp. *725-747*, 2012. DOI: 10.1080/00423114.2011.637566.

[105] S. Kotz, T. Kozubowski and K. Podgorski, "The Laplace Distribution and Generalizations", *2nd* ed. Birkhäuser Basel, Basel, 2001. DOI: 10.1007/978-1-4612-0173-1.

[106] C.J. Dodds and J.D. Robson, "The description of road surface roughness", *Journal of Sound and Vibration*, vol. *31*, no. *2*, pp. *2*, 1973. DOI: 10.1016/S0022-460X(73)80373-6.

[107] ISO 8608, "Mechanical vibration – Road surface profiles – Reporting of measured data. ISO 8608: 1995, 1995", 1995.

[108] H. B. Pacejka, "Tire and vehicle dynamics", *3rd* ed. Amsterdam: Elsevier/BH, 2012.

[109] L. Romano, F. Timpone, F. Bruzelius and B. Jacobson, "Analytical results in transient brush tyre models: theory for large camber angles and classic solutions with limited friction", *Meccanica*, vol. *57*, no. *1*, pp. *1663-1679*. DOI: 10.1007/s11012-021-01422-3.

[110] H. P. Hsu, "Schaum's Outline of Probability, Random Variables, and Random Processes", *4th* ed. McGraw-Hill Education: New York, Chicago, San Francisco, Athens, London,

Madrid, Mexico City, Milan, New Delhi, Singapore, Sydney, Toronto, 2020.

[111] L. Romano, P. Johannesson, F. Bruzelius and B. Jacobson, "An enhanced stochastic operating cycle description including weather and traffic models", *Transportation Research Part D: Transport and Environment*, vol. *97*, pp. *102878*, 2013. DOI: 10.1016/j.trd.2021.102878.

[112] A. Ramesh Babu, J. Andric, B. Minovski and S. Sebben, "System-Level Modeling and Thermal Simulations of Large Battery Packs for Electric Trucks", *Energies*, vol. *14*, no. *16*, 2021. Available: https://doi.org/10.3390/en14164796.

[113] Garrett J. Marshall, Colin P. Mahony, Matthew J. Rhodes, Steve R. Daniewicz, Nicholas Tsolas, Scott M. Thompson, "Thermal Management of Vehicle Cabins, External Surfaces, and Onboard Electronics: An Overview", *Engineering*, vol. *5*, iss. *5*, no. *2095-8099*, pp. *954-969*, 2019. DOI: 10.1016/j.eng.2019.02.009.

[114] Y. Liu and M. C. Roberts and R. Sioshansi, "A vector autoregression weather model for electricity supply and demand modeling", *Journal of Modern Power Systems and Clean Energy*, vol. *6*, no. *4*, pp. *763-776*, 2018.

[115] A. Eymen and Ü. Köylü, "Seasonal trend analysis and ARIMA modeling of relative humidity and wind speed time series around Yamula Dam", *Meteorol Atmos Phys*, vol. *131*, pp. *601-6012*, 2019.

[116] P. La Rocca, D. Riggi and F. Riggi, "Time series analysis of barometric pressure data", *European Journal of Physics*, vol. *31*, no. *3*, pp. *645-655*, 2010. Available: https://doi.org/10.1088/0143-0807/31/3/022.

[117] Mohamed M. Ahmed, Ali Ghasemzadeh, "The impacts of heavy rain on speed and headway Behaviors: An investigation using the SHRP2 naturalistic driving study data", *Transportation Research Part C: Emerging Technologies*, vol. *91*, no. *0968-090X*, pp. *371-384*, 2018. DOI: 10.1016/j.trc.2018.04.012.

[118] Jiho Yeo, Jooyoung Lee & Kitae Jang (2021) The effects of rainfall on driving behaviors based on driving volatility, International Journal of Sustainable Transportation, 15:6, 435-443, DOI: 10.1080/15568318.2020.1756543.

[119] B. N. J. Persson, U. Tartaglino, O. Albohr, and E. Tosatti, "Rubber friction on wet and dry road surfaces: The sealing effect", *Phys. Rev. B*, vol. *71*, 2005. DOI: 10.1103/PhysRevB.71.035428.

[120] K. R. Gabriel and J. Neumann, "A Markov chain model for daily rainfall occurrence at Tel Aviv", *Quarterly Journal of the Royal Meteorological Society*, vol. *88*, no. *375*, pp. *90-95*, 1962. DOI: 10.1002/qj.49708837511.

[121] E. H. Chin, "Modeling daily precipitation occurrence process with Markov Chain", *Water Resources Research*, vol. *13*, no. *6*, pp. *949-956*, 1977. DOI: 10.1029/WR013i006p00949.

[122] G. J. Husak, J. Michaelsen and C. Funk, "Use of the gamma distribution to represent monthly rainfall in Africa for drought monitoring applications", *International Journal of Climatology*, vol. *27*, no. *7*, pp. *935-944*, 2007. DOI: 10.1002/joc.1441.

[123] V. Kumar and S. Jahangeer, "Statistical distribution of rainfall in Uttarakhand, India", *Appl Water Sc*, no. *7*, pp. *4765–4776*, 2017. DOI: 10.1007/s13201-017-0586-5.

[124] F. O. Hocaoğlu, Ö. N. Gerek and M. Kurban, "A novel wind speed modeling approach using atmospheric pressure observations and hidden Markov models", *Journal of Wind Engineering and Industrial Aerodynamics*, vol. *98*, no. *8*, pp. *472-481*, 2010. Available: https://doi.org/10.1016/j.jweia.2010.02.003.

[125] E. Cadenas, W. Rivera, R. Campos-Amezcual and C. Heard, "Wind Speed Prediction Using a Univariate ARIMA Model and a Multivariate NARX Model", *Energies*, vol. *9*, no. *2*, 2016. Available: https://www.mdpi.com/1996-1073/9/2/109.

[126] E. Erdem and J. Shi, "ARMA based approaches for forecasting the tuple of wind speed and direction", *Applied Energy*, vol. *88*, no. *4*, pp. *1405-1414*, 2011. Available: https://doi.org/10.1016/j.apenergy.2010.10.031.

[127] N. I. Fisher, "Statistical Analysis of Circular Data". Cambridge, 1993.

[128] A. Eriksson, "Simulation based methods and tools for comparison of powertrain concepts", Chalmers University of Technology, 1997.

[129] J. A. Michon, "A Critical View of Driver Behavior Models: What Do We Know, What Should We Do?", *Human Behavior and Traffic Safety*, pp. *485–524*. Springer US, Boston MA, 1985.

[130] P. A. Brodtkorb, P. Johannesson, G. Lindgren, I. Rychlik, J. Rydén E. and Sjö, "WAFO – a Matlab Toolbox for the Analysis of Random Waves and Loads", *Proc. 10'th Int. Offshore and Polar Eng. Conf., ISOPE, Seattle, USA*, vol. *3*, pp. *343–350*, 2000.

[131] WAFO-group, "WAFO – A Matlab Toolbox for Analysis of Random Waves and Loads - A Tutorial", Math. Stat., Center for Math. Sci., Lund Univ., Lund, Sweden, 2000. Available: http://www.maths.lth.se/matstat/wafo.

[132] H. Tennekes, "The Logarithmic Wind Profile", *Journal of Atmospheric Sciences*, vol. *30*, no. *2*, pp. *234–238*, 1973. Available: https://journals.ametsoc.org/view/journals/atsc/30/2/1520-0469_1973_030_0234_tlwp_2_0_co_2.xml.

[133] L. I. Rudin, S. Osher and E. Fatemi, "Nonlinear total variation based noise removal algorithms", *Physica D: Nonlinear Phenomena*, vol. *60*, iss. *1-4*, pp. *259-268*, 1992. DOI: 10.1016/0167-2789(92)90242-F.

[134] T. F. Chan, G. H. Golub and P.Mulet "A nonlinear primal-dual method for total variation-based image restoration", in Berger MO., Deriche R., Herlin I., Jaffré J., Morel JM. (eds) ICAOS '96. Lecture Notes in Control and Information Sciences, vol 219. Springer, Berlin, Heidelberg. DOI: 10.1007/3-540-76076-8_137

[135] Y. Li and F. Santosa, *An affine scaling algorithm for minimizing total variation in image enhancement*, 1994.

[136] P. Blomgren and T. F. Chan, "Color TV: total variation methods for restoration of vector-valued images", in IEEE Transactions on Image Processing, vol. *7*, no. *3*, pp. *304-309*, March 1998. DOI: 10.1109/83.661180.

[137] N. Andréasson, A. Evgrafov, M. Patriksson et al, "An Introduction to Continuous Optimization", *3rd* ed. Malmö AB, Sweden: Studentlitteratur, 2018.

[138] B. Øksendal, "Stochastic Differential Equations", *6th* ed. Springer Berlin, Heidelberg, 2003. Available: https://doi.org/10.1007/978-3-642-14394-6.

[139] M. Grigoriu, "Stochastic Calculus", Birkhäuser Boston, MA, 2013. Available: https://doi.org/10.1007/978-0-8176-8228-6.

[140] H. Risken, "The Fokker-Planck Equation", *1st* ed. Springer Berlin, Heidelberg, 1996. Available: https://doi.org/10.1007/978-3-642-61544-3.

[141] L. Johnson, A. J. Nedzesky, "A comparative study of speed humps, speed slits and speed cushions", *Tech. Rep. Annual meeting compendium*, U.S. Department of Transportation Federal Highway Administration, 2004.

Paper A

An enhanced stochastic operating cycle description including weather and traffic models

Paper B

A classification method of road transport missions and applications using the operating cycle format

Paper C

Development of the Västra Götaland operating cycle for long-haul heavy-duty vehicles

Paper D

A method to build energy-metric-optimal (EMO) classification systems for road transport missions

Paper E

Stochastic modeling of mission stops and variable cargo weight for heavy-duty trucks